THE ROLE OF K_V7 IN PERIPHERAL NEURONS

Chih Houng King

A DISSERTATION

in

Neuroscience

Presented to the Faculties of the University of Pennsylvania in Partial Fulfillment of the Requirements for the Degree of Doctor of Philosophy

2012

Supervisor of Dissertation

_____

Dr. Steven S. Scherer

Professor, Department of Neurology

Graduate Group Chairperson

_____

Dr. Rita Balice-Gordon

Professor, Department of Neuroscience

Dissertation Committee

Dr. Erika Holzbaur, Professor, Department of Physiology

Dr. Rita Balice-Gordon, Professor, Department of Neuroscience

Dr. Dejian Ren, Associate Professor, Department of Biology

Dr. Wenqin Luo, Assistant Professor, Department of Neuroscience

THE ROLE OF K_V7 IN PERIPHERAL NEURONS

Dedication

For my grandparents, for being the genesis of my journey here.

ACKNOWLEDGMENTS

Being a Ph.D. student is certainly a very unique experience that I will never forget, and though all of the ups and downs I have learned that the one constant that I could always count on are the support from the following people, so I would like to express my brief, but sincere, gratitude to these people here, for without them it would not have been possible for me to reach this point.

I like to first thank Steve, for being like a scientific father to me. Steve was the first faculty member that I spoke to during my interview at Penn, and even at that first interaction I could tell that he is a fantastic mentor. Thank you for being stern with me when you needed to be, for giving me encouragement when things got tough, for your enthusiasm to share with me everything that you know about the nervous system, and most importantly, for never losing your patience and faith in me. I could only hope that one day I can be a mentor like you, and to pass down everything that I have learned from you during my years in your lab.

In extension, I would also like to thank the past and present members of the Scherer lab: Eric Lancaster, Sarah, Joel, Toby, Junxian, Meryl, Jenn, Sabrina, Sam, and Eric Sirkowski. I really enjoy all of the times that we have spent together, and I will miss you all very much after I have said my goodbye.

I like to thank the past and present members of my thesis committee. I appreciate all of the guidance and feedback provided by Erika, Rita, Dejian, and Wenqin toward my thesis work, and Ed Cooper for all of the advices and reagents. Like Steve, all of you have kept your support and faith in me, and for that I am very grateful.

I like to thank my friends both here and in New York City for reminding me that there is always a life outside science, and for all of the fond memories and adventures during these years. I look forward to sharing the next chapter of my life with you.

Last but not least, I like to thank my girlfriend Sophia and my family, which are the things most dear to my heart. My girlfriend Sophia, who I first met here in Philly, kept me going with her love, support, and for always being there for me when I needed someone to talk to. My family for believing in me when I first decided to come to Penn to pursue my Ph.D., and for the unconditionally support during all of these years. I hope that in completing this thesis, I have made all of you proud.

ABSTRACT

THE ROLE OF K_V7 IN PERIPHERAL NEURONS

Chih Houng King

Supervisor: Steven S. Scherer

The Kv7 (KCNQ) channel is a family of voltage-gated potassium channels that is considered to be important in the regulation of cellular excitability and axonal conduction. Previous studies have shown that peripheral sensory neurons express Kv7.2, Kv7.3, and Kv7.5 subunits, and that suppression of Kv7 activity with pharmacological blockers can lead to increased nociception. However, the specific localization and the functional role of each Kv7 subunits within the peripheral sensory system have not been fully elucidated. In this thesis, I first investigate the expression pattern of Kv7.5 with immunohistochemical techniques, which allow me to show that Kv7.5 is localized in the axons of the Remak bundles (unmyelinated axons and their associated Schwann cells), including their cutaneous branches, and is not detected at nodes of Ranvier. In addition, I demonstrate that small diameter neurons in the dorsal root ganglia (DRG), which are the origin of these unmyelinated afferents, express relatively more Kv7.5 than do large DRG neurons. Thus, Kv7.5 may be the relevant Kv7 channel expressed by C-fibers. Next I examined Kv7.2 with the generation of conditional *Kcnq2*-null mice that lacked Kv7.2 expression in all peripheral sensory neurons. I show that *Kcnq2*-null mice have a complete loss of Kv7.2 expression in the peripheral sensory neurons, but retain normal Kv7.3 nodal expression and other molecular components of the node, paranode, and

juxtaparanode. Furthermore, the *Kcnq2*-null mice exhibit normal motor performance, but have increased thermal hyperalgesia and mechanical allodynia. Finally, by utilizing whole cell patch recording technique, I demonstrate that *Kcnq2*-null DRG neurons have increased excitability and reduced spike-frequency adaptation. Taken together, the results that I have generated in this thesis suggest that in the peripheral sensory system, Kv7.5 provides the primary M-current in unmyelinated axons, while Kv7.2 regulates the excitability of myelinated axon.

TABLE OF CONTENTS

LIST OF TABLES

LIST OF ILLUSTRATIONS

CHAPTER 1: GENERAL INTRODUCTION

Peripheral myelinated and unmyelinated axons

The axons in the peripheral nervous system (PNS) can be divided into two broad classes - the myelinated and the unmyelinated axons. The myelinated axons are organized into several domains - the node of Ranvier, the paranode, the juxtaparanode, and the internode, and this organization is critical to the propagation of action potential by the mechanism of saltatory conduction (Poliak and Peles, 2003, Salzer et al., 2008). Schwann cells, which unlike oligodendrocytes in the central nervous system (CNS) can only myelinate one internode of a single axon, form myelin sheath by enwrapping their membrane several times around the axon (Poliak and Peles, 2003); the multi-lamellar structure of the myelin sheath serves to both increase membrane resistance as well as limit the generation of action potentials to the nodes, thus dramatically increasing the conduction velocity of myelinated axons. Of course, the most important domain of the myelinated axon is the node, where there is a very high concentration of voltage-gated sodium channels (Poliak and Peles, 2003, Salzer et al., 2008), and is also where the voltage-gated Kv7 potassium channels are expressed (Devaux et al., 2004); the co-localization of Kv7 channels with the voltage-gated sodium channels (Na_v) at nodes (and axonal initial segments) allows Kv7 channels to contribute to the regulation axonal excitability, as I will discuss below. Notably, the co-localization of both Na_v and the Kv7.2 and Kv7.3 channels owes to a consensus ankyrin-G binding domain at their C-termini (Pan et al., 2006), which is absent in all other Kv7 subunits. Finally, the nodes of peripheral axon are normally ~1 μm long and are contacted by Schwann cell microvilli,

which closely appose the nodal axolemma (Salzer et al., 2008); in chapter 3 of this thesis I will compare the ultrastructure of *Kcnq2*-null myelinated axons against wild-type myelinated axons.

Unlike the CNS, which contains relatively few unmyelinated axons, the PNS contains many unmyelinated axons (Griffin and Thompson, 2008). The unmyelinated fibers, referred to as Remak fibers (because they were first characterized by Robert Remak 170 years ago; (Remak, 1838)), include the C-fibers, the postganglionic sympathetic fibers, and some of the preganglionic sympathetic and parasympathetic fibers (Griffin and Thompson, 2008). Unmyelinated axons lack the distinct domains of myelinated axons, and Na_v and Kv7 channels are expressed along the entire length of the membrane (Giuliodori and DiCarlo, 2004); the lack of saltatory conduction, along with decrease membrane resistance, result in the substantially slower conduction velocity of the Remak fibers. For example, C-fibers, have a conduction velocity of < 1 m/s, versus 5-30 m/s for the thinly-myelinated A-delta fibers (Fields, 1987). Lastly, unlike myelinating Schwann cells, Remak Schwann cells often ensheath more than one axon (Griffin and Thompson, 2008).

Kv7 channels and M-current

The Kv7 (KCNQ) family of potassium channels is made up of five members: Kv7.1 to Kv7.5, and mutation of *KCNQ* genes contribute to a number of inherited neuropathies. Kv7.1 is the only Kv7 subunit known to be expressed in the heart, and dominant mutation of Kv7.1 can lead to long-QT syndrome, a potentially fatal form of cardiac arrhythmia (Wang et al., 1996). Kv7.2 and Kv7.3 is found in a wide variety of nervous tissues within

the CNS and PNS (Jentsch, 2000, Robbins, 2001), and dominant mutation of *KCNQ2* or *KCNQ3* cause benign familial neonatal convulsions, a form of generalized epilepsy during the neonatal period (Singh et al., 1998). The expression of Kv7.4 is primarily restricted to the auditory and vestibular system, and dominant mutant of *KCNQ4* can lead to progressive hearing loss caused by degeneration (Van Camp et al., 2002). Lastly, Kv7.5 has been found to be expressed in the brain (Schroeder et al., 2000), peripheral sensory neurons (Passmore et al., 2003), as well as muscles; unlike the other Kv7 subunits, no human disease has yet been linked to mutation of *KCNQ5* (Jentsch, 2000). These Kv7-mediated channelopathies illustrate the important functional role that Kv7 channels play in the regulation of cellular excitability, by generating a type of potassium current known as the M-current (I_M) (Wang et al., 1998). The M-current (so-called because it can be modulated by muscarinic agonists (Brown and Adams, 1980), is a type of slowly activating current that does not become inactivated. Because of its low activation threshold (at around -60 mV) (Lamas et al., 2002, Brown and Passmore, 2009), it helps to maintain the resting membrane potential. In addition, because M-current does not become inactivated after depolarization, it plays an important role in the regulation of neuronal excitability by reducing firing frequency during prolonged stimulation (Rivera-Arconada et al., 2009), thus mediating spike-frequency adaptation (Gu et al., 2005, Peters et al., 2005). Indeed, numerous studies have demonstrated that the administration of M-blockers decrease spike-frequency adaptation and increase firing rates of both central (Aiken et al., 1995, Yue and Yaari, 2004, Gu et al., 2005, Shah et al., 2008) and peripheral (Passmore et al., 2003, Wladyka and Kunze, 2006, Wladyka et al., 2008) neurons.

Beside the aforementioned ankyrin-G binding motif, the C-termini of Kv7 subunits also contains a putative assembly domain that is thought to be involved in subunit assembly, at least in Kv7.1 (Jentsch, 2000, Schmitt et al., 2000). All Kv7 channels can form homomeric channels (i.e. with themselves) *in vitro* (Jentsch, 2000), while a subset of the Kv7 subunits can form heteromeric channels. For example, while Kv7.1 can only form homomeric channels, Kv7.2, Kv7.4, and Kv7.5 can form heteromeric channels with Kv7.3 (Kubisch et al., 1999, Schroeder et al., 2000, Cooper, 2011), and Kv7.4 and Kv7.5 can also form heteromeric channels (Bal et al., 2008). In the myelinated axon, Kv7.2 and Kv7.3 had been shown to co-localize at nodes (Pan et al., 2006), and a recent study suggest that proper localization of Kv7.3 at nodes and axon initial segment depends on Kv7.2 (Gomez-Posada et al., 2010). I will address these points in chapter 3 of this thesis by examining the expression pattern of both Kv7.2 and Kv7.3 in the myelinated axons of my *Kcnq2*-null mice.

Kv7 blockers and enhancers

As mentioned earlier, in studies of the Kv7 channels, one of the most common tools that the researchers utilized is M-channel blockers, and the two most commonly used compounds are linopirdine and its successor XE991; linopirdine was the first selective Kv7 blocker developed, originally designed as a cognitive enhancer for the treatment of neurodegenerative diseases such as Alzheimer's disease (Tam and Zaczek, 1995); however, due to the relatively high dose required to inhibit M-current, linopirdine was found to cause tremors through cholinergic hyperstimulation (Miceli et al., 2008, Brown and Passmore, 2009), and other compounds, such as XE991, were later designed

to try to overcome this shortcoming. However, with the exception of Kv7.5 (Schroeder et al., 2000), both linopirdine and XE991 are relatively non-selective again other Kv7 channels (Wang et al., 1998), so utilizing these compounds for both experimental and treatment purposes carry the risk of inhibiting cardiac Kv7.1 channels and causing fatal arrhythmia (Wang et al., 2000). However, one compound that does not share this disadvantage is tetraethylammonium (TEA), which is much more sensitive against the Kv7.2 subunit (Hadley et al., 2000). Specifically, the TEA's IC_{50} value for Kv7.2 (0.3 mM) is at least 10 times less than for the other Kv7 subunits (the IC_{50} values for Kv7.1, Kv7.3, Kv7.4, and Kv7.5 are: 5.0mM, >30 mM, 3.0 mM, and 70 mM, respectively; (Hadley et al., 2000, Schroeder et al., 2000)), and this sensitivity is likely due to the presence of a tyrosine residue in the pore loop of the channel (Kavanaugh et al., 1991). Indeed, I used TEA at a Kv7.2-specific concentration (at 3mM) in chapter three of my thesis to investigate if the decreased spike-frequency adaptation exhibited by my *Kcnq2*-null neurons could be attributed to the lack of Kv7.2 expression.

In several of the aforementioned studies on neuronal excitability, the authors had also used Kv7 enhancers such as retigabine in order to increase Kv7 channel activity. Interestingly, the Kv7.1 subunit is completely insensitive to retigabine, and this selectivity was used to determine that retigabine binding requires the presence of a tryptophan in the S5 domain of Kv7 channels (Schenzer et al., 2005) and also that retigabine enhances Kv7 activity by stabilizing the open state and increasing the opening time of the channel (Tatulian and Brown, 2003). In addition, retigabine's selectivity for Kv7.2-7.5 over the cardiac Kv7.1 subunit also provides a practical safety advantage when used in animals. Finally, when administered to both central and peripheral neurons,

retigabine produces the opposite effect of linopirdine or XE991, and results in hyperpolarization and decreased firing rates (Passmore et al., 2003, Yue and Yaari, 2004, Gu et al., 2005, Lang et al., 2008).

Kv7 and nociception

In general, there are three major classes of nociceptors - thermal, mechanical, and polymodal, whose cell bodies are all located in the dorsal root ganglia (DRG) and the trigeminal ganglia. Both thermal (> 45^{o}C or < 5^{o}C) and mechanical nociceptors have thinly myelinated A-delta fibers, and polymodal nociceptors have unmyelinated C-fibers (Fields, 1987). As was mentioned earlier, A-delta fibers have a much higher conduction velocity compared to C-fibers, therefore when noxious stimuli are sensed, the sharp "first pain" is carried by the A-delta fibers, while the dull "second pain" is carried by the C-fibers; these signals are then passed onto projection neurons in the dorsal horn of the spinal cord (Fields, 1987). It should be noted that pain can be divided into two general classes - acute pain and persistent pain, and the latter class can further be subdivided into nociceptive and neuropathic pain. While both acute and nociceptive pain usually can be controlled with traditional analgesics, neuropathic pain, which is pain caused by a primary dysfunction of the nervous system, is much more refractory to treatments (Suzuki and Dickenson, 2000, Suzuki et al., 2002). Because DRG neurons express Kv7.2, Kv7.3, and Kv7.5 (Passmore et al., 2003), Kv7 channels are thought to play an important role in the regulation of nociception, and Kv7 enhancers represent a promising method for the treatment of pain, especially for neuropathic pain. Both chapter 2 and chapter 3 of this thesis are devoted to investigating the expression of Kv7.2, Kv7.3, and Kv7.5 in

peripheral sensory neurons. First, I used immunohistochemical techniques to determine which Kv7 subunit is expressed by the unmyelinated C-fibers and their cell bodies in the dorsal root ganglia. Next, I use the Cre-Lox system (Sauer and Henderson, 1988) to selectively knockout Kv7.2 expression in all peripheral sensory neurons. I then assess the nociceptive behaviors of the *Kcnq2*-null mice to noxious thermal and mechanical stimuli with the Hargreaves' test and the von Frey hair filament test, respectively. Finally, because previous studies have shown that the application of Kv7-blockers in peripheral sensory neurons decrease spike frequency adaptation and increase firing rate (Passmore et al., 2003, Wladyka and Kunze, 2006), I use whole cell patch-recording technique to see if *Kcnq2*-null DRG neurons have decreased spike frequency adaptation.

CHAPTER 2: $K_V7.5$ IS THE PRIMARY K_V7 SUBUNIT EXPRESSED IN C-FIBERS

INTRODUCTION

The Kv7 (KCNQ) family of K^+ channels was originally characterized by their modulation by muscarinic agonists, giving rise to the name M-currents (Brown and Adams, 1980, Wang et al., 1998). In mammals, there are five Kv7 channels, Kv7.1-7.5; all can form homomeric channels, and Kv7.3 can form heteromeric channels with either Kv7.2 or Kv7.5 (Jentsch, 2000, Schroeder et al., 2000). All Kv7 channels are slowly activated by depolarization and play an important role in maintaining normal resting membrane potential. Dominant mutations of *KCNQ2* or *KCNQ3* cause benign familial neonatal convulsions, a form of generalized epilepsy confined to the neonatal period (Singh et al., 1998). In addition, at least one *KCNQ2* mutation also causes neuromyotonia (Dedek et al., 2001), which is characterized by excessive excitability of distal motor axons.

We have previously shown that Kv7.2 and Kv7.3 channels are highly enriched in axon initial segments (AISs) and nodes of Ranvier (Devaux et al., 2004). Their localization owes to a consensus ankyrinG-binding motif in the intracellular carboxy-terminus (Pan et al., 2006). This motif is present in all vertebrate voltage-gated Na^+ channels (Nav1.1-1.9), Kv7.2, and Kv7.3, but not in Kv7.1, Kv7.4, or Kv7.5 - a unique example of convergent evolution at the molecular level (Hill et al., 2008).

Kv7.5 mRNA has been detected in the small neurons of the dorsal root ganglia (DRG) (Passmore et al., 2003), but the localizations of the Kv7.5 protein in peripheral nerves and DRG are unknown. We show here that Kv7.5 is localized in the axons of the Remak bundles (unmyelinated axons and their associated Schwann cells), including their cutaneous branches, and is not detected at nodes of Ranvier. Furthermore, small diameter DRG neurons, the origin of these unmyelinated afferents, express relatively more Kv7.5 than do large DRG neurons. Thus, Kv7.5 may be the relevant Kv7 channel expressed by C-fibers.

MATERIALS AND METHODS

Animal and tissue sections

All procedures involving rodents were approved by the Institutional Animal Care and Use Committee of the University of Pennsylvania. 8-10 weeks old adult Sprague Dawley rats (n=3) or C57BL/6 mice (n=3) were anesthetized with ketamine/xylazine mix and killed by decapitation. Sciatic nerves, dorsal root ganglia (from L4-L6 spinal levels), and skin (both hairy and glabrous) were dissected, and quickly embedded in OCT cooled in an acetone/dry ice slurry. The sciatic nerve fibers were teased apart with fine needles, mounted on SuperFrost Plus glass slides (Fisher Scientific, Pittsburgh, PA), dried overnight, and stored at -20^{o}C. Ten μm thick cryostat sections were thaw-mounted onto Superfrost slides, and stored at -20^{o}C.

Immunohistochemistry

Teased fibers and OCT sections were immersed in -20^{o}C acetone for 10 minutes, rinsed in PBS, blocked at room temperature for one hour in PBS containing 5% fish skin gelatin and 0.5% Triton X-100, and incubated overnight at 4^{o}C with various combination of primary antibodies diluted in blocking solution. The slides were washed with PBS, incubated with the appropriate FITC-, TRITC-, and Cy5-conjugated donkey cross-affinity-purified secondary antibodies (Jackson ImmunoResearch, 1:200) at room temperature for one hour, washed with PBS, counterstained with 4',6-diamidino-2-phenylindole dihydrochloride (DAPI; Invitrogen), mounted with Vectashield (Vector Laboratories), examined by epifluorescence on a Leica DMR light microscope with a cooled Hamamatsu camera under the control of Openlab software (Openlab, Improvision). When necessary, digital images were cropped and RGB histogram adjusted to fill entire tonal range using Photoshop (Adobe).

Antibody Characterization

Please see Table 2-1 for a summary of all primary antibodies used. The KCNQ2N antiserum (Cooper et al., 2001) stained nodes and AISs of teased nerve fibers in an identical pattern as previously shown (Devaux et al., 2004, Pan et al., 2006) In addition, using the Lipofectamine 2000 kit (Invitrogen) with method as previously described (Rasmussen et al., 2007), the KCNQ2N antiserum positively stained Hela cells that were transiently transfected with the cDNA encoding human Kv7.2 (kindly provided by Dr. Edward Cooper), but did not stain Hela cells transfected with human Kv7.5 cDNA

(kindly provided by Dr. Thomas Jentsch). Finally, the nodal staining by the KCNQ2N antiserum was abolished in tissues of a Kv7.2 conditionally-null mouse, but was preserved in tissues of a wild-type littermate. The KCNQ3C antiserum also stained nodes in an identical pattern as previously described (Pan et al., 2006).

The sequences of immunogen targeted by the KCNQ5 antiserum (Chemicon AB5599) and the Kv7.5 antiserum (Chemicon AB9792) are shown in Figure 2-1. Both antisera were able to positively label Hela cells transfected by the Kv7.5 cDNA but did not label Hela cells transfected by the Kv7.2 cDNA. In addition, peptide-blocking was performed, whereby slides of rat sciatic nerves and DRG were stained according to the above protocol, except that the AB5599 and the AB9792 Kv7.5 antisera (along with the panNav antibody) were preincubated with the purified peptide for the AB9792 antiserum (10 μg peptide per 1 μg of antibody in 100μl for 12 hours at 37°C. The mixtures were then centrifuged for 15 minutes at 13,000 rpm, and the supernatant was used in the primary antibody step); the blocking experiment was repeated three times, and when images were taken with the microscope, identical exposure time was used for all blocking conditions. Pre-incubation with immunogen of AB9792 was able to diminish AB9792 staining of all tissues, but did not change AB5599's staining.

The panNav monoclonal antibody targets multiple voltage-gated Na^+ channels, and has previously been shown to specifically stain the AISs and nodes of a wide range of nervous tissues (Rasband et al., 2001, Devaux et al., 2004, Pan et al., 2006) in our stainings it recognized the nodes of both rat and mouse sciatic nerves, as expected.

The TrkA antiserum has been shown by the manufacturer to be able to detect rat TrkA in both direct ELISAs and Western blots, with less than 1% cross-reactivity with recombinant mouse TrkB and TrkC. It has been previously shown to label primarily small and medium sized rat DRG cells (Averill et al., 1995), and in our immunostaining of rat DRG sections the TrkA antiserum labeled primarily small and medium size neurons as well.

IB4 lectin is derived from *Bandeiraea simplicifolia* and binds to cells surface glycoprotein of GDNF-sensitive small diameter DRG neurons (Kashiba et al., 2001). In our staining we used biotin-conjugated IB4 lectin, and we observed that it preferentially labeled small diameter DRG neurons, as had been shown previously (Ivanusic, 2009).

The MAG antiserum recognizes the extracellular domain of rat myelin-associated glycoprotein, and was able to recognize rat MAG in direct ELISAs and Western blots according to the manufacturer's datasheet. In our evaluation of immunohistochemical staining, it strongly labeled myelin shealth, as expected.

The NFH monoclonal antibody, recognized neurofilament heavy subunits as was previously shown both by ELISA, and also by the peroxidase-antiperoxidase method to specifically stained axons and neurons in human cerebellum sections (Lee et al., 1982). In our immunostaining of rat sciatic nerve it labeled axons, but not myelin sheath.

The glial fibrillary acidic protein (GFAP) antiserum recognizes a single band of 51 kDa band on immunoblot of cytoskeleton-enriched rat spinal cord lysate, and has been shown to stain glial elements and astrocytes (Lee et al., 1984). When we stained rat sciatic nerve, the antibody labeled non-myelinated Schwann cells, consistent with other

studies using anti-GFAP antisera (Jessen et al., 1985, Jessen et al., 1990, Cheng and Zochodne, 2002).

Kv7.5 Quantification

DRG sections from three rats were triple-stained with Kv7.5 AB5599 antiserum, IB4 lectin, and TrkA antiserum, and imaged with a Leica Sp2 confocal microscope system. The embedding, sectioning, staining, and imaging were done in parallel. Intensities of the three secondary antibodies specific to each of the primary antisera were measured by using NIH ImageJ, and cytoplasmic intensity were calculated by subtracting the nucleus intensity from the whole cell intensity. Data collected in Microsoft Excel, and the Student's t-tests were performed using SAS 9.2 (SAS). For the comparison between IB4 and TrkA staining, a threshold of 20 was selected as the cutoff for clear positive staining.

To quantify mRNA level of Kv7.5, 3 samples of total RNA isolated from young adult rat sciatic nerve and DRG by CsCl2 gradient centrifugation (Chirgwin et al., 1979) was amplified and analyzed with the SuperScript One-Step RT-PCR with Platinum Taq system (Invitrogen 10928-042) according to manufacturer protocol. NCBI Primer-BLAST using known *Rattus norvegicus* mRNA sequence was used to design primer sets complementary to rat KV7.5 (forward, ACGTCACCACCTGCCTTGTTG; reverse, TGTAAGTTCAGTTCCTCTGTCGATCT) and myelin-associated glycoprotein (MAG; forward, AGCCACCGCCTTCAACCTGT; reverse, TGGCAAAGGCGACCACAGCA). To rule out genomic DNA contamination, 2 units of Platinum Taq DNA polymerase

(Invitrogen 10966-034) were used instead of the RT/Platinum Taq Mix in the reaction. The RT-PCR of the sciatic nerve total RNA sample was repeated 3 times.

Axotomy was performed on anesthetized (60 mg/kg of ketamine, 7.5 mg/kg of xylazine) 30-day-old Sprague Dawley rats (n=3). The sciatic nerve was exposed at the sciatic notch and transected with iridectomy scissors, and the skin incision was closed with wound clips. Four days after the surgery the animals were euthanized, and the sciatic nerve segment distal to the transection site, as well as the corresponding contralateral sciatic nerve segment, were dissected and teased onto slides, and were immunostained with previously described antisera. For image recording, identical exposure times were used for both the transected and contralateral teased fibers.

RESULTS

Kv7.5 is localized to Remak bundles

We immunostained unfixed teased fibers from rat sciatic nerves for Kv7.2 or Kv7.5, combined with a mouse monoclonal antibody against voltage-gated Na^+ channels (panNav). As shown in Figure 2-2, nodes of Ranvier were strongly Kv7.2- and panNav-positive, as we have previously shown (Devaux et al., 2004, Pan et al., 2006). Remak bundles were panNav-positive, but were not detectably labeled by the Kv7.2 antiserum. The Kv7.5 antiserum (Chemicon AB9792) produced the reciprocal result: nodes were not labeled, whereas Remak bundles were Kv7.5- (and panNav-) positive. Another Kv7.5 antiserum produced the same staining pattern (Chemicon AB5599; data not shown).

Because Kv7.5 can form heteromeric channels with Kv7.3 *in vitro* (Schroeder et al., 2000), we investigated whether Kv7.3 is also present in Remak bundles. The KCNQ3C antiserum we have used does not label rat tissues well (due to the possibility that targeted residues of KCNQ3C is not conserved in rat; see Pan et al. (2006)), so we immunostained unfixed mouse teased fibers with the Kv7.2, Kv7.3, or Kv7.5 (Chemicon AB5599) antisera, combined with the panNav mouse monoclonal antibody. Similar to the above results, the Kv7.2 and Kv7.3 antisera labeled nodes but not the Remak bundles (Figure 2-3), while the Kv7.5 antiserum produced the opposite result, labeling the Remak bundles but not the nodes. Therefore, Kv7.5 likely forms homomeric channels, but not heteromeric channels with Kv7.3, in Remak bundles. In a separate experiment, the Kv7.2 antiserum was used on a *Kcnq2*-null mouse, and the Kv7.2 staining of the nodes was abolished (with intact Kv7.3 nodal staining), thereby demonstrating the specificity of our Kv7.2 antiserum (Chapter 3).

The Chemicon AB9792 and AB5599 Kv7.5 antisera also produced granular staining of myelinated fibers (Figure 1, chevrons). Specifically, much of the granular staining lies outside of the neurofilament-positive axons, but resides with the myelin sheaths (Figure 2-4). These two Kv7.5 antisera were raised against partially overlapping sequences of the intracellular N-terminus; this entire region shares little homology with Kv7.2. To ascertain their specificity, HeLa cells were transiently transfected to express either Kv7.2 or Kv7.5. Cells expressing Kv7.5, but not Kv7.2, were strongly labeled by both Kv7.5 antisera. Conversely, cells expressing Kv7.2, but not Kv7.5, were robustly labeled with the Kv7.2 antiserum but not by either Kv7.5 antisera (Figure 2-5).

To determine whether the Kv7.5 expression in the Remak bundles originates from axons or the surrounding Schwann cells, we immunostained teased fibers from the distal nerve stump of sciatic nerves 4 days post-transection. At this time, axons distal to the injury have degenerated, while their associated Schwann cells persist (Griffin and Thompson, 2008). Denervated Remak bundles were not panNav- or Kv7.5-positive, whereas Remak Schwann cells were GFAP-positive (Figure 2-6). These results support the idea that Remak axons and not Remak Schwann cells express Kv7.5. While there exist the possibility that the disappearance of Kv7.5 staining is due to a loss of its expression from the Schwann cells rather than from the axons after nerve injury, we feel that this is a less likely explanation given the concurrent loss of panNav staining with the retention of robust GFAP staining, suggesting the loss of axons and the continued presence of its associated Schwann cells. In addition, as we will show, expression of Kv7.5 by the small diameter DRG neurons also indicate that the loss of Kv7.5 staining is from the axons, since they originate from these DRG neurons. Finally, we performed a blocking experiment, utilizing the purified immunogen for the AB9792 antiserum. As shown in Figure 2-7, pre-incubation with the peptide eliminated the labeling of Remak bundles, and seemed to reduce granular staining of myelinated axons.

We were suspicious that the granular staining of Kv7.5 represents background staining, as we are unaware of other antigens that are localized in this pattern. To investigate this, we performed RT-PCR on RNA samples prepared from rat sciatic nerve and DRG, with primer pairs for rat Kv7.5 and MAG (Figure 2-8). Both the MAG and the Kv7.5 primers amplified the correctly sized products in both the sciatic nerve and the DRG RNA samples. In order to rule out the possibility of genomic DNA contamination

in the RNA samples, we substituted DNA polymerase in place of the RT-PCR polymerase mix. In this case, the Kv7.5 primers did not amplify a product in either the sciatic nerve or the DRG sample, but it did amplify the expected size product from a DNA sample (result not shown). Thus, we cannot rule out the possibility that the granular staining of Kv7.5 of myelin sheaths is authentic.

Small DRG neurons express Kv7.5

The largest and smallest axons in peripheral nerves originate from the largest and smallest neurons in DRG, respectively (Perry et al., 1991, Lozeron et al., 2004). To determine which neurons expressed Kv7.2 and Kv7.5, we immuno-stained unfixed sections of rat dorsal root ganglia (Figure 2-9). The Kv7.2 antiserum predominantly labeled large diameter neurons (which were largely panNav-negative), including their stem processes, which have many of the molecular features of nodes (Figure 2-10). In contrast, the AB9792/Kv7.5 antiserum predominately labeled the smaller neurons, which were mostly panNav-positive. The other Kv7.5 antiserum (AB5599) gave similar results (data not shown). To quantify these results, we used NIH ImageJ to calculate the mean Kv7.5 (AB9792) immuno-fluorescence for individual DRG neurons imaged by confocal microscopy. As shown in Figure 2-11, for three different rats, there is a negative correlation between cell size and Kv7.5 labeling, with the majority of the highly labeled cells (fluorescence intensity >20) having small diameters. Similar to the sciatic nerve, pre-incubation with the cognate peptide greatly diminished the staining of neurons by AB9792 (Figure 2-12).

Small DRG neurons can be divided into either NGF sensitive neurons that express TrkA (Averill et al., 1995) and the GDNF sensitive neurons that express glycoprotein that can bind to IB4 (Kashiba et al., 2001), and because both of these neurons give off unmyelinated C fibers, both IB4 and TrkA serve as neurochemical markers of nociceptive neurons (Averill et al., 1995, Molliver et al., 1997, Kashiba et al., 2001, Priestley et al., 2002). To investigate this issue further, we triple-labeled sections of DRG from three individual rats for Kv7.5, IB4, and TrkA (Figure 2-13). As expected, almost all of the small DRG neurons were either IB4- or TrkA-positive. Of the small neurons (diameter <30 μm), a similarly high proportion of IB4-positive and TrkA-positive were Kv7.5-positive neurons (Table 2-2). In contrast, all of the large diameter, Kv7.2-positive neurons were IB4-negative, and a few were TrkA-positive. Taken together, these data show that Kv7.5 is mainly expressed by small diameter neurons.

Peripheral axons of cutaneous nociceptors express Kv7.5

Because Kv7 channel enhancers have local effects in the skin (Passmore et al., 2003), we wished to determine whether cutaneous afferents express Kv7.5. We immuno-stained unfixed sections of glabrous and hairy skin from rats for Kv7.2 or Kv7.5 and panNav. As shown in Figure 2-14, the panNav-positive unmyelinated axons were predominately Kv7.5-positive, and almost all were Kv7.2-negative. Pre-incubation of Kv7.5 antiserum with its cognate antigen greatly diminished the labeling of unmyelinated axons (Figure 2-15).

DISCUSSION

In this present study, we found that C-fibers, including their cutaneous branches, express Kv7.5 and not Kv7.2 or Kv7.3. Small diameter DRG neurons also preferentially express Kv7.5 along with either IB4 or TrkA. Thus, Kv7.5 is the predominant Kv7 channel expressed by nociceptors, from their cell bodies to their terminals. In contrast to Kv7.2 and Kv7.3, Kv7.5 expression was not found at nodes of Ranvier. Although Kv7.5 subunits can form heteromeric channels with the Kv7.3 subunits (Schroeder et al., 2000), Kv7.3 was not co-localized with Kv7.5 in C-fibers, suggesting that the Kv7.5 forms homomeric channels in C-fibers.

Although a previous study found that cultured DRG neurons express Kv7.2, Kv7.3, and/or Kv7.5 (Passmore et al., 2003), the authors did not emphasize that Kv7.5 is mainly localized to small diameter neurons as we report here. However, they did show that the M-current was the dominant subthreshold sustained current in small sensory neurons, and that many were capsaicin-sensitive, confirming that they are nociceptors (Passmore et al., 2003). This observation is in agreement with our finding that the Kv7.5-positive small diameter DRG neurons are also positive for either IB4 or TrkA, both neurochemical markers of nociceptors. Interestingly, several studies of nerve function suggest that C-fibers and their terminals are refractory to the M-channel blocker XE991 (Lang et al., 2008, Roza and Lopez-Garcia, 2008), while A-fibers are sensitive to inhibition (Schwarz et al., 2006, Brown and Passmore, 2009). Since the IC_{50} for XE991 inhibition is much higher for Kv7.5 (50-70μM; Schroeder et al. (2000)) than it is for Kv7.2/7.3 subunits (0.6μM; Wang et al. (2000)), the preferential expression of Kv7.5 by

C-fibers may explain its insensitivity to XE991. Large neurons, in contrast, were IB4-negative and Kv7.2-positive, consistent with a previous study showing that IB4-negative neurons had a TEA-sensitive Kv current (with properties of slow kinetics and no inactivation) that was inhibited by 25 mM TEA (Vydyanathan et al., 2005), which should block Kv7.2 but not Kv7.5 (Hadley et al., 2000, Schroeder et al., 2000, Hadley et al., 2003). Our results contradict a recent report that Kv7.2-immunoreactivity is predominately localized to small sensory neurons and abundantly expressed in sciatic nerve axons (Rose et al., 2011). These findings are at odds with several reports that Kv7.2 is localized to nodes (Devaux et al., 2004, Pan et al., 2006, Schwarz et al., 2006) and our finding that large and not small sensory neurons are Kv7.2-positive. We have, furthermore, found that Kv7.2-immunoreactivity is lost in both nodes and large diameter DRG neurons from a Kv7.2-conditional null mouse (chapter 3), demonstrating the authenticity of our results. Taken together, different populations of sensory neurons express different levels of Kv7.2 and Kv7.5 (and likely Kv7.3); these channels likely affect their electrophysiological characteristics, akin to the differential expression of different voltage-gated Na channels in different kinds of sensory neurons (Waxman et al., 1999).

Whether Kv7.5 functions in the conduction of normal C-fibers remains uncertain. Devaux et al. (2004) showed that retigabine [a Kv7-specific enhancer (Lerche et al., 2000, Brueggemann et al., 2007)] mildly slows the conduction velocity of myelinated axons; they did not investigate C-fibers. In biopsied human sural nerves, retigabine increased the membrane threshold and modified the post spike recovery cycle of C-fibers (Lang et al., 2008), but these nerves were recovered from patients suffering from

neuropathy or peripheral vascular disease. However, Roza and Lopez-Garcia (2008) reported that retigabine had no effect on C-fiber conduction in mouse saphenous nerve, but they only used one type of stimulus (a von Frey probe) and had a small sample size (5 units). These results are not definitive in our opinion.

In contrast, Kv7 enhancers have substantial effects in rodent models of neuropathic/inflammatory pain. Kv7 enhancers (retigabine or flupirtine) reduce the excitability of injured axons to both mechanical and chemical stimuli (Passmore et al., 2003, Roza and Lopez-Garcia, 2008), as well as the behavioral responses of rodents following nerve ligation or cutaneous injections of irritants (Blackburn-Munro and Jensen, 2003, Passmore et al., 2003, Dost et al., 2004, Nielsen et al., 2004). Because these effects can be blocked by co-administrating Kv7 blockers, they most likely stem from enhanced Kv7 activity. Our finding that Kv7.5 is the main Kv7 subunit expressed by C-fibers, focuses attention on the possible role of Kv7.5 in these models of pain, and the expression of Kv7.5 during the development of neuropathic pain warrants further investigation.

The ability of G-protein-coupled receptors (GPCRs) to modulate Kv7 channels gives rise to the possibility that GPCRs expressed by nociceptive axons modulate neuropathic/inflammatory pain. Local injection of inflammatory mediators that bind to GPCRs, such as bradykinin and certain proteases, can cause pain, presumably through the excitation and sensitization of the peripheral terminals of nociceptors (Linley et al., 2010). In small cultured DRG neurons, bradykinin (via the B_2R receptor) increases intracellular Ca^{2+}, which inhibits M-currents (Liu et al., 2010); *in vitro* study using CHO

cells specifically shows intracellular Ca^{2+} only inhibits Kv7.2, Kv7.4, and Kv7.5 subunits (Gamper et al., 2005). Furthermore, injecting bradykinin into rat hind paws produced nocifensive behavior that is reversed by retigabine, suggesting that bradykinin induces acute pain, at least in part, through its modulation of Kv7 channels (Liu et al., 2010). Similarly, ligands for protease-activated receptor 2 (PAR-2) inhibit M-current in small cultured DRG neurons by increasing intracellular Ca^{2+} (Linley et al., 2008). Injecting PAR-2 agonists into rat hind paws produce nocifensive behavior similar to that produced by Kv7 blocker (XE991) injection, and the simultaneous injection of both compounds does not produce additive pain response, indicating that PAR-2 agonists act primarily through the Kv7 channels. Finally, beta-alanine, the ligand for MrgD receptors, inhibits the M-current in cultured IB4-positive sensory neurons (Crozier et al., 2007); the electrophysiological effects of beta-alanine are absent in *Mrgprd*-null sensory neurons, but the M-current was not measured (Rau et al., 2009). Taken together, the endogenous ligands of GPCRs may decrease the M-current of nociceptors, which we have reason to believe is largely generated by Kv7.5 channels, and lead to increased nociception.

Acknowledgments. We thank Drs. Edward Cooper, Virginia Lee, Thomas Jentsch, and Alvaro-Villarroel for the cDNAs and antisera.

Figure 2-1

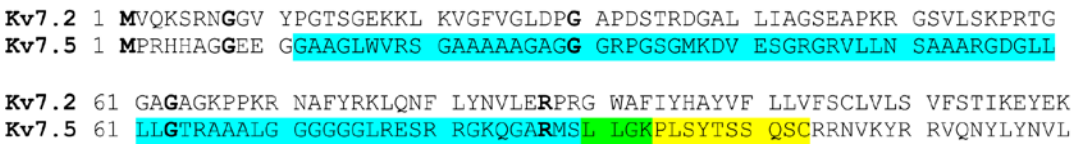

Figure 2-1: Primary structure of Kv7.2 and Kv7.5 (*Rattus norvegicus*).

The first 120 amino acids of Kv7.2 (NCBI Reference Sequence: NP_001153611.1) and Kv7.5 (NCBI Reference Sequence: NP_034741.2) are aligned with NCBI COBALT. Residues that are identical between Kv7.2 and Kv7.5 are shown in bold. The sequences targeted by the Chemicon AB5599 antibody are highlighted in blue (Caminos et al., 2007), while the immunogen for the Chemicon AB9792 antibody is highlighted in yellow (information from Chemicon). The region common between the two antibodies is shown on a green background.

Figure 2-2

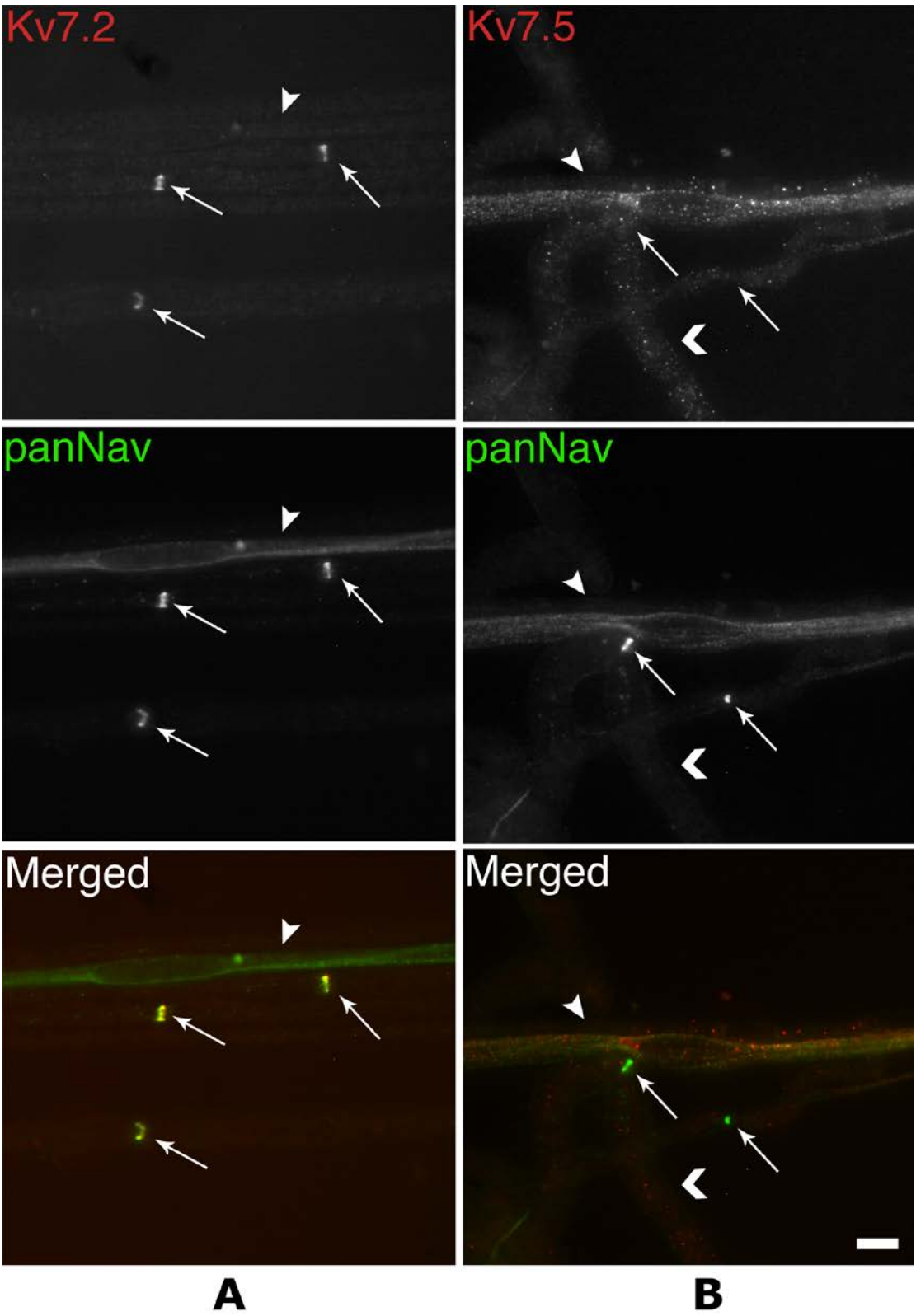

Figure 2-2: Remak bundles, but not nodes, express Kv7.5.

These are digital images of unfixed teased fibers, double-labeled for either Kv7.2 or Kv7.5 (Chemicon AB9792; red) and voltage-gated sodium channels (panNav; green). In column A, note that Kv7.2 and panNav are co-localized at nodes (arrows), but Kv7.2 is not localized in a Remak bundle (arrowhead). In column B, Kv7.5 is not detected at nodes (arrows), but is expressed in a Remak bundle (arrowhead), and as a granular staining on myelinated axons (chevrons). Scale bar: 10 μm.

Figure 2-3

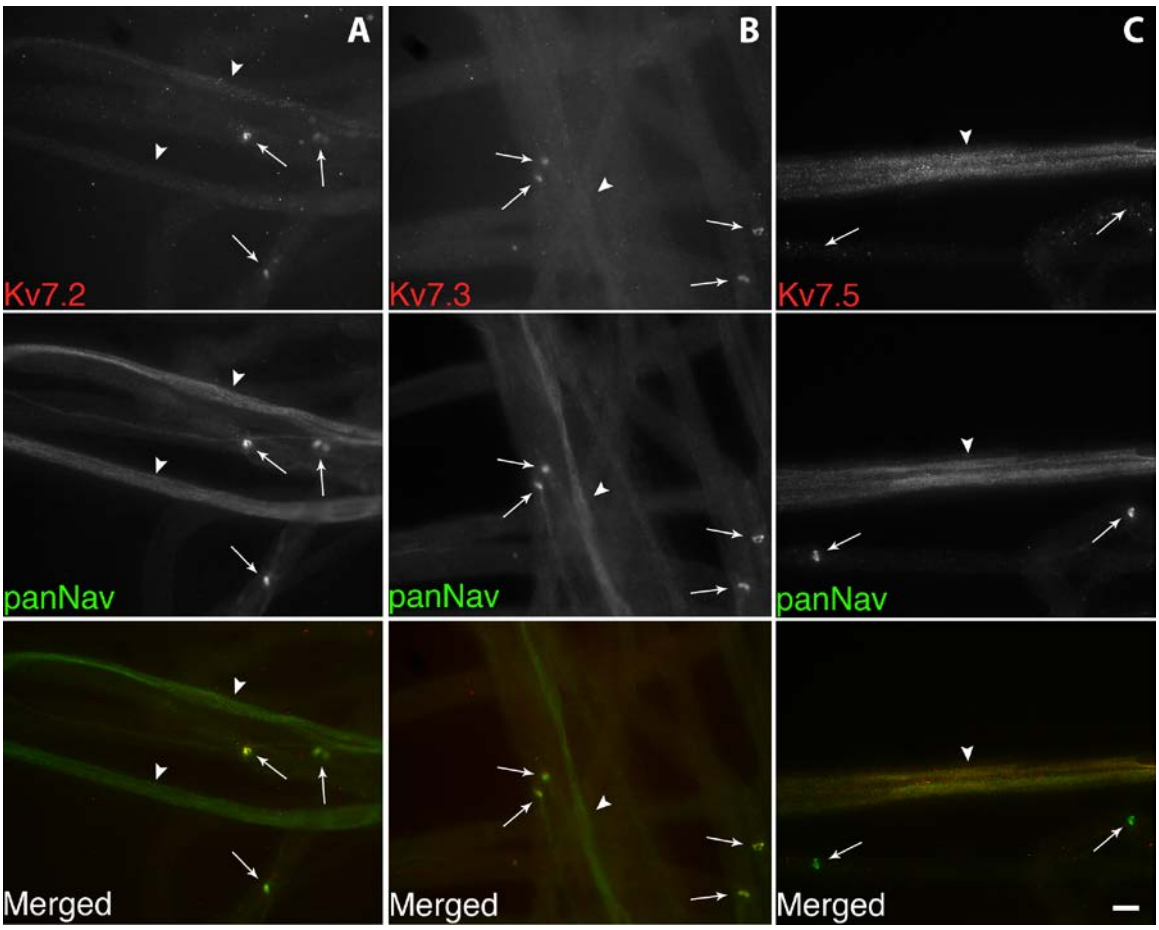

Figure 2-3: Remak bundles do not express Kv7.3.

These are digital images of unfixed mouse teased nerves, double-labeled for either Kv7.2, Kv7.3, or Kv7.5 (AB5599; red) and voltage-gated sodium channels (panNav; green). In columns A and B, note that Kv7.2 and Kv7.3 are co-localized with panNa_v at nodes (arrows), but not in Remak bundles (arrowheads). In column C, the Kv7.5 antiserum labels Remak bundles (arrowheads) but not nodes (arrow). Scale bar: 10 μm.

Figure 2-4

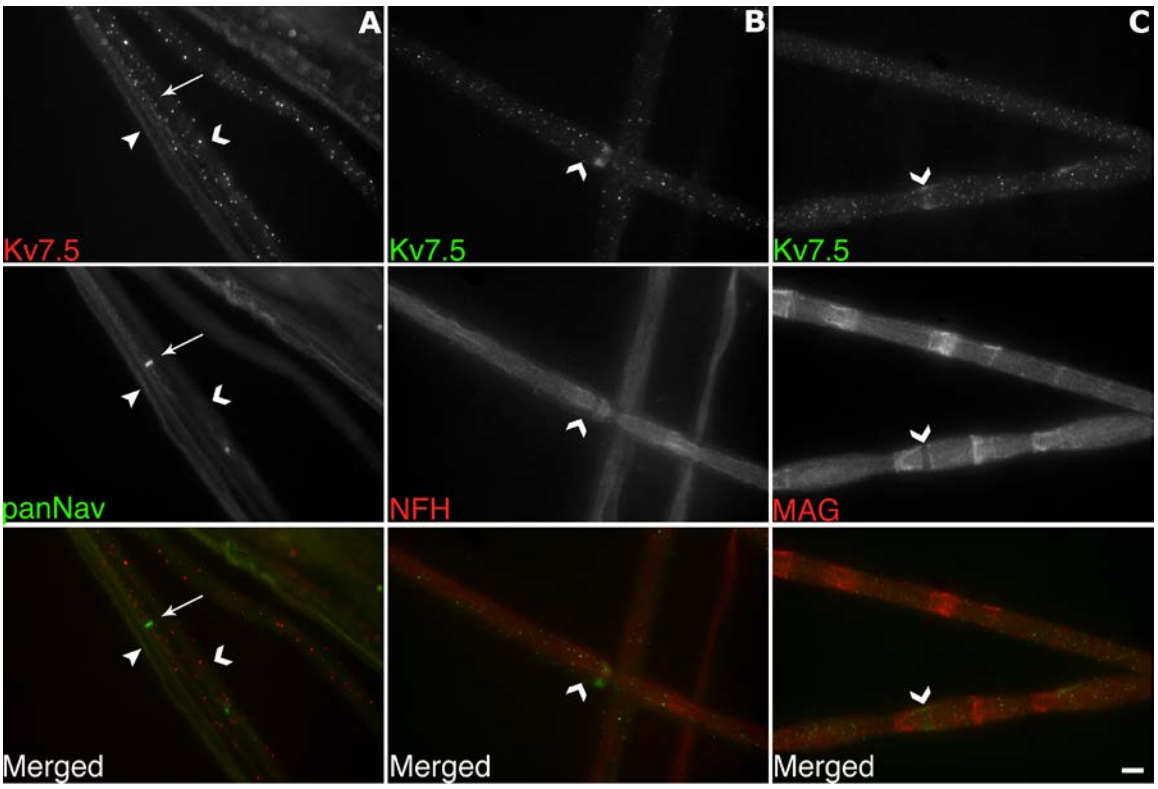

Figure 2-4: Granular staining of myelin sheaths with the AB9792 Kv7.5 antiserum.

These are unfixed teased fibers, double-labeled for Kv7.5 (red) and panNav (green), neurofilament heavy (NFH, red), or myelin-associated glycoprotein (MAG, red), as indicated. Note that the granular staining is associated with myelinated axons (chevrons), as shown by the their co-localization with MAG, but not with axons (NFH staining) or Remak bundles (arrowheads). The arrows indicate a node. Scale bar 10 μm.

Figure 2-5

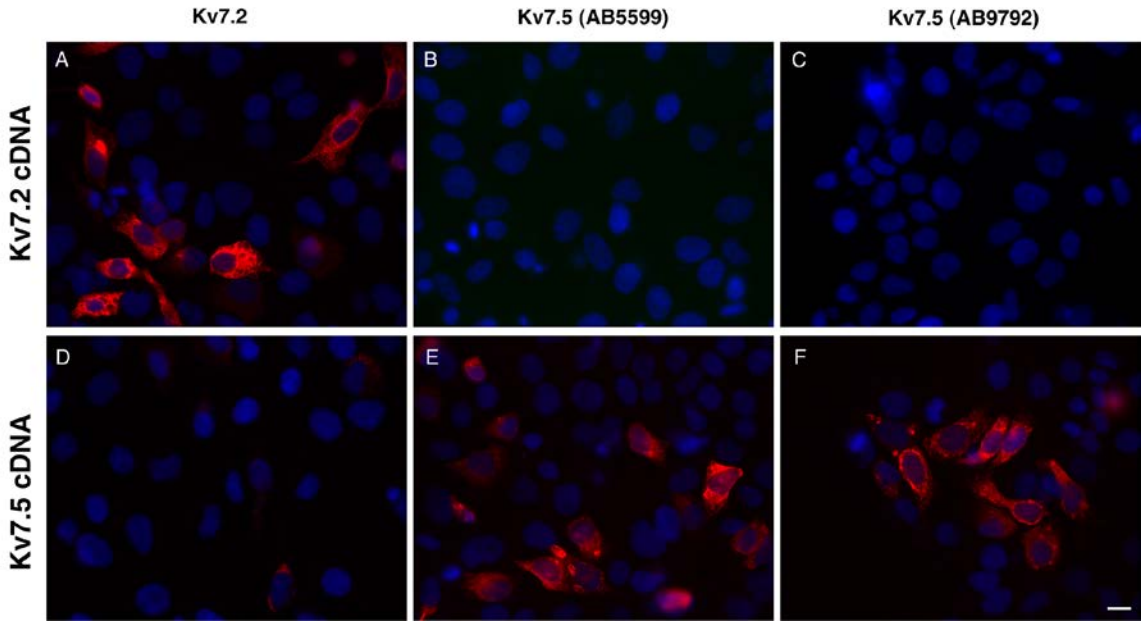

Figure 2-5: AB5599 and AB9792 antisera recognize Kv7.5 but not Kv7.2.

These are images of HeLa cells transiently transfected to express human Kv7.2 or Kv7.5, labeled with the indicated antiserum and counterstained with DAPI. Note that the Kv7.2 antiserum (A) labels cells expressing Kv7.2 and not Kv7.5, and that the AB5599 (B) and AB9792 (C) antisera label cells expressing Kv7.5 but not Kv7.2. Scale bar: 20 μm.

Figure 2-6

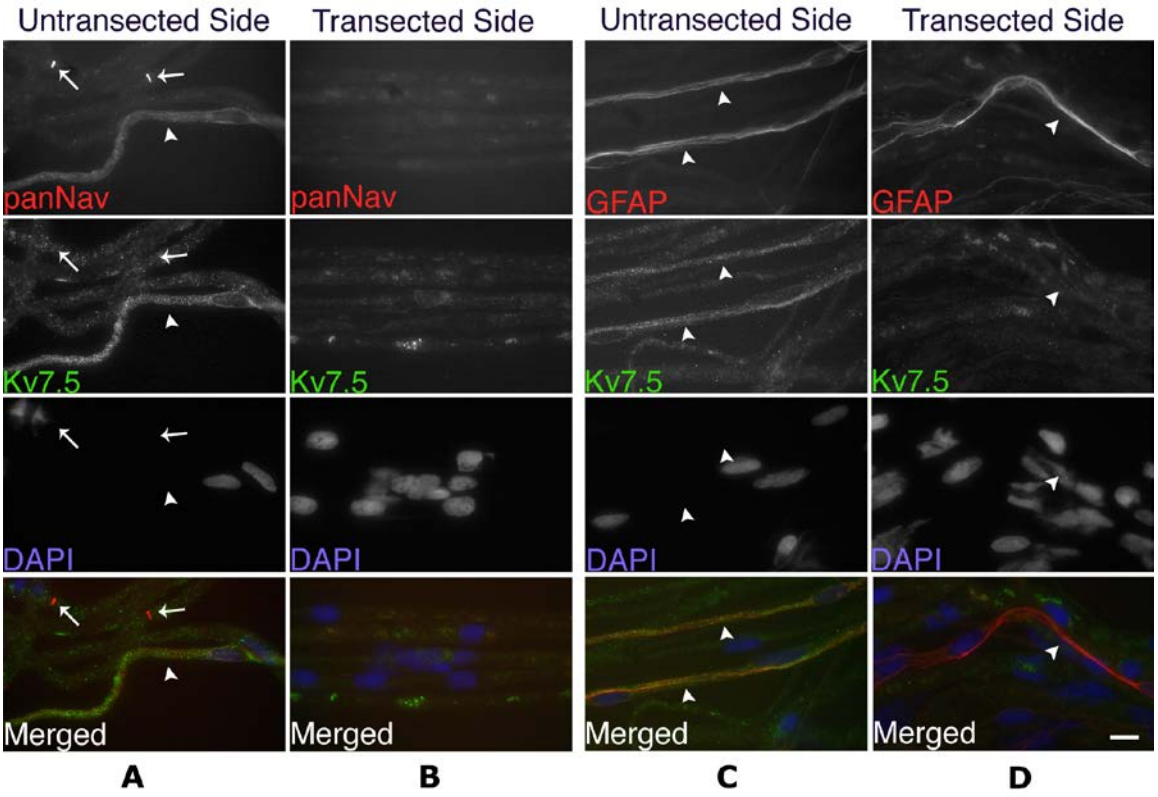
Untransected Side
Transected Side
Untransected Side
Transected Side
panNav
panNav
GFAP
GFAP
Kv7.5
Kv7.5
Kv7.5
Kv7.5
DAPI
DAPI
DAPI
DAPI
Merged
Merged
Merged
Merged
A
B
C
D

Figure 2-6: Axotomy abolishes Kv7.5 expression.

These are digital images of unfixed rat teased fibers, taken from the nerve segment distal to the lesion (columns B and D) 4 days post-transection, or the corresponding segment of an unlesioned nerve (columns A and C). The fibers were double-labeled for Kv7.5 (Chemicon AB9792; green) and either voltage-gated sodium channels (panNav; red) or glial fibrillary acidic protein (GFAP; red, labels Remak Schwann cells), and counterstained with DAPI to visualize nuclei (blue). Note that panNav-immunoreactivity is associated with nodes (arrows) and a Remak bundle (arrowhead), which is lost after axotomy (columns A and B), and that Kv7.5-immunoreactivity in Remak bundles (arrowheads) is lost after axotomy, whereas GFAP-immunoreactivity persists. Scale bar: 20 μm.

Figure 2-7

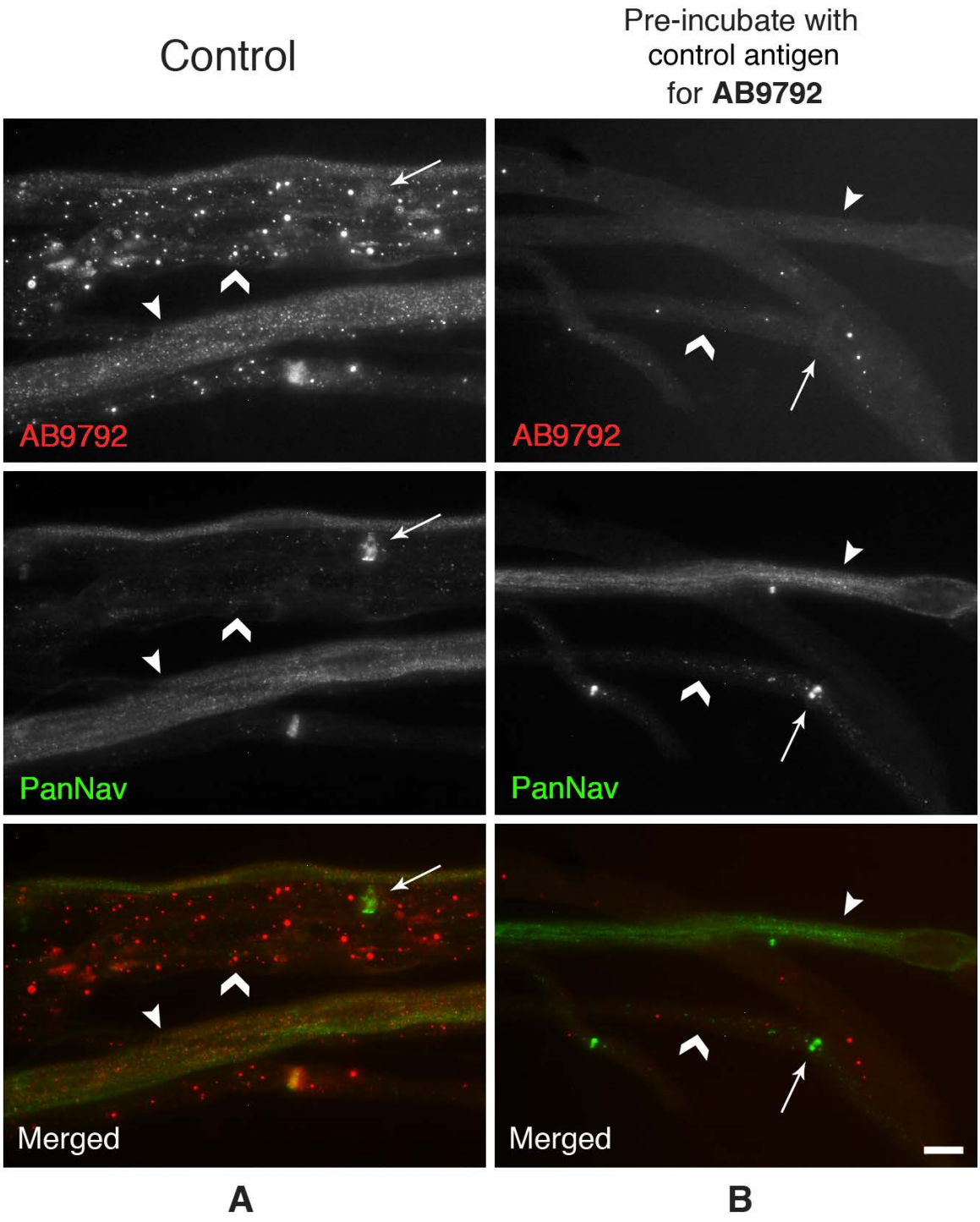
Control
Pre-incubate with control antigen for AB9792
AB9792
AB9792
PanNav
PanNav
Merged
Merged
A
B

Figure 2-7: Cognate antigen reduces immunostaining of Remak bundles with Kv7.5 antiserum AB9792.

These are images of unfixed teased fibers that were double-labeled for Kv7.5 (AB9792; red) and panNav (green), as indicated. The images were exposed for the same amount of time to facilitate direct comparison. Compared to teased fibers labeled with the AB9792 antiserum alone (column A), pre-incubation with the control antigen (column B) reduced the granular staining of myelinated axons (chevrons) and abolished the staining of Remak bundles (arrowheads), which are also labeled by the panNav antibody. Arrows indicate nodes. Scale bar: 10 μm.

Figure 2-8

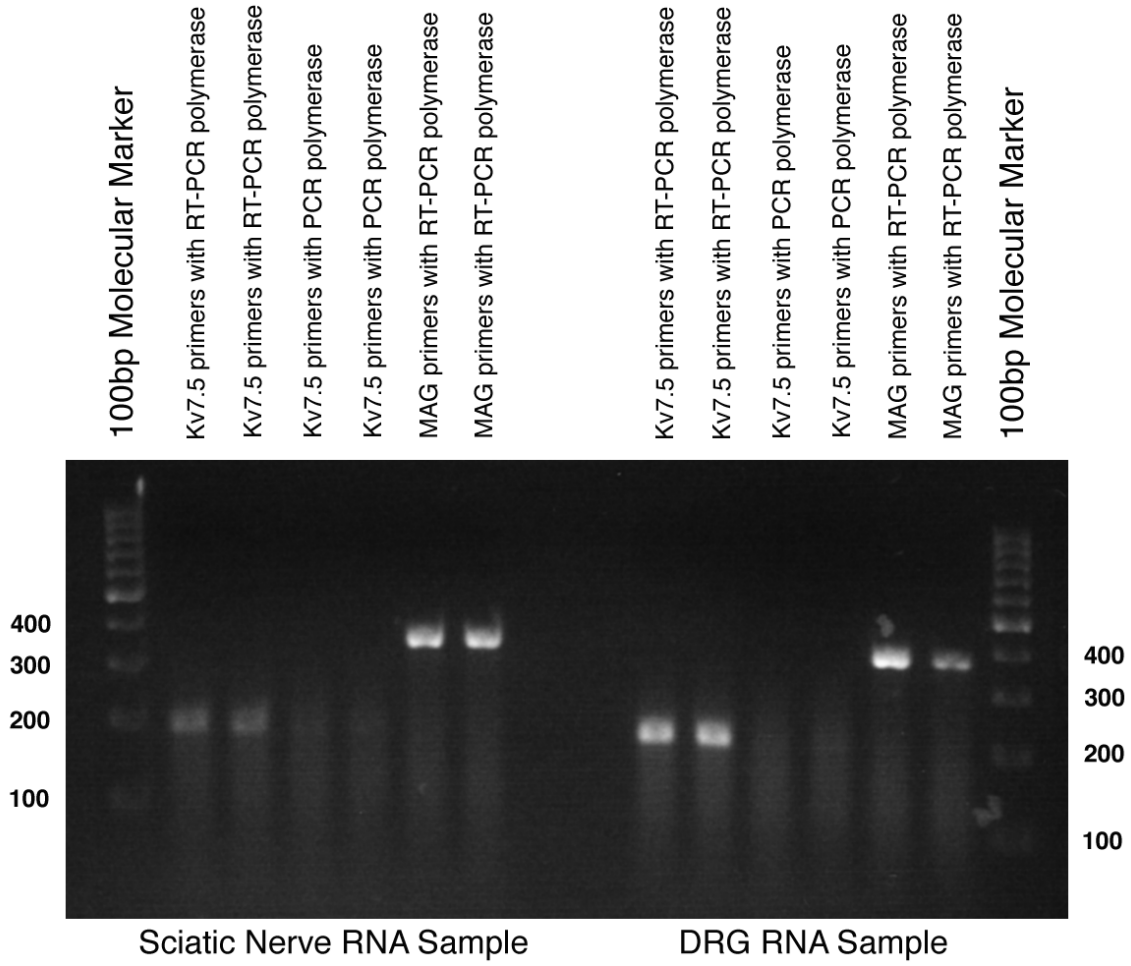
100bp Molecular Marker
Kv7.5 primers with RT-PCR polymerase
Kv7.5 primers with RT-PCR polymerase
Kv7.5 primers with PCR polymerase
Kv7.5 primers with PCR polymerase
MAG primers with RT-PCR polymerase
MAG primers with RT-PCR polymerase
Kv7.5 primers with RT-PCR polymerase
Kv7.5 primers with RT-PCR polymerase
Kv7.5 primers with PCR polymerase
Kv7.5 primers with PCR polymerase
MAG primers with RT-PCR polymerase
MAG primers with RT-PCR polymerase
100bp Molecular Marker
400
300
200
100
400
300
200
100
Sciatic Nerve RNA Sample
DRG RNA Sample

Figure 2-8: RT-PCR expression analysis of rat sciatic nerve and DRG RNA.

Total RNA was isolated from adult rat tissues, duplicate samples were subjected to RT-PCR with the indicated primers and polymerases, and the reaction products were separated by gel electrophoresis. A ~200 bp band, corresponding to the predicted size of the Kv7.5 mRNA sequence, was detected in both the DRG and the sciatic nerve RNA samples. When PCR polymerase is used instead of RT-PCR polymerase, the Kv7.5 primers did not amplify a similarly sized product from the RNA samples, indicating that they were not contaminated by genomic DNA. A ~370 bp band, corresponding to the predicted size of MAG mRNA, was present in both RNA samples. Molecular markers are located in the first and last lanes (in 100 bps).

Figure 2-9

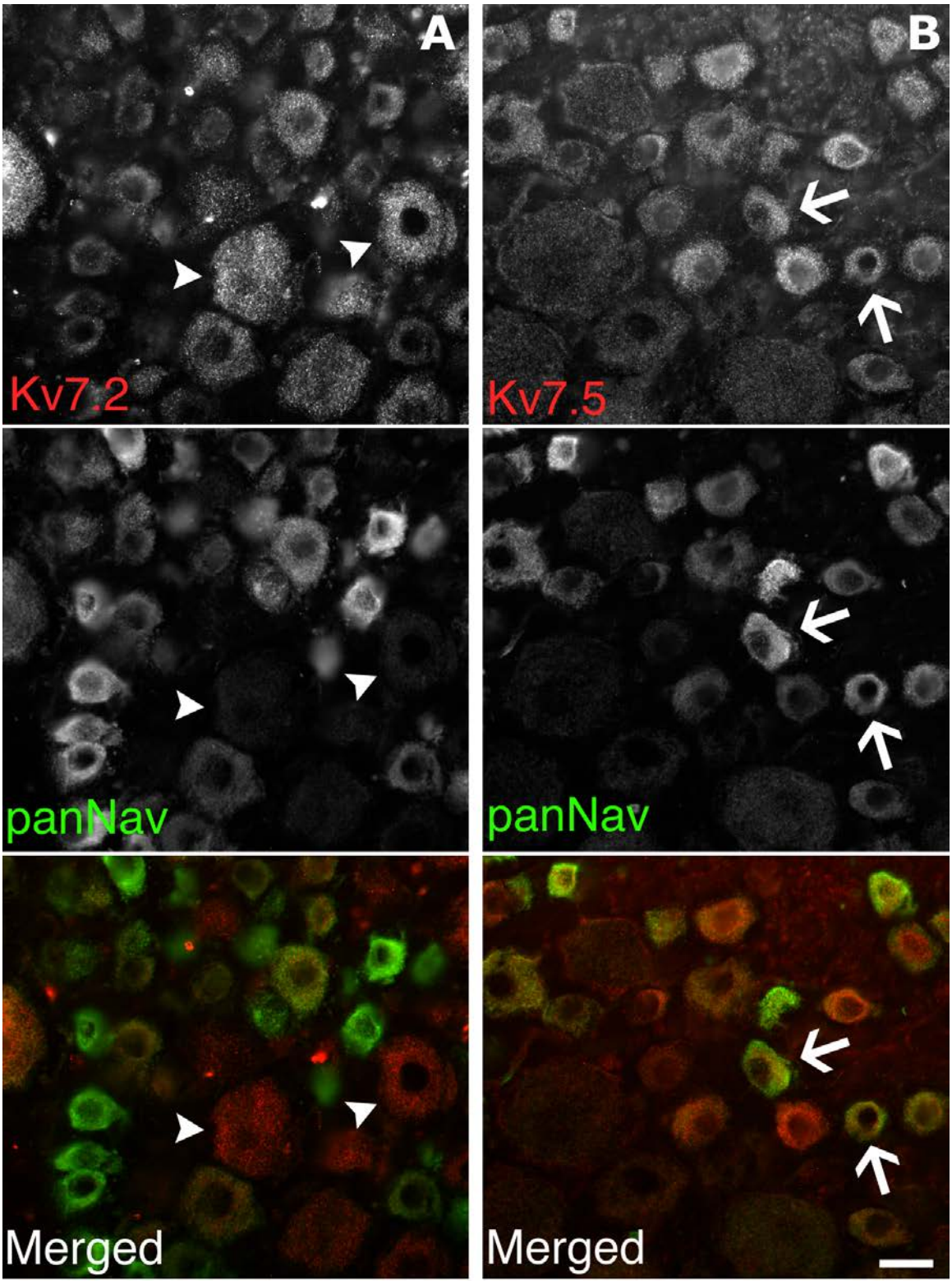

Figure 2-9: Kv7.5 is predominately expressed by the small DRG neurons.

These are images of unfixed sections of rat lumbar DRG, double-labeled with rabbit antisera (magenta) against Kv7.2 or Kv7.5 (AB9792) and a panNav monoclonal antibody (green). Note that in column A, the Kv7.2 antiserum predominately labels large diameter neurons (two examples denoted with arrowheads), which are relatively unlabeled by the panNav antibody. In contrast, in column B, the Kv7.5 antiserum and the panNav antibody preferentially label small diameter neurons (two examples denoted with arrows). Scale bar: 20 μm.

Figure 2-10

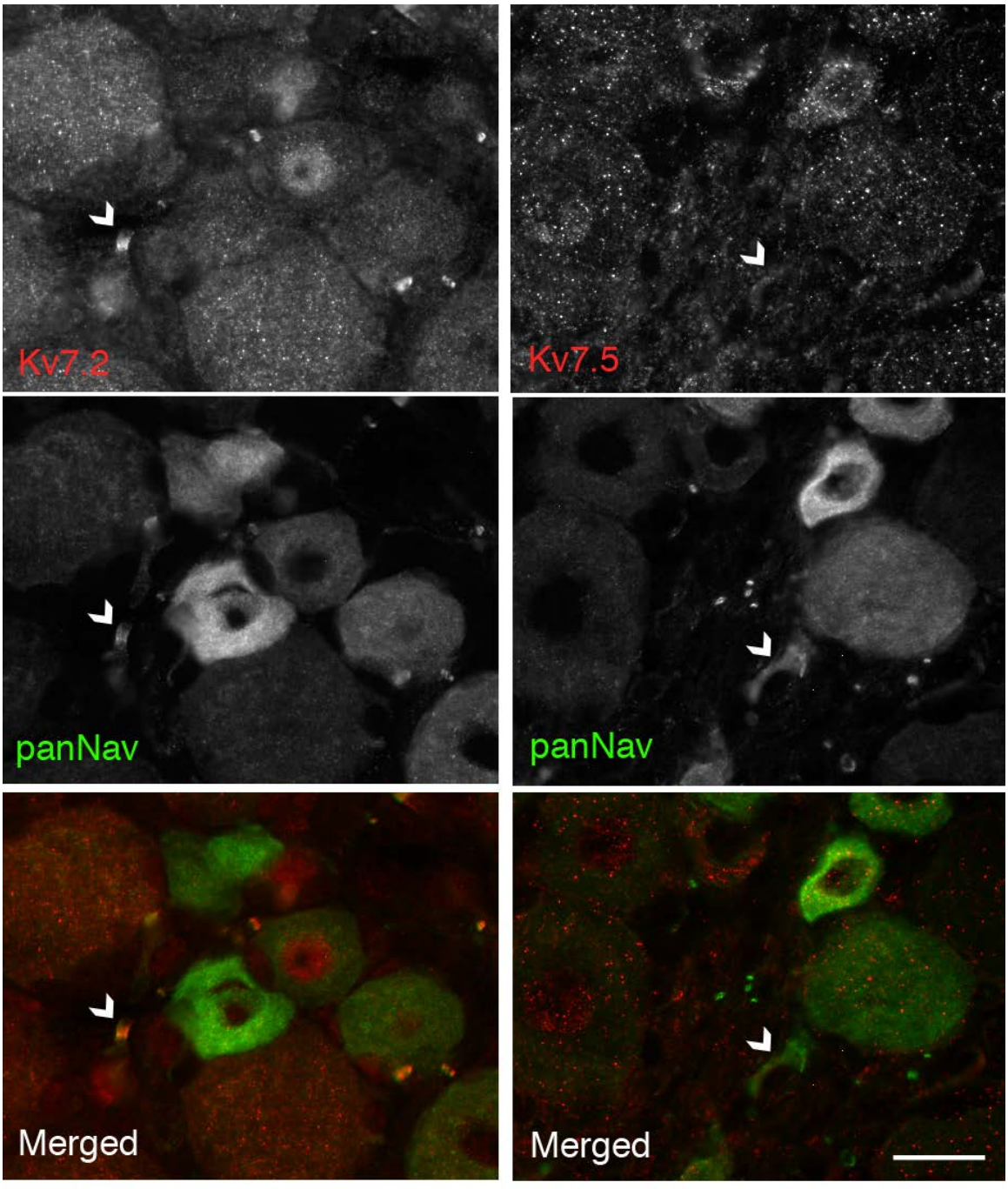

Figure 2-10: Stem processes are Kv7.5-negative.

These are images of unfixed sections of rat lumbar DRG, double-labeled with rabbit antisera (red) against Kv7.2 or Kv7.5 (AB9792) and a panNav monoclonal antibody (green). In column A, note that Kv7.2 and panNav are co-localized in a stem process (chevron). In column B, the Kv7.5 antiserum does not label the stem process, which is panNav-positive (chevron). Scale bar: 20 μm.

Figure 2-11

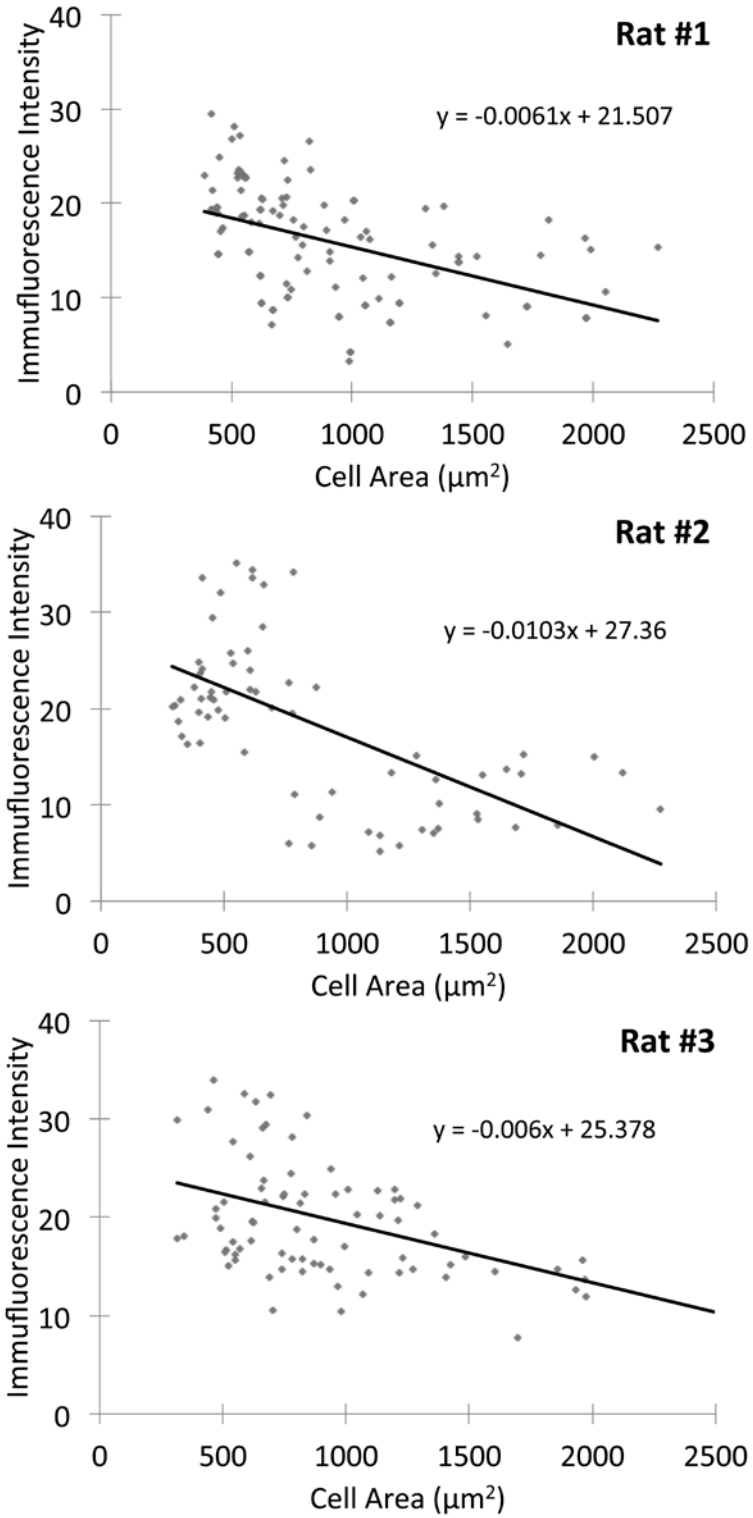
Rat #1
y = -0.0061x + 21.507
Immufluorescence Intensity
Cell Area (µm²)
Rat #2
y = -0.0103x + 27.36
Immufluorescence Intensity
Cell Area (µm²)
Rat #3
y = -0.006x + 25.378
Immufluorescence Intensity
Cell Area (µm²)

Figure 2-11: Smaller DRG neurons express relatively higher levels of Kv7.5.

The level of Kv7.5/AB9792-immunoreactivity was measured in sections from lumbar DRG neurons from 3 adult rats. Note that Kv7.5-immunoreactivity is inversely related to the size of the DRG neurons, with the majority of the labeled cells (fluorescence intensity >20) being small [cell diameter less than 30 μm, or 701 μm^2 (Rasband et al., 2001). The slope of the inverse relationship for each rat is statistically different as compared to the slope of no relationship (slope of 0), with a p value of < 0.05 (Student's t-test).

Figure 2-12

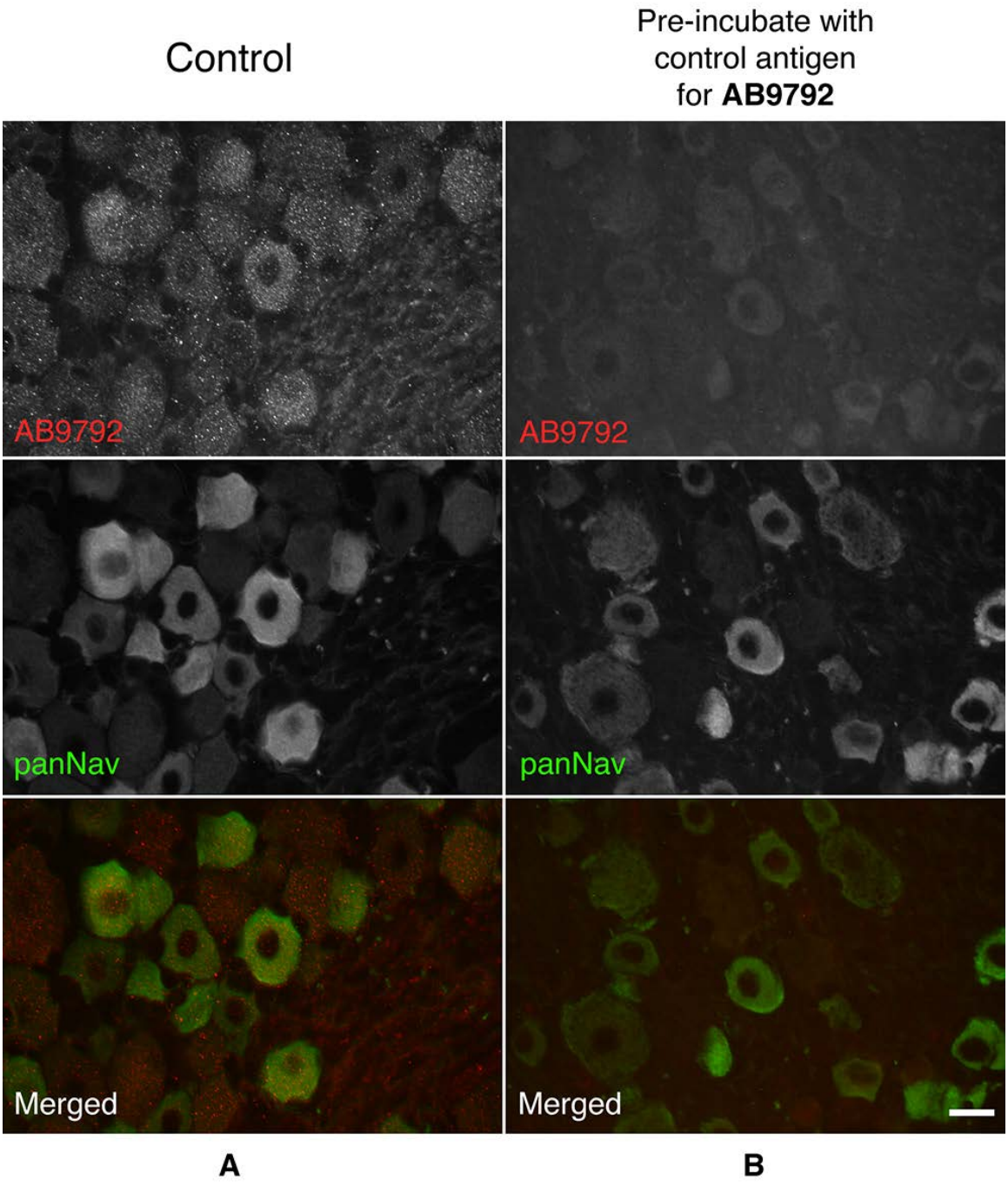
Control
Pre-incubate with control antigen for AB9792
AB9792
AB9792
panNav
panNav
Merged
Merged
A
B

Figure 2-12: Cognate antigen blocks immunostaining of DRG neurons with Kv7.5 antiserum AB9792.

These are images of sections of unfixed rat DRG, double-labeled for Kv7.5 (AB9792; red) and panNav (green), as indicated. The images were exposed for the same amount of time to facilitate direct comparison. Pre-incubation with the control antigen (column B) reduced the neuronal staining of the AB9792 antiserum. Scale bar: 20 μm.

Figure 2-13

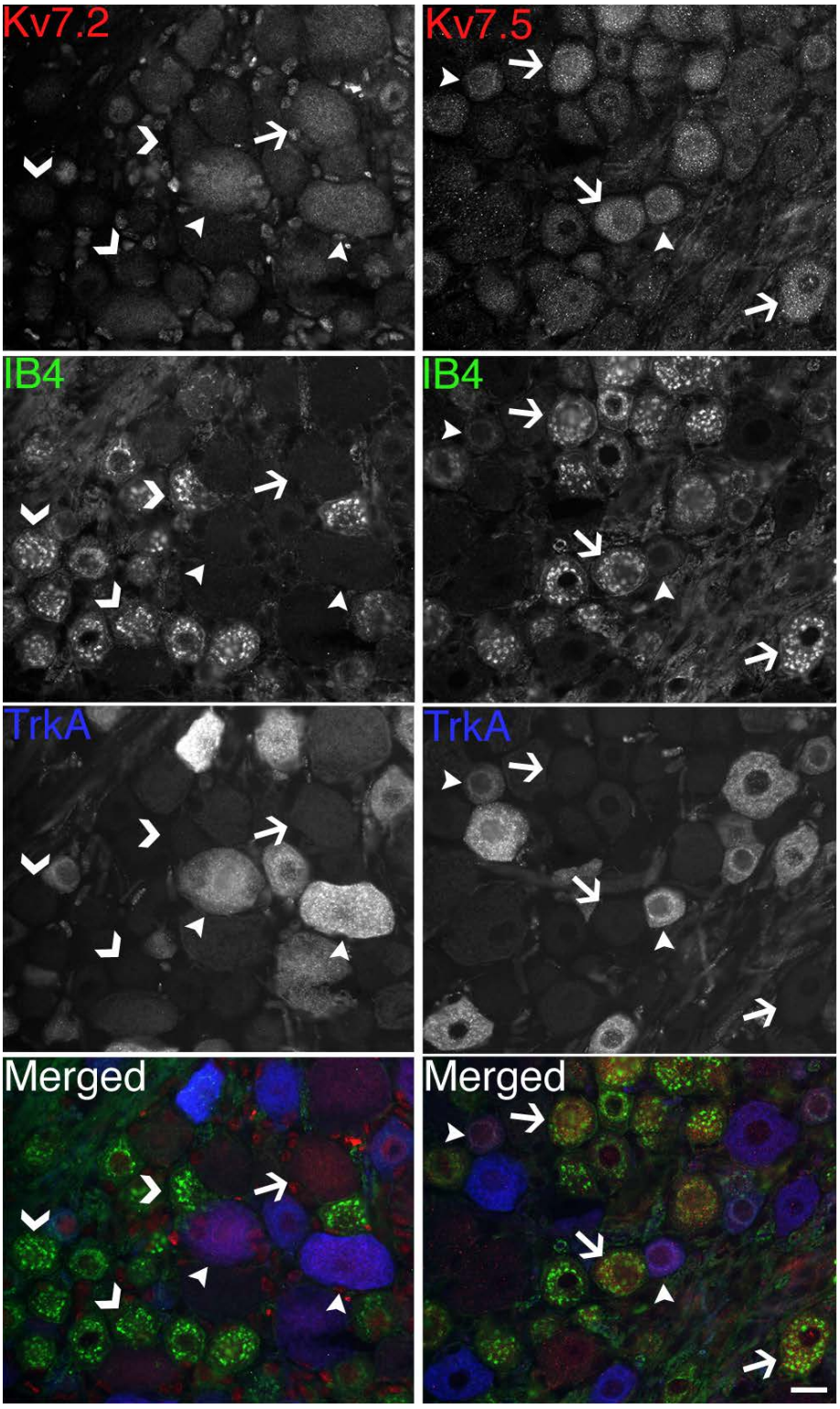

Figure 2-13: Kv7.5-positive DRG neurons are mostly IB4- or TrkA-positive.

These are images of unfixed sections of rat DRG, triple-labeled as indicated for either Kv7.5 (AB9792; red) or Kv7.2 (red), as well as IB4 (green) and TrkA (blue). Note that most Kv7.5-positive neurons are IB4-positive (arrows); fewer are TrkA-positive (arrowheads). In contrast, none of the Kv7.2-positive neurons are IB4-positive (arrow), but some are TrkA-positive (arrowheads); all of the IB4-positive neurons are Kv7.2-negative (chevrons). Scale bar: 20 μm.

Figure 2-14

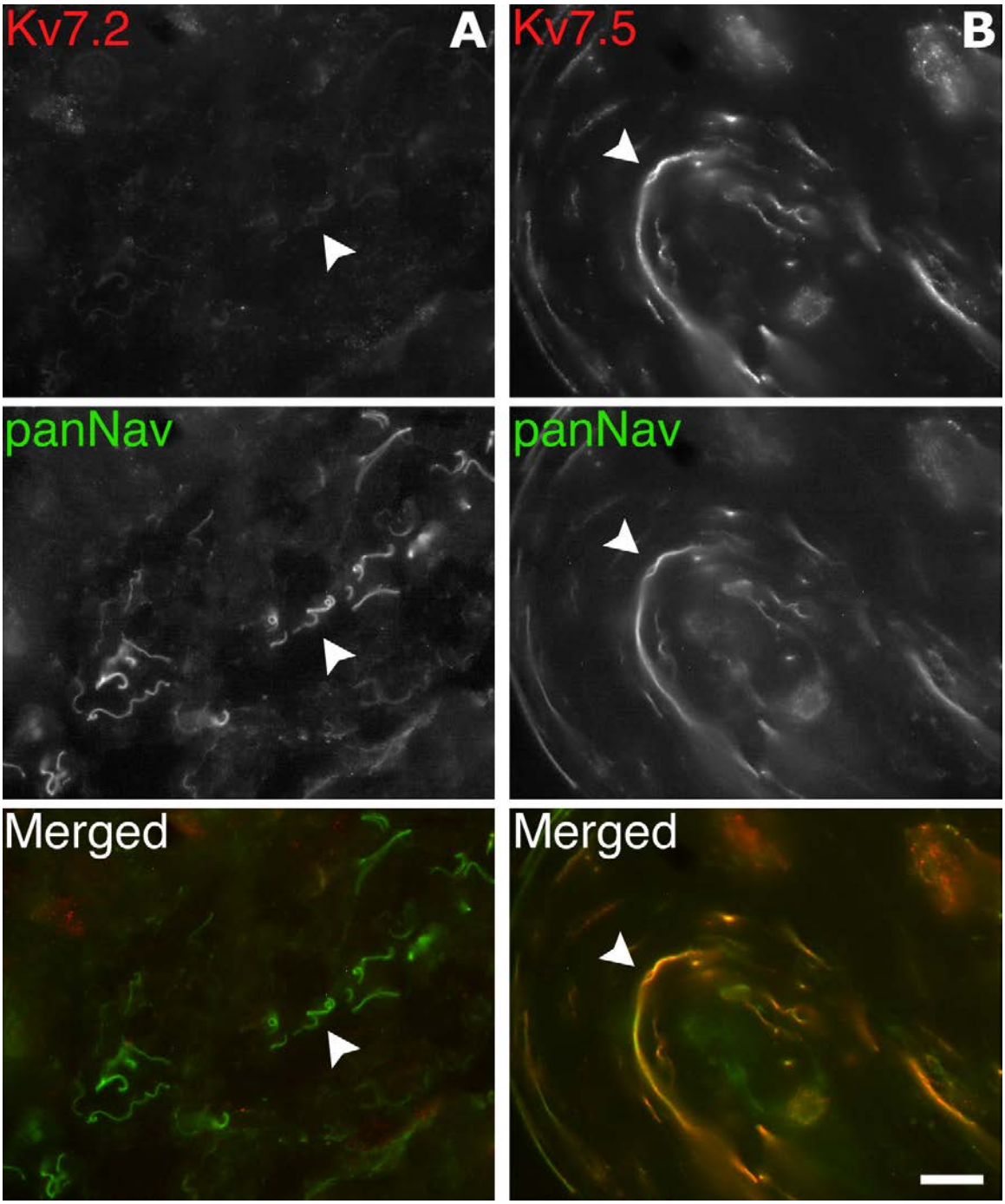

Figure 2-14: Cutaneous afferents express Kv7.5.

These are digital images of unfixed section of hairy skin, double-labeled for Kv7.2 (red), Kv7.5 (Chemicon AB9792; magenta), and voltage-gated sodium channels (panNav; green). In column A, the unmyelinated axons are labeled by the panNav antibody but not by the Kv7.2 antiserum (one example is denoted with an arrowhead). In column B, the unmyelinated axons are labeled by both the Kv7.5 antiserum and the panNav antibody (arrowhead). Scale bar: 20 μm.

Figure 2-15

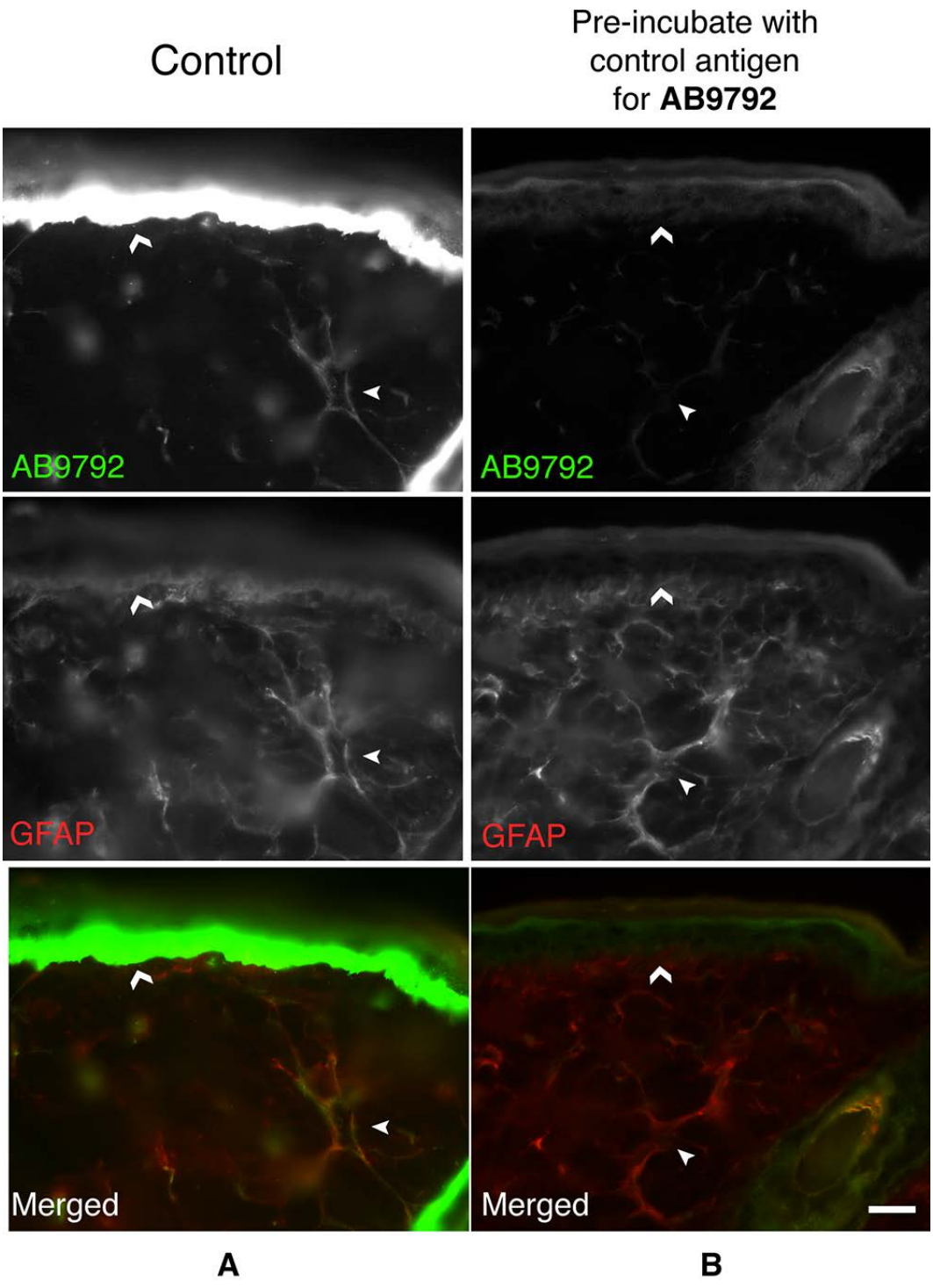
Control
Pre-incubate with control antigen for AB9792
AB9792
AB9792
GFAP
GFAP
Merged
Merged
A
B

Figure 2-15: Cognate antigen blocks immunostaining of cutaneous afferents with Kv7.5 antiserum AB9792.

These are images of sections of unfixed hairy skin, double-labeled for Kv7.5 (AB9792; green) and glial fibrillary acid protein (GFAP; a marker of non-myelinating Schwann cells; red), as indicated. The images were exposed for the same amount of time to facilitate direct comparison. Compared to rat skin labeled with the AB9792 antiserum alone (column A), pre-incubation with the control antigen (column B) reduced the staining of cutaneous afferents (arrowheads), but not the GFAP-staining of their associated Schwann cells. The pre-incubation also diminished Kv7.5-immunoreactivity of the stratum basale (chevron). Scale bar: 20 μm.

Table 2-1

Name	Manufacturer	Dilution	Species	Type	Immunogen
KCNQ2 N	A gift from Dr. Edward Cooper	1:200	Rabbit	Polyclonal	KCNQ2 N-terminus (residues 13-37)
KCNQ3 C	A gift from Dr. Edward Cooper	1:200	Rabbit	Polyclonal	KCNQ3 C-terminus (residues 578-604)
KCNQ5	Chemicon; AB5599	1:1000	Rabbit	Polyclonal	KCNQ5 N-terminus (residues 12-93)
Kv7.5	Chemicon; AB9792	1:200	Rabbit	Polyclonal	KCNQ5 N-terminus (residues 89-103)
panNav	Sigma; clone K58/35	1:250	Mouse	Monoclonal	CTEEQKKYYNAMKKLGSKK from the intracellular III-IV loop of Na^+ channels
TrkA	R&D Systems; AF1056	1:100	Goat	Polyclonal	Recombinant rat TrkA (Ala33Pro418)
IB4	Sigma; L2140	1:100	Biotin-conjugated	N/A	Major affinity for terminal α-D-galactosyl residues of blood group B
MAG	R&D Systems; AF538	1:100	Goat	Polyclonal	Recombinant rat MAG extracellular domain (rrMAG)
NF-H	A gift from Dr. Virginia Lee	1:500	Rat	Monoclonal	Clone Ta51; bovine neurofilament-heavy subunit
GFAP	A gift from Dr. Virginia Lee	1:200	Rat	Monoclonal	Highly enriched glial filament proteins from bovine spinal cord

Table 2-1: List of Primary Antibodies Used

Table 2-2

	IB4-positive only	TrkA-positive only	Total Neurons
Rat #1	12/17 (70.6%)	5/6 (83.3%)	17/23 (73.9%)
Rat #2	17/21 (81.0%)	9/9 (100%)	23/30 (76.7%)
Rat #3	17/20 (85.0%)	8/10 (80%)	25/30 (83.3%)

Table 2-2: A high proportion of small, IB4- and TrkA-positive neurons are Kv7.5-positive.

The cell soma size as well as the fluorescence intensity of IB4, TrkA, and Kv7.5 was measured for ~100 DRG neurons from 3 rats. For each rat, we counted the number of small neurons (diameter < 30 μm) that were either IB4- or TrkA-positive (fluorescence intensity >20), and also determined whether they were Kv7.5-positive. For each rat, the fraction of Kv7.5-positive small neurons to the total number small DRG neurons is shown. A similarly high proportion of IB4-positive and TrkA-positive small neurons are Kv7.5-positive.

CHAPTER 3: IMMUNOHISTOCHEMICAL, BEHAVIORAL, AND ELECTROPHYSIOLOGICAL ANALYSIS OF *Kcnq2*-NULL PERIPHERAL SENSORY MYELINATED AXONS

INTRODUCTION

The Kv7 (KCNQ) family of K^+ channels is made up of five members, Kv7.1 to Kv7.5 (Jentsch, 2000, Delmas and Brown, 2005, Brown and Passmore, 2009). While many PNS and CNS neurons have been shown to express Kv7.2, Kv7.3, and K7.5, recently Kv7.1 and Kv7.4 have also been found in certain neuronal populations (Goldman et al., 2009, Heidenreich et al., 2011). In addition, Kv7.1 and Kv7.4 are prominently expressed in the cochlea, and Kv7.1 is expressed in the heart (Brown and Passmore, 2009). Kv7 channels contribute to the normal resting membrane potential, and also form the non-inactivating M-current, because muscarinic agonists modulation it (Brown and Adams, 1980, Wang et al., 1998). Their importance in maintaining normal cellular excitability is demonstrated by the effects of dominant mutations of *KCNQ1*, *KCNQ*2, *KCNQ3,* and *KCNQ4* – all decrease the Kv7 current and cause hereditary diseases in a cell autonomous manner (Singh et al., 1998) - in the heart (*KCNQ1*), brain (*KCNQ2* and *KCNQ3*), and inner ear (*KCNQ1* and *KCNQ4*) (Jentsch, 2000, Brown and Passmore, 2009). One *KCNQ2* mutation causes neuromyotonia (Dedek et al., 2001), which is likely the result of diminished Kv7.2 and Kv7.3 current at nodes of Ranvier, where Kv7.2 and Kv7.3 are localized (Devaux et al., 2004). A conserved ankyrin-G binding motif located at the C-

termini mediates the localization of Kv7.2 and Kv7.3 at nodes and axon initial segments (Pan et al., 2006).

Previous investigations of the role of Kv7 in regulating neuronal excitability and nociceptive behaviors utilized pharmacological M-channel blockers and/or enhancers (Passmore et al., 2003, Yue and Yaari, 2004, Rivera-Arconada and Lopez-Garcia, 2006, Lang et al., 2008, Roza and Lopez-Garcia, 2008). Because homozygous *Kcnq2*-null mice die at birth due to pulmonary atelectasis, investigators studied heterozygous *Kcnq2*-knockout mice (Watanabe et al., 2000, Yang et al., 2003, Otto et al., 2006, Tzingounis and Nicoll, 2008), *Kcnq3*-null mice (Tzingounis and Nicoll, 2008), or mice expressing a dominate negative mutant allele of human *KCNQ2* as a transgene (Peters et al., 2005). None of these studies, however, satisfy the need to develop an animal model with a complete absence of Kv7.2 expression. In addition, previous studies of heterozygous *Kcnq2*-knockout mice found that reduction of Kv7.2 expression can lead to decreased seizure threshold (Watanabe et al., 2000, Yang et al., 2003).

In the present study, we characterize mice in which *Kcnq2* has been deleted in all somatic sensory neurons, using the Cre-Lox system (Sauer and Henderson, 1988, Nagy, 2000). These mice are viable and their myelinated sensory axons have a normal ultrastructure and normal molecular composition of nodes (including Kv7.3), paranodes, and juxtaparanodes. *Kcnq2* mutant mice showed increased signs of thermal hyperalgesia and mechanical allodynia, and *Kcnq2*-null dorsal root ganglia (DRG) neurons showed increased excitability and reduced spike-frequency adaptation. Taken together, our results

suggest that Kv7.2 regulates neuronal excitability, and a reduction of Kv7.2 expression could lead to altered nociception.

MATERIALS AND METHODS

All procedures involving rodents were approved by the Institutional Animal Care and Use Committee of the University of Pennsylvania. Except when specified, all chemicals were from Sigma.

Generation of conditional *Kcnq2*-null mice

A floxed allele of *Kcnq2* was designed (Fig. 1A) to delete exons 3-5; these correspond to 463 bp (amino acid 130-285) of mouse *Kcnq2* cDNA (GeneBank AF490773; (Wen and Levitan, 2002); this deletion has been shown to result in a functional null allele (Watanabe et al., 2000). Two DNA fragments (*EcoRV* and *Xhol*) were cloned from R1 ES-cells genomic DNA, and used to generate a targeting vector in which a FRT-neomycin-FRT-loxP cassette was inserted into a unique Xhol site, with flanking 7kb and 3.4kb of homologous genomic DNA. An additional loxP site was inserted in an EcoRI site just upstream of the third exon. The targeting vector also includes a diphtheria toxin (DT) gene as a negative selection marker against ES clones which have randomly integrated the targeting vector. The linearized targeting vector was electroporated into R1 embryonic stem cells, selected with G418, and colonies were picked and analyzed by duplication. Positive ES cells were used to first generate chimeras and then heterozygous mice (Gollan et al., 2003, Poliak et al., 2003). The presence of the targeted locus was confirmed by PCR analysis of tail DNA. Heterozygous mice were first mated with mice

carrying the FLP recombinase (129S4/SvJaeSor-Gt(ROSA)26Sortm1(FLP1)Dym/J; (Farley et al., 2000), to remove the *Neo* cassette and to create a floxed *Kcnq2* allele.

We crossed mice expressing *Pax3-Cre* (Jackson Laboratory; stock number 005549) with mice carrying the *Rosa26* reporter gene (Jackson Laboratory; stock number 003504). We examined X-gal expression in the brains, spinal cords, and lumbar DRG of 3 *Pax3-Cre*-positive // *Rosa26* mice and 3 *Pax3-Cre*-negative // *Rosa26* littermates, all 1-month-old, as previously described (Feltri et al., 1992, Arroyo et al., 1998). The mice were perfused with 0.5% glutaraldehyde (in 0.1M PB, pH 7.4), their cerebra, cerebelli, and spinal cords were dissected and cut into slabs with a razor blade, and the resulting sections along with L4 and L5 DRG were fixed for 3 hours at 4^{o}C, stained in X-Gal (Roche Diagnostic) at 37^{0}C for 24-48 hours, rinsed in 0.1M PB, then re-fixed in 3% glutaraldehyde (in 0.1M PB) at 4^{o}C overnight. The samples were photographed using a Nikon Coolpix 5000 camera mounted on a Leica MZ16 FA stereomicroscope. The DRG were osmicated, dehydrated, and embedded with the Embed 812 kit (EMS). Semi-thin sections (1 μm thick) were photographed using a cooled Hamamatsu camera mounted on Leica DMR light microscope.

Kcnq2 was deleted in sensory axons by crossing with mice that were heterozygous for both the floxed *Kcnq2* allele and *Pax3-Cre* (*Kcnq2*$^{f/+}$ // *Pax3-Cre*). We chose this approach because it generates relatively mice of the desired genotype, and homozygous *Pax3-Cre* mice fail to develop past E18.5 according to Jackson Laboratory. All offspring were genotyped by PCR. Tail DNA was digested with DirectPCR (Viagen) and proteinase K overnight at 55^{o}C, heated to 85^{o}C for 45 minutes to denature proteinase

K, then PCR were then performed with REDTaq ReadyMix PCR reaction mix following manufacturer's protocol in a Bio-Rad DNA Engine peltier thermal cycler. Three primers were used together: KCNQ2A (GGGGCAGTTGTCTAACCCTC), KCNQ2C (TATGTGGTGCTCCCCAGAAG), and KCNQ2E (GGGAGGCTCTAGTGTCAGTG); see Figure 1B. After amplification, samples were separated in 1.5% agarose (GeneMate) gel in 1xTBS at 125V for 1 hour.

Anatomical studies

One-month-old *Kcnq2*-mutant mice (*Kcnq2*$^{fl/fl}$ *// Pax3-Cre*; n=3) and their control littermates (*Kcnq2*$^{+/+}$ *// Pax3-Cre*; n=3) were anesthetized with ketamine/xylazine mix and killed by decapitation. Sciatic nerves, dorsal root ganglia (from L4-L6 spinal levels) with the ventral and dorsal roots attached, and femoral nerves (motor and sensory branches separately) were dissected, and quickly embedded in OCT cooled in an acetone/dry ice slurry. The sciatic and femoral nerve fibers were teased apart with fine needles, mounted on SuperFrost Plus glass slides (Fisher Scientific, Pittsburgh, PA), dried overnight, and stored at -20^{o}C. Ten μm thick cryostat sections were thaw-mounted onto SuperFrost slides, and stored at -20^{o}C. Teased fibers and OCT sections were immersed in -20^{o}C acetone for 10 minutes, rinsed in Tris-buffered saline (TBS; pH 7.4), blocked at room temperature for one hour in TBS containing 5% fish skin gelatin and 0.5% Triton X-100, and incubated overnight at 4^{o}C with various combination of primary antibodies diluted in blocking solution - a rabbit antiserum against a peptide from the N-terminus of Kv7.2 (KCNQ2N, 1:200 (Cooper et al., 2001) or a rabbit antiserum against a

peptide from the C-terminus of Kv7.3 (KCNQ3C, 1:200 (Pan et al., 2006), combined with a mouse monoclonal antibody either against all voltage-gated Na^+ channels (panNav; Sigma clone K58/35, 1:250), Kv1.1 (NeuroMab clone K20/78, 1:200), or contactin-associated protein (Caspr; clone 2751:100 (Poliak et al., 1999). The slides were washed with TBS, incubated with the appropriate FITC- and TRITC-conjugated donkey cross-affinity-purified secondary antibodies (Jackson ImmunoResearch, 1:200) at room temperature for one hour, washed with TBS, counterstained with 4',6-diamidino-2-phenylindole dihydrochloride (DAPI; Invitrogen), mounted with Vectashield (Vector Laboratories), then examined with a Leica DMR light microscope with a cooled Hamamatsu camera under the control of Openlab software (Openlab, Improvision).

To ascertain the specificity of the Kv7.2 antisera, Hela cells were transiently transfected with the cDNA encoding human Kv7.2 or Kv7.3, (kindly provided by Dr. Edward Cooper) using the Lipofectamine 2000 (Invitrogen) method as previously described (Rasmussen et al., 2007), and immunostained 1 day post-transfection with the Kv7.2 (gifts of Drs. Edward Cooper and Jérôme Devaux) and Kv7.3 (gift of Dr. Edward Cooper) antisera.

To analyze the structure of myelinated axons, one-month-old *Kcnq2* mutant mice (*Kcnq2*$^{fl/fl}$ *// Pax3-Cre*; n=3) and littermates controls (*Kcnq2*$^{+/+}$ *// Pax3-Cre*; n=3) were perfused with 2% glutaraldehyde/2% paraformaldehyde mix (in 0.1M PB) for 10 minutes, then the femoral sensory and motor branches as well as the L4 and L5 DRG were dissected, fixed for 4 hours at 4^{o}C, osmicated, dehydrated, and embedded with the Embed 812 kit. Semi-thin (1 μm) sections were stained with toluidine blue and examined

as above; thin (80 nm thick) sections were stained with lead citrate and examined with a JEM-1010 transmission electron microscope (JEOL USA) outfitted with a digital camera.

Behavior Testing

Three-month-old *Kcnq2*-mutant mice (*Kcnq2*$^{fl/fl}$ *// Pax3-Cre*; n=9) and their littermates (*Kcnq2*$^{+/+}$ *// Pax3-Cre*; n=9), derived from 3 litters were studied. Mechanical allodynia was measured using Chaplan's up-down threshold method (Chaplan et al., 1994, Hubbard and Winkelstein, 2005, Lee et al., 2008, Quinn et al., 2010). Mice were confined in plexiglass enclosure placed on a wire-mesh platform and allowed to acclimate for at least 30 minutes before each test. Three rounds of testing was performed over three consecutive days, with each round comprised of five stimulations of either the right or the left mid-plantar hindpaw in a random order, with a series of ascending von Frey filament strength (0.4 g, 0.6 g, 1.0 g, 1.4 g, 2.0 g; Stoelting Co.) held perpendicular for 8-10 seconds with enough force to cause slightly buckling against the skin. A positive response is recorded for sharp paw withdrawal or if immediate flinching was observed upon removal of filament. If two consecutive filament strengths elicited a withdrawal response, the lower of the two filament strengths was recorded as the threshold. Any mouse that failed to display a response with the highest filament strength was recorded as having a threshold of 2.0 g. Testing in the opposite direction (descending filament strength) was also performed during each round to confirm the withdrawal threshold. The average threshold of the three rounds was recorded for each mouse.

Thermal nociceptive response was assessed using a paw thermal stimulator

system (UARDG, University of California San Diego; otherwise referred to as Hargreaves' apparatus) as previously described (Hargreaves et al., 1988, Dirig et al., 1997). Four rounds were performed over four consecutive days. Briefly, the mice were allowed to acclimate on the glass plate of the apparatus (maintained at 30^{o}C) for at least 30 minutes, then either the left or the right mid-plantar hindpaw was randomly heated with a thermocouple set at 5 amperes. A timer is automatically started with the thermal source, and response latency is defined as the time required for the hindpaw to show an abrupt withdrawal (maximum 20 seconds). Paw withdrawal is automatically detected by an array of photodiode motion sensors mounted on the stimulus tower that stops the timer and terminates the stimulus. Stimulus current is monitored continuously. Six trials were performed during each round, with a minimum of 5 minutes between each trial to allow the hindpaws to return to normothermic baseline (Dirig et al., 1997). The average threshold of the four rounds was recorded for each mouse.

Motor function was measured with a rotarod apparatus (Ugo Basile, Stoelting Co.) as previously described (Wood et al., 2005, Oliveira et al., 2006). Briefly, the rotarod has a 3-cm diameter rotating rod raised 16 cm above a platform and divided into five sections for testing multiple mice simultaneously. Mice were acclimated on the first day by allowing them to run on the rotarod with the slowest rotation speed. Three rounds of testing were performed during the three subsequent days, with three trials during each round. For each trial, mice were placed on the rotarod, and the rotation speed was gradually increased from 4 to 40 rpm over the course of 5 minutes. Each trial ended when mice fell off (maximum 300 seconds), and the latency to fall was recorded for each trial. Test was considered valid if mice ran forward on the rotarod for at least 10 seconds. Mice

were given 1-hour rest between each trial. The average time to fall of each mouse was used as the outcome.

Whole cell patch recording

DRG neurons were dissected and cultured from three-month-old *Kcnq2* mutant mice (*Kcnq2*$^{fl/fl}$ *// Pax3-Cre*; n=5) and their littermate controls (*Kcnq2*$^{+/+}$ *// Pax3-Cre*; n=5) from 2 litters, as previously described (Malin et al., 2007). Lumbar DRGs were rapidly removed, transferred to ice-cold Ca^{2+}/Mg^{2+}-free HBSS (GIBCO), then incubated first in papain solution (60U papain; Worthington), 3µl saturated NaHCO3, 1 mg L-Cys free base, 1.5ml Ca^{2+}/Mg^{2+}-free HBSS (GIBCO) for 10 minutes at 37^{o}C, then in collagenase/dispase solution (0.1U/ml collagenase 0.8U/ml dispase (Roche), 3 ml Ca^{2+}/Mg^{2+}-free HBSS) for 1 hour at 37^{o}C. Neurons were dissociated by trituration using fire-polished glass Pasteur pipettes, suspended in F12 medium (GIBCO) containing 10% FCS (Invitrogen) and 1% penicillin/streptomycin (Invitrogen), then plated onto laminin /poly-D-lysine (Beckton Dickson) coated coverslips (Fisher). DRG neurons adhered to coverslips and were maintained in culture for 12-48 hours after plating at 37^{o}C prior to recording.

Whole cell patch-clamp techniques (Hamill et al., 1981, Lancaster et al., 2001) were employed with an Axopatch 200B amplifier and PCLAMP 9 software (Axon Instruments). Patch pipettes (1–4 M**Ω**) were fabricated from glass capillaries (MTW150F-4, World Precision Instruments). Pipettes were filled with a variant of a solution described previously (Ikeda et al., 1986), with a composition of (in mM) 140

KCl, 2 MgATP, 10 *N*-[2-hydroxyethyl] piperazine-*N*9-[2-ethanesulfonic acid] (HEPES), 11 ethylene glycolbis(b-aminoethyl ether)-*N*,*N*,*N*9,*N*9-tetraacetic acid (EGTA), and 2 $CaCl_2$; titrated to pH 7.3 with KOH, and to 314 mOsm with sucrose. Pipette voltage offset was neutralized prior to the formation of a giga-seal. Membrane input resistance (R_{in}), series resistance (R_s), and capacitance (C_m) were determined from current transients elicited by 5 mV depolarizing steps from a holding potential of -60 mV, delivered using the Membrane Test application of PCLAMP9. Criteria for cell inclusion in the study were as follows: $R_s \leq 10$ MV, $R_m \geq 100$ MV, and stable recording during the entire experiment. Cover slips were superfused (2–4 ml/min) continuously during recording at 34–36°C extracellular solution (composition in mM: 10 glucose, 140 NaCl, 3 KCl, 0.6 $MgCl_2$, 2.5 $CaCl_2$, 10 HEPES, titrated to pH 7.4 with TRIS base, to 325 mOsm with sucrose if needed). Tetraethylammonium (TEA) was fully dissolved in the extracellular solution prior to application; 3 mM TEA was applied for at least 2 minutes before determining its effects on membrane properties. To prevent bias in cell selection or analysis, the electrophysiologist was blinded to genotypes of the cells (control versus *Kcnq2*-null) during the experiments and measurements of cell properties. A total of 25 neurons from mutant mice, and 25 neurons from control littermates, were recorded and analyzed.

Statistical Tests

Other than the following exceptions, all comparisons between two samples were explored using unpaired two-samples Student's t-test, with equal variance first established with the equality of variance test. All statistical tests were performed with

SAS 9.2 (SAS), with all data given as mean ± standard error of mean (SEM). Comparison of Kv7.2- and Kv7.3-positive nodes in different peripheral nerves was tested with two-way ANOVA; motor function results over the course of nine sessions were analyzed with repeated measures ANOVA; two-way repeated measures ANOVA was used to compare mutant and control neurons before and after 3 mM TEA across multiple rheobase, followed by the Tukey test to identify specific significant differences. The minimum *a priori* criteria for statistical significance is $p < 0.05$.

RESULTS

Generation of conditional *Kcnq2*-null mice

We generated mice lacking *Kcnq2* expression in sensory neurons by using the Cre-Lox system (Sauer and Henderson, 1988, Nagy, 2000). Mice containing a floxed allele of *Kcnq2* (Fig. 1A) were crossed with mice expressing a *Pax3-Cre* transgene, which is expressed by cells derived from the neural crest (Li et al., 2000). To determine whether *Pax3-Cre* deleted exons 3-5 of *Kcnq2*, we examined three $Kcnq2^{fl/fl}$ *// Pax3-Cre* mice by amplifying genomic DNA with PCR and appropriate primers (Fig. 3-1A). As shown in Figure 3-1C, while both the floxed and recombined *Kcnq2* alleles were detected in the DRG and trigeminal ganglia, only the floxed allele was detected in the liver, indicating that the *Kcnq2* allele was being selectively deleted in neural-crest-derived tissues.

We examined the expression of the *Pax3-Cre* by crossing the mice with *Rosa26 lacZ* reporter mice, in which Cre removes a floxed stop cassette so that *lacZ* is expressed

(Soriano, 1999). Using litters that contained mice of the informative genotypes, we stained the brain, spinal cord, and DRG for beta-galactoside activity with X-gal as the chromogen. As shown in figure 3-2, none of the samples taken from any of the control animals showed X-gal staining. In contrast, a majority of the cerebellum, regions of the cerebrum (including the cortex, the hippocampus, the thalamus, and the hypothalamus), and the dorsal part of the spinal cord (including the dorsal roots) of *Wnt1-Cre*-positive mice were stained with X-gal. *Pax3-Cre*-positive mice also exhibited similar X-gal staining pattern (but with more intense thalamic staining and no detectable hippocampal or hypothalamic staining). Lastly, mice expressing *Avil*-Cre showed much less cerebellum X-gal labeling, with cerebrum staining primarily seen in the cortex and the hippocampus, as well as staining of the dorsal part of the spinal cord (including the dorsal roots). The ventral part of the spinal cords and the ventral roots from all three Cre lines were unstained, suggesting that motor neurons lack Cre expression. In contrast, as shown in figure 3-3, all DRG neurons from all three Cre lines showed X-gal staining, provide support that all DRG neurons were *Wnt1-Cre*-, *Pax3-Cre*, or *Avil-Cre*-positive. Interestingly, our observed pattern of *Avil-Cre* X-gal staining, especially within the cerebrum, was more extensive than had been previously described (Hasegawa et al., 2007), but was more consistent with the *Avil in situ* hybridization data from the Allen Mouse Brain Atlas (experiment 69527692; Allen Mouse Brain Atlas), suggesting that *Avil-Cre* expression is not limited to sensory neurons.

After analyzing the results of our X-gal experiment, we decided to use the *Pax3-Cre*, which is expressed by cells derived from the neural crest (Li et al., 2000), including all sensory neurons (Toth, 1966). The *Pax3-Cre* mediated deletion of exons 3-5 of the

floxed *Kcnq2* allele (figure 3-1, panel A), which resulted in a complete knockout of *Kcnq2* expression in neural crest derived tissues.

Primary sensory neurons in conditional *Kcnq2*-null mice lacked Kv7.2

To determine whether *Pax3-Cre* resulted in the loss of Kv7.2 expression in sensory neurons, we examined three mutants (*Kcnq2*$^{fl/fl}$ *// Pax3-Cre*) and three control littermates (*Kcnq2*$^{+/+}$ *// Pax3-Cre*). We immunostained unfixed teased nerve fibers from femoral sensory and motor branches, and from dorsal and ventral roots, as well as sections of the lumbar DRG, for Kv7.2 or Kv7.3, combined with a mouse monoclonal antibody against voltage-gated Na^+ channels (panNav). As shown in figure 3-4, in the control mice, all nodes of Ranvier of both the motor and sensory branches of the femoral nerve were Kv7.2- and panNav-positive, agreeing with previously published results (Devaux et al., 2004, Pan et al., 2006). In mutant animals, all nodes were panNav-positive, but none of the nodes of the femoral sensory branch, and only some nodes of the femoral motor branch, were Kv7.2-positive. The lack of nodal staining of the *Kcnq2*-null sensory axons supports for the specificity of the Kv7.2 antiserum, which also selectively labeled HeLa cells transiently transfected to express human Kv7.2, but did not label transfected cells expressing Kv7.3 (Fig. 3-5). Similarly, none of the nodes in the dorsal roots (which are purely sensory), and all of the nodes in the ventral roots (which are purely motor), were Kv7.2-positive (Fig. 3-7). Another Kv7.2 antiserum (provided by Dr. Jérôme Devaux) gave similar results (data not shown).

Because Kv7.3 can form heteromeric channels with Kv7.2 *in vitro* (Wang et al., 1998, Selyanko et al., 2001, Shah et al., 2002, Maljevic et al., 2003), and Kv7.2 and Kv7.3 co-localize at nodes *in vivo* (Pan et al., 2006, Schwarz et al., 2006), we wish to investigated whether proper Kv7.3 nodal expression require Kv7.2. Unlike Kv7.2, both the femoral motor and sensory branches of mutant mice showed robust Kv7.3 immunostaining at all nodes (Figure 3-6), indicating that proper Kv7.3 nodal expression does not require Kv7.2. Similarly, in the dorsal and ventral roots of mutant animals (Figure 3-7), Kv7.2 nodal staining is absent in the dorsal root and present in the ventral root, while Kv7.3 nodal staining is present at both dorsal and ventral roots. Notably, because the dorsal root is composed entirely of sensory axons, and the ventral root is predominately composed of motor axons (Karlsson and Hildebrand, 1993), the total absence of Kv7.2 immunostaining in the dorsal root coupled with the presence of Kv7.2 staining in the ventral root provide strong evidence that *Kcnq2* expression is being selectively knocked-out in the sensory neurons of our mutant animals. To quantify these results, we calculated the percentages of Kv7.2- or Kv7.3-positive nodes in each of the four nerve branches (femoral sensory, femoral motor, ventral root, and dorsal root) out of all panNav-positive nodes. As shown in figure 3-8, there were significant decreases in the percentage of Kv7.2-positive nodes in the dorsal root (1.43 ± 0.06%), femoral sensory branch (0.48 ± 0.48%), and femoral motor branch (47.13 ± 1.56%) of the mutant animals versus the wild-type littermates (99.45 ± 0.55%, 97.66 ± 0.53%, 96.36 ± 0.95% respectively). However, the percentage of Kv7.2-positive nodes in the ventral root is not different between the mutant animals (99.40 ± 0.60%) and the wild-type littermates (97.46 ± 0.41%), suggesting intact Kv7.2 expression in the motor neurons. In contrast,

the percentages of Kv7.3-positive nodes in all four nerve branches were found to approach 100% in both mutant and wild-type mice.

After demonstrating intact nodal Kv7.3 and voltage-gated sodium channels expression, we wanted to study the molecular components of the paranodes and juxtaparanodes of the *Kcnq2*-null axons. Therefore we double-labeled the sciatic nerve of mutant mice for Kv7.2 and either panNav, Caspr, or Kv1.1 antibodies. As shown in figure 3-9, the selected nodal (panNav), paranodal (Caspr) and juxtaparanodal (Kv1.1) components are the same for myelinated axons for both Kv7.2-positive (motor axons) or Kv7.2-negative (sensory axons) nodes. Thus, the molecular components of nodes, paranodes, and juxtaparanodes appeared to be maintained in *Kcnq2*-null sensory axons. Lastly, to determine if the microstructure and ultrastructure of the *Kcnq2*-null is normal, we examined epon-embedded cross-section of femoral nerves and DRG, and longitudinal sections of femoral sensory axons of mutant and wild-type animals. As shown in figure 3-10, the cross-section of both motor and sensory axons of the mutant animals showed normal shape and myelin sheath, while the ultra-thin sections of femoral sensory nerves showed that the appearance of the paranodal loops, the nodal microvilli, and the nodal axolemma of the *Kcnq2*-null sensory axons were all similar to wild-type axons (Figure 3-11). Finally, because we had previously demonstrated that Remak fibers, but not nodes of Ranvier, express Kv7.5 (King et al, publication in press), we wished to determine whether this pattern of expression is retained in *Kcnq2*-mutant mice. In both the femoral sensory and femoral motor branches, Remak fibers of both control and mutant mice showed robust Kv7.5 immunostaining. Nodes were Kv7.5-negative (Fig. 3-12), indicating that Kv7.3 forms homomeric channels in the *Kcnq2*-null axons.

Because our X-gal staining appears to show that all DRG neurons express *Pax3-Cre*, we confirmed that Kv7.2 expression is abolished in *Kcnq2*-null DRG by immunostaining unfixed DRG sections taken from both mutant and wild-type animals with the Kv7.2 antiserum (Figure 3-13). In the wild-type animals the Kv7.2 antiserum predominately labeled larger diameter DRG neurons (which were panNav-negative), while the panNav antibody primarily labeled smaller diameter neurons. In contrast, in the mutant animals, we did not detect Kv7.2 staining in any neuron, while the panNav antibody retained its wild-type staining pattern. Similar to our teased nerve results, nodes in the *Kcnq2*-null DRG lack Kv7.2 immunostaining. In addition, we had also examined unfixed trigeminal ganglia sections taken from the same groups of animals (Figure 3-14), and we detected a similar loss of Kv7.2 immunostaining in the neurons and nodes of mutant animals. As the trigeminal ganglion is analogues to the DRG, and also is neural crest-derived, this result further indicate that Kv7.2 expression was lost in all neural crest-derived sensory neurons. Finally, in order to demonstrate the lack of recombined *Kcnq2* allele in non-neural crest derived-tissue, we performed PCR on DNA samples isolated from DRG, trigeminal, and liver of mutant animals. As shown in figure 3-1 panel C, while both the floxed and recombined *Kcnq2* alleles were detected in the DRG and trigeminal ganglia, only the floxed allele was detected in the liver, indicating that the *Kcnq2* allele was being selectively deleted in neural crest-derived tissues.

Conditional *Kcnq2*-null mice exhibited normal motor performance

Although our immunohistochemical assays seem to indicate normal *Kcnq2* expression in the peripheral motor axons of our mutant animals, our X-gal staining suggest that it is possible for Kv7.2 expression to be altered in non-sensory tissues of our *Kcnq2-null* animals. Therefore we used the rotarod to test the motor performance of the mutant animals. As shown in figure 3-15, all mice tested (nine mutant and nine wild-type littermates) learned the test equally well, and showed similar performance improvement over the nine testing sessions. The average time to fall for all sessions was statistically equal between the mutant (162.63 ± 12.87 seconds) and wild-type (169.89 ± 6.12 seconds) groups ($P = 0.62$). Therefore, the conditional deletion of *Kcnq2* did not appear to affect the motor performance of mutant animals.

Conditional *Kcnq2*-null mice showed increased signs of mechanical allodynia and thermal hyperalgesia

A previous study on the role of M-current in behavior models of pain have reported that local injection of the Kv7-blocker XE991 in normal uninjured rat hindpaws did not produce mechanical allodynia (Linley et al., 2008). However, because XE-991 is not Kv7.2-specific (Wang et al., 1998, Wang et al., 2000, Schwarz et al., 2006), we examined our *Kcnq2*-null mice to see if decreased Kv7.2-expression correlates to increased mechanical allodynia. To do so, we measured pain withdrawal threshold using von Frey filaments. As shown in figures 3-16, the *Kcnq2*-null mice on average had a lower withdrawal threshold (0.65 ± 0.07g) compared to the wild-type littermates by a statistically significant amount (0.93 ± 0.09g; $P < 0.05$).

Dost et al. (2004) reported that intraperitoneal injection of retigabine was able to reduce signs of thermal hyperalgesia in rats, but another study found oral administration of retigabine had no effect against acute noxious thermal stimuli in rats (Blackburn-Munro and Jensen, 2003). To address this conflict, and to investigate if lower Kv7.2 expression can increase thermal hyperalgesia, we measured the withdrawal latency of the mutant and wild-type animals from noxious thermal stimuli using the Hargreaves' test. As shown in figure 3-17, the *Kcnq2*-null mice on average exhibited shorter withdrawal latency (3.73±0.164 seconds) versus the wild-type littermates by a statistically significant amount (4.28 ± 0.158 seconds; $p < 0.05$). Taken together, our results suggest that loss of Kv7.2 expression can lead to increased mechanical allodynia and thermal hyperalgesia.

Conditional *Kcnq2*-null mice showed increased AHP peak undershoot and decreased spike frequency adaptation

In a previous study using a dominant negative mutation of Kv7.2 to suppress M currents in the mouse hippocampus, Peters et al. (2005) found that the mutant CA1 pyramidal neurons exhibited decreased spike-frequency adaptation, and these changes can be replicated in the control neurons by the application of XE991, demonstrating that the altered biophysical properties of the mutant neurons were a result of M-current suppression. In this study we examined the electrophysiological properties of the *Kcnq2*-null DRG neurons. In addition, we utilized the M-channel blocker TEA, which at 3 mM should primarily affect only Kv7.2 (and Kv7.2/Kv7.3 heteromers) but no other Kv7 subunits (Wang et al., 1998, Hadley et al., 2000, Lerche et al., 2000, Hadley et al., 2003).

We first dissociated and cultured twenty-five lumbar DRG neurons from each genotype (five wild-type and five mutant mice), then we used whole cell patch-clamp recording techniques to examine the passive membrane properties and firing properties of DRG neurons (Table 3-1). While we recorded from various neuron sizes, the average cell size recorded from each genotype (as estimated from membrane capacitance) was not statistically different between the control and *Kcnq2*-null groups (38.75 ± 3.3 pF versus 45.3 ± 4.14 pF, respectively).

To investigate the afterhyperpolarization (AHP) properties, we elicited single AP with brief (3-ms) depolarizing current steps, and measured both the peak undershoot (most negative potential during the AHP, in mV) as well as the duration (in ms) of AHPs from each neuron. As shown in figure 3-18, prior to TEA application the average AHP peak undershoot of mutant DRG neurons was 3.92% more negative than wild-type neurons (-85.7 ± 0.97 mV versus -82.47 ± 1.28 mV, respectively; $P < 0.05$), while the AHP duration was not statistically different between the two groups (262.9 ± 39.91 ms versus 205.97 ± 31.79 ms, respectively). After 3mM TEA application, both the AHP duration and peak magnitude of the wild-type neurons did not change by a statistically significant amount (221.63 ± 48.58 ms and -83.92 ± 1.21 mV, respectively). Furthermore, the AHP properties of the mutant neurons also were not affected by TEA application.

Next, we examined the AP firing patterns and spike-frequency adaptation by injecting 500-ms depolarizing current steps into DRG neurons. For each neuron, a threshold current (rheobase) was determined with incremental (100 pA) 500-ms current

steps, starting from 0.1 nA. Then we applied 500-ms depolarizing current steps to 1, 2, and 3 times rheobase and recorded the number of APs evoked by each current step. To determine the responsiveness of DRG neurons to absolute (as opposed to relative threshold) depolarizing stimuli, we injected a series of 500-ms incremental current steps (0.1-0.9 nA). As shown in figure 3-19, the *Kcnq2*-null neurons produced significantly more APs and exhibited less spike-frequency adaptation than control neurons. In addition, 3 mM TEA was able to significantly increase the number of APs and decrease spike-frequency adaptation in control neurons more than in cells from mutant mice. Lastly, TEA decreased the rheobase of wild-type neurons by 49% (Table 1; 0.39 ± 0.07 nA from 0.77 ± 0.23 nA; $P < 0.05$), which is also statistically different than mutant neurons after TEA (0.88 ± 0.19 nA); on the other hand, the rheobase of the mutant was not affected by TEA (0.88 ± 0.19 nA from 0.81 ±0.16 nA). Therefore, the lack of *Kcnq2* expression in mutant DRG neurons was associated with increased excitability and decreased spike-frequency adaptation, and this hyper-excitability could be replicated in wild-type neurons by the application of Kv7.2-specific concentration of TEA.

DISCUSSION

Deleting *Kcnq2* enabled us to investigate directly the role of Kv7.2 in sensory neurons. Deleting Kv7.2 had no discernible effect on the structure of myelinated axons, or on the motor performance of the mutant animals. There were modest effects on both acute thermal and mechanical nociceptive behaviors, and on the electrophysiological properties of sensory neurons.

Kv7.3 nodal expression does not depend on Kv7.2

Our data confirm that Kv7.2 and Kv7.3 are found at nodes (Devaux et al., 2004, Pan et al., 2006, Schwarz et al., 2006), although we document an even greater extent of their colocalization. This finding suggests that Kv7.2/Kv7.3 heteromers are the main Kv7 channels at PNS nodes. The localization of Kv7.3 at *Kcnq2*-null nodes demonstrates that nodal Kv7.3 expression does not require Kv7.2, in contrast to previous in vitro studies (Schwake et al., 2000, Gomez-Posada et al., 2010). Because both Kv7.2 and Kv7.3 contain an ankyrin-G binding domain in their C-termini (Pan et al., 2006), it is reasonable to expect that Kv7.3 could be selectively retained at nodes and AIS. Indeed, the deletion of the ankyrin-G binding motif in Kv7.2 alone does not alter the AIS localization of Kv7.2/Kv7.3 heteromers (Rasmussen et al., 2007). In addition, the normal molecular components of nodes (panNav), paranodes (Caspr), and juxtaparanodes (Kv1.1), as well as ultrastructure of *Kcnq2*-null sensory myelinated axons, shows that these features do not depend on Kv7.2. Finally, we found that Kv7.5 expression in Remak bundles is maintained in *Kcnq2*-null nerves. While Kv7.5 and Kv7.3 can form heteromeric channels *in vitro* (Schroeder et al., 2000), we did not detect Kv7.5-immunoreactivity at *Kcnq2*-null nodes, suggesting that in our mutant animals, the nodal Kv7 channels are comprised of Kv7.3 homomers.

Kv7.2 contributes to the regulation of neuronal excitability

Kv7 channels activate at subthreshold potentials and do not become inactivated, thereby contributing to the regulation of neuronal excitability (Brown and Passmore, 2009). This has been documented with a variety of ways: Kv7 blockers (linopridine or XE991), dominant-negative Kv7.2 mutants, or decreased Kv7.2 expression have all been shown to increase excitability (decreased spike-frequency adaptation and/or increased number of action potentials) of hippocampal neurons (Aiken et al., 1995, Yue and Yaari, 2004, Gu et al., 2005, Peters et al., 2005, Shah et al., 2008) and of somatic and visceral sensory neurons (Passmore et al., 2003, Rivera-Arconada and Lopez-Garcia, 2005, Wladyka and Kunze, 2006, Wladyka et al., 2008). Kv7 enhancer (retigabine) produces the opposite effects (Lerche et al., 2000, Brueggemann et al., 2007). In isolated rat peripheral nerves, retigabine slows axonal conduction, and these effects can be reversed by application of 20 μM linopridine or 10 mM TEA (Devaux et al., 2004). Schwarz et al. (2006) showed that XE991 both abolishes the slow accommodation to the depolarization and the post-depolarization undershoot of action potential at nodes, as well as increases repetitive firing and decreases spike-frequency adaptation in rat motor axons. Taken together, these results indicate that Kv7 channels regulate both neuronal and axonal activity.

Our analysis of *Kcnq2*-null DRG neurons confirmed and extended these prior works. By using TEA at a Kv7.2-specific concentration (Wang et al., 1998, Hadley et al., 2000, Lerche et al., 2000, Hadley et al., 2003), we showed that Kv7.2 contributes to the spike-frequency adaptation of sensory neurons. Because TEA did not further decrease spike-frequency adaptation in *Kcnq2*-null neurons, decreased Kv7.2 activity is the most parsimonious explanation for the increased excitability of the *Kcnq2*-null neurons. While

we did not see any decrease in the rheobase of the mutant neurons pre-TEA application, it is possible that Kv7.3, which is also expressed in DRG neurons (Passmore et al., 2003), is sufficient to maintain normal rheobase in the absence of Kv7.2.

Classically, AHP can be subdivided into three phases: fast (1-5 ms), medium (50-200 ms), and slow (500 ms to several seconds) AHP (Madison and Nicoll, 1984, Storm, 1990, Gu et al., 2005). Because the slow activation speed of the M channels (tens of milliseconds), they do not contribute materially to the fast AHP (Brown and Passmore, 2009), which is instead considered to be mediated by the Big Potassium (BK) family of potassium channels (Storm, 1990). Indeed, our *Kcnq2*-null neurons exhibited only slightly more negative fast AHP amplitude compared to control neurons, and the application of TEA did not produce statistically significant changes in fast AHP amplitudes in both mutant and control neurons. The negative TEA results indicate that Kv7.2 does not play an appreciable role in the fast AHP. While we cannot explain why the fast AHP amplitude of our *Kcnq2*-null neurons was actually slightly more negative compared to the control neurons, the fact that Kv7.2-specific concentration of TEA did not change the fast AHP amplitude of the control neurons suggest that this difference may not be due to the lack of Kv7.2 activity.

On the other hand, the identity of the channel(s) that mediates the slow AHP is still uncertain (Tzingounis and Nicoll, 2008, Matthews et al., 2009), but decreases in Kv7.2 or Kv7.5 activity has been shown to reduce slow AHP in mouse hippocampal neurons (Tzingounis and Nicoll, 2008, Tzingounis et al., 2010). Our *Kcnq2*-null DRG neurons also displayed a decrease in slow AHP amplitude compared to control neurons,

and 3mM TEA was able to reduce the slow AHP amplitude of control neurons, while having no effect on mutant neurons. While a previous study have shown that 10 μM XE991 application in hippocampal had actually enhanced slow AHP, other experiments showed that muscarine, which suppresses Kv7 channels (Brown and Adams, 1980), was able to inhibit slow AHP (Ghamari-Langroudi and Bourque, 2004, Hu and Mooney, 2005). Therefore, while the exact contribution of Kv7 channels to slow AHP remained uncertain, our results raise the possibility that Kv7.2 activity does contribute, at least in part, to slow AHP in DRG neurons.

Increased mechanical allodynia and thermal hyperalgesia in *Kcnq2*-null mice

There results regarding the role of Kv7 channels on mechanical allodynia and thermal hyperalgesia are inconsistent. Retigabine increases the tail withdrawal threshold to noxious thermal stimuli at a dose-dependent manner (Dost et al., 2004). Because this effect was not reversed by the co-administration of linopridine, it may be due to non-Kv7-specific effect of retigabine, and it also conflicts with another study using different methodology, in which found that retigabine did not affect the withdrawal response from noxious thermal stimuli (Blackburn-Munro and Jensen, 2003). Lastly, intraplantar injections of XE991 into the mice hindpaws did not induce thermal hyperalgesia or mechanical allodynia, with the caveat that the actual concentration of XE991 that reached the sensory axons cannot be established (Linley et al., 2008). The above studies shared the important limitation that the enhancers and blockers likely act on most or all Kv7 subunits, and potentially other channels (for example $GABA_A$ (Otto et al., 2002)), and the

distribution of these subunits may be heterogenous. For example, we found that unmyelinated axons express Kv7.5 (King et al, publication in press), which could also be the site of these pharmacological agents.

In our current study we sought to minimize these confounding factors by analyzing a type of myelinated sensory axons that lacks Kv7.2, the A-delta fibers. While the technical limitations of our behavior tests do not allow us to completely differentiate A-delta fiber mediated nociception from C-fiber mediated nociception, previous studies suggest that withdrawal reflex behavior from both acute noxious thermal stimuli (Price and Dubner, 1977, Dubner and Bennett, 1983, Yeomans and Proudfit, 1996, Hargreaves et al., 1998, Cuellar et al., 2010) and punctate mechanical stimuli (Dubner and Bennett, 1983, Koltzenburg et al., 1993, Ziegler et al., 1999) are both primarily mediated by A-delta fibers. Specifically, Yeomans and Proudfit (1996) found that radiant heating of rat hindpaw at a high rate of 6.5^{o}C/sec for 6 seconds primarily evokes A-delta fiber response, while a low rate of 0.9^{o}C/sec for 20 seconds primarily activates C-fibers response; notably, the C-fiber response at either heating rate did not begin until 5-8 seconds after onset of heating. Because the thermocouple of our Hargreaves apparatus had been shown to raise rat hindpaw temperature from 30^{o}C to 49^{o}C in 5 seconds (3.8^{o}C/sec) (Dirig et al., 1997), and because the average withdrawal latency of both mutant and control animals in our Hargreaves' test were less than 5 seconds (3.7 sec and 4.3 sec, respectively), our results suggest that the increased thermal hyperalgesia behavior of our *Kcnq2*-null mutant animal was, at least in part, as a result of increased A-delta fiber activity. Furthermore, Ji et al. (2007) reported that rats treated with spinal nerve ligation displayed decreased mechanical threshold of A-delta fibers, but not of C-fibers, and simultaneously exhibited

increased mechanical allodynia (as tested with von Frey filaments), suggesting that the increased mechanical allodynia of our *Kcnq2*-null animals may also be due to increase A-delta fiber activity. Taken together, the increased thermal hyperalgesia and mechanical allodynia exhibited by our *Kcnq2*-null mice suggest that the lack of Kv7.2 expression in the A-delta fibers may produce increased acute thermal and mechanical nociception. Because our rotarod test provided no evidence of different motor performance between our mutant and control animals, the increased nociceptive responses observed in the *Kcnq2*-null mice is unlikely to be a consequence of altered motor behavior. However, because our X-gal stainings indicate that *Pax3*-Cre expression may also be present in regions of the brain, the possibility exists that the loss of Kv7.2 expression within the central nervous system may also have played a role in the increased thermal hyperalgesia and mechanical allodynia exhibited by our *Kcnq2* mutant mice.

Taken together, our work raises the possibility that a decrease in Kv7.2 activity can increase sensory neuronal excitability, and lead to increased pain perception.

Acknowledgments. We like to thank Drs. Edward Cooper and Virginia Lee for the cDNAs and antisera, Dr. Fan Wang for providing us with the *Avil-Cre* mice, Dr. Gordon Barr for loaning us the Hargreaves' Apparatus, Dr. Ted Abel for loaning us the rotarod, Dr. Beth Winkelstein for advices regarding the von Frey hair filament test, Dr. Marc Dichter for the use of their electrophysiology rig, and Dr. Jian Li for the processing and sectioning of the epon-embedded samples.

Figure 3-1

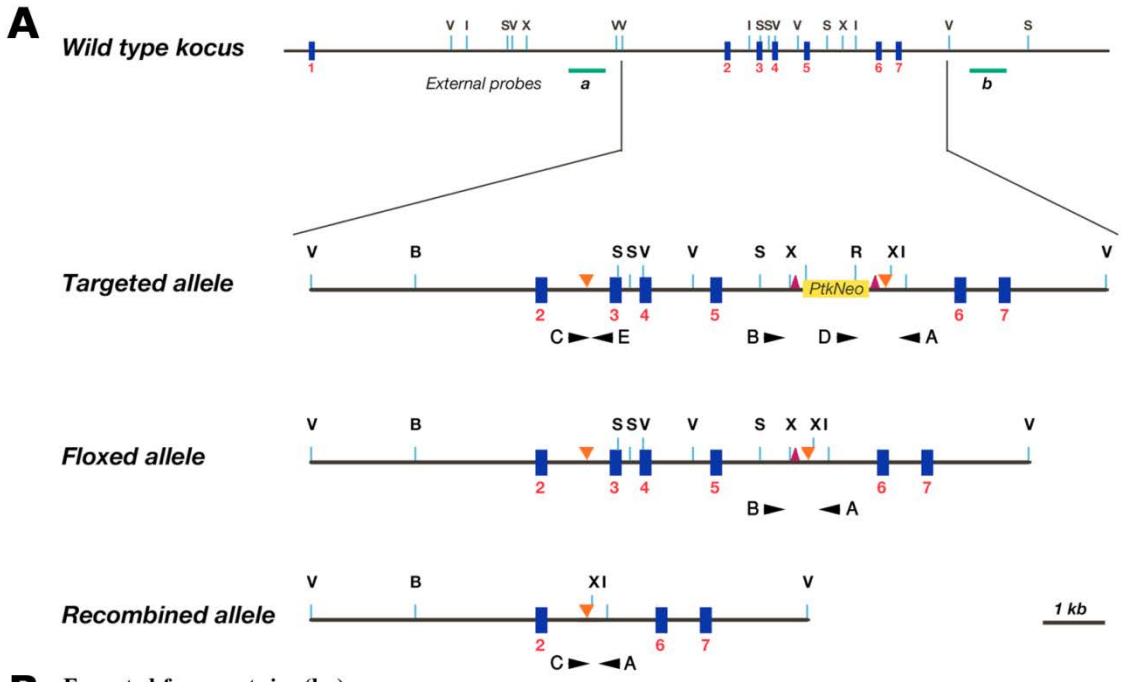

B

Expected fragment size (bp):

Primer set	*WT*	*FRTlox*	*Floxed*	*KO*
A-D	-	400	-	-
A-B	280	1620	394	-
*A-C**	(3800)	(5000)	(3800)	380
C-E	270	300	300	-

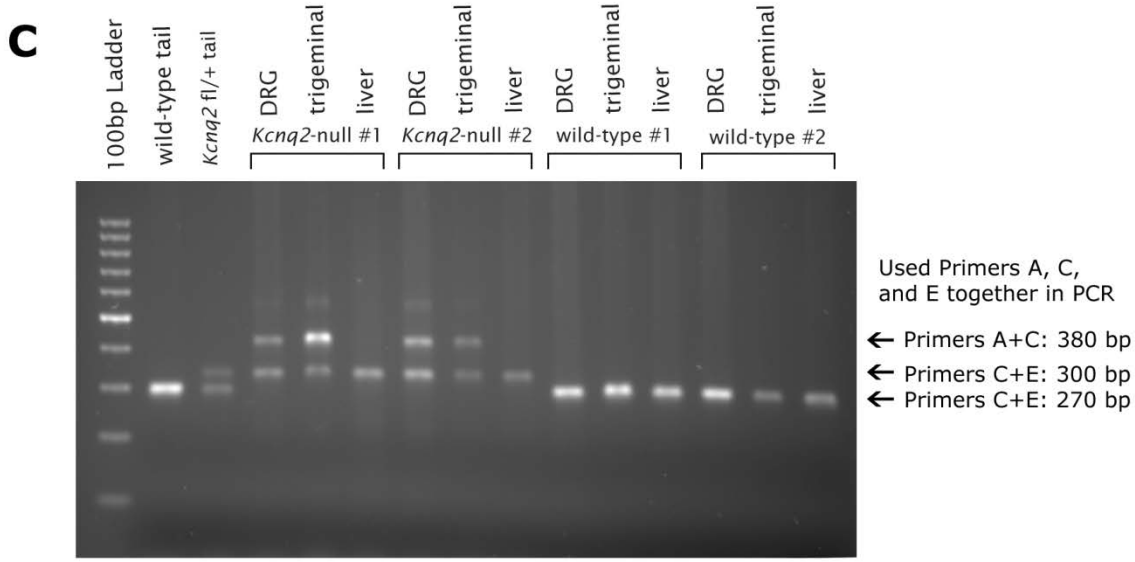

Figure 3-1: Targeting strategy to generate an inducible deletion allele of *Kcnq2*.

Panel A shows the genomic arrangement of the first seven exons of wild type *Kcnq2*. The external probes *a* and *b* are indicated as horizontal green lines. The targeted allele contains two *loxP* sites (orange triangles facing down) before the third, and after the fifth exons. A cassette containing a *neo* gene under the herpes simplex *Tk* promoter (*PtkNeo*; yellow box), flanked by two FRT sites (purple triangles facing up) is inserted in a unique XhoI site in the intron between the fifth and the sixth exons. The targeting vector (not shown) is the same as the pictured targeted allele except that it includes a diphtheria toxin (DT) gene as a negative selection marker after the last EcoRV site. Mice carrying the floxed allele were obtained after the removal of the *PtkNeo* cassette by mating the targeted mice with a general FRT-deleter strain. The recombined allele lacks exons 3-5, is generated after Cre-mediated deletion.

Panel B show the expected sizes of the amplified DNA with the different primer pairs.

Panel C shows the PCR results of DNA isolated from DRG, trigeminal ganglia, and liver of *Kcnq2*-null mice and their control littermates, along with tail DNA from control and heterozygous floxed *Kcnq2* mice (*Kcnq2* fl/+). Samples were subjected to PCR with the indicated primers, and the reaction products were separated by gel electrophoresis. A ~270 bp band, corresponding to the predicted size of wild-type *Kcnq2* allele, was detected in both tail samples, as well as in all of the samples from the control littermates. A ~300 bp band, corresponding to the predicted size of the floxed *Kcnq2* allele, was detected in the heterozygous tail, as well as in all of the *Kcnq2*-null samples. A ~380 bp

band, corresponding to the predicted size of the recombined *Kcnq2* allele, was detected in both the DRG and the trigeminal ganglia of the *Kcnq2*-null mice, but not in their liver.

Figure 3-2

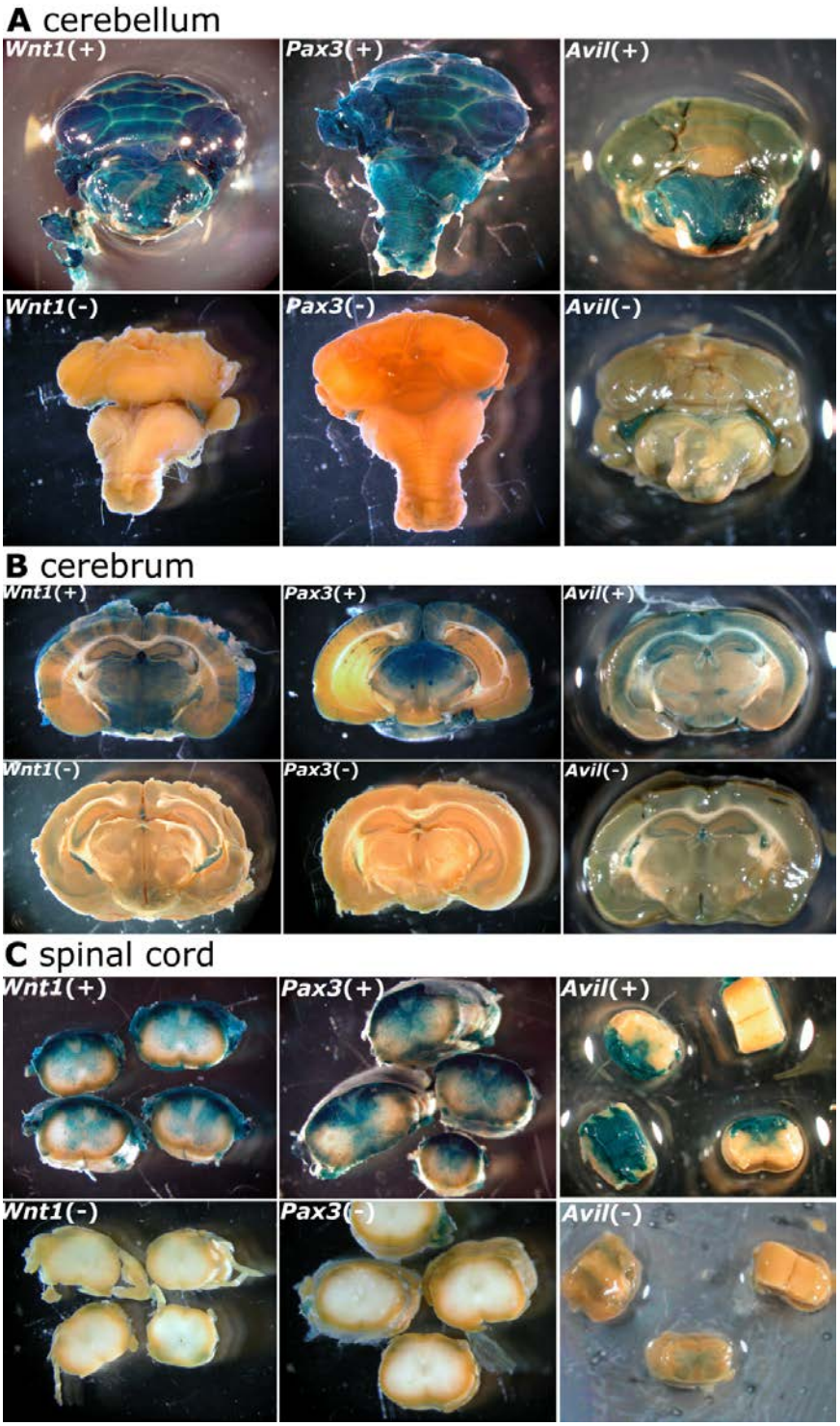
A cerebellum
Wnt1(+)
Pax3(+)
Avil(+)
Wnt1(-)
Pax3(-)
Avil(-)
B cerebrum
Wnt1(+)
Pax3(+)
Avil(+)
Wnt1(-)
Pax3(-)
Avil(-)
C spinal cord
Wnt1(+)
Pax3(+)
Avil(+)
Wnt1(-)
Pax3(-)
Avil(-)

Figure 3-2: Expression of *Wnt1-Cre, Pax3-Cre, and Avil-Cre*.

These are digital images of samples taken from *Wnt1-Cre*-positive (n=3), *Pax3-Cre*-positive (n=3), *Avil-Cre*-positive (n=3), and their *Cre*-negative littermates (n=3 for each genotype) that also expressed the *Rosa26* reporter gene. The sections were stained for beta-galactoside activity (X-gal was the chromogen), and photographed with a stereo dissecting microscope. None of the samples taken from any of the control animals showed any X-gal staining. In contrast, a majority of the cerebellum, regions of the cerebrum (including the cortex, the hippocampus, the thalamus, and the hypothalamus), and the dorsal part of the spinal cord (including the dorsal roots) were stained with X-gal in mice expressing *Wnt1-Cre*. These regions of the brain and spinal cord were also stained in mice expressing *Pax3-Cre* (but with more intense thalamic staining and no hippocampal or hypothalamic staining). Lastly, mice expressing *Avil*-Cre showed much less cerebellum labeling, with cerebrum staining primarily seen in the cortex and the hippocampus, as well as staining of the dorsal part of the spinal cord (including the dorsal roots).

Figure 3-3

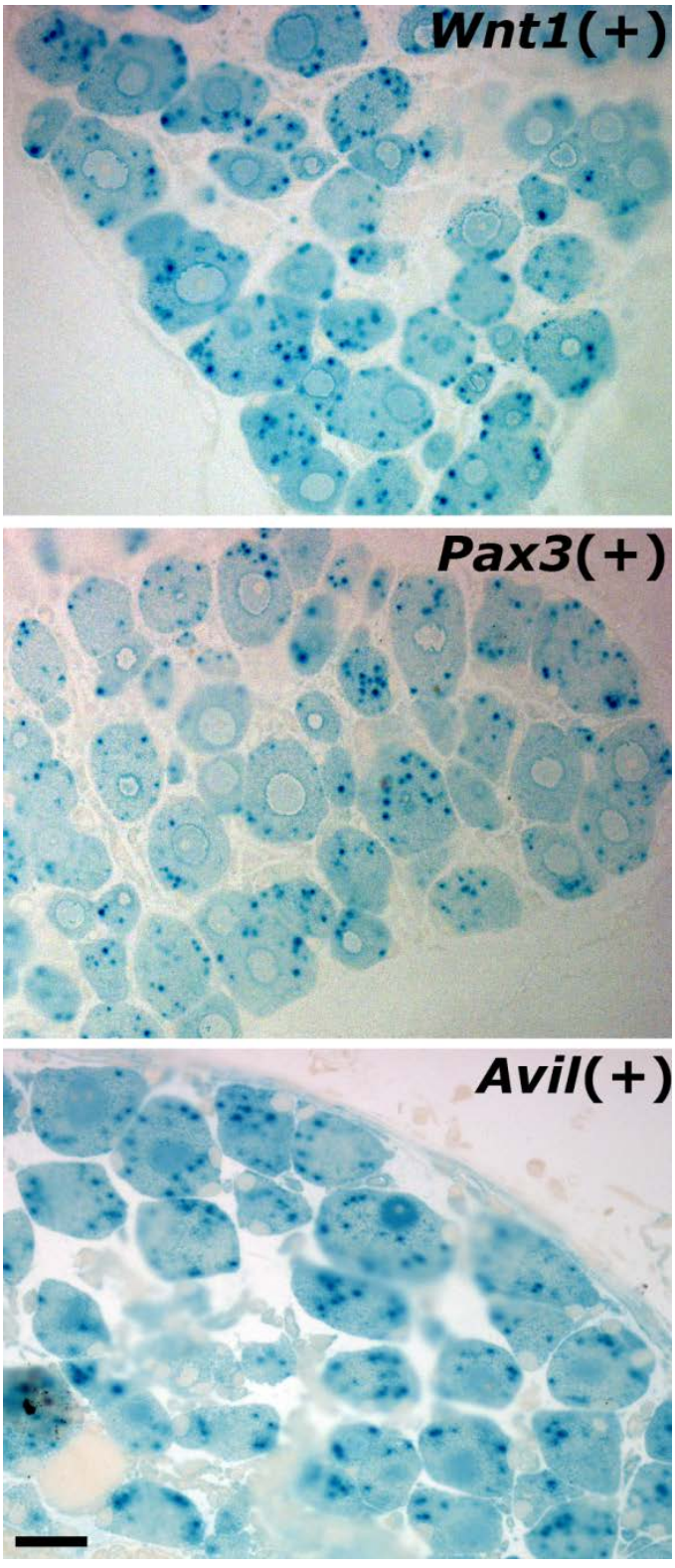

Figure 3-3: All sensory neurons expressed *Wnt1-Cre, Pax3-Cre,* and *Avil-Cre*.

These are digital images of 1 μm thick epoxy sections of DRG neurons from *Wnt1-Cre*-positive (n=3), *Pax3-Cre*-positive (n=3), and *Avil-Cre*-positive (n=3) mice that also expressed the *Rosa26* reporter gene. The DRGs had been labeled with X-gal. All of the *Wnt1-Cre, Pax3-Cre, and Avil-Cre*-positive neurons showed X-gal staining (blue). Scale bar: 20 μm.

Figure 3-4

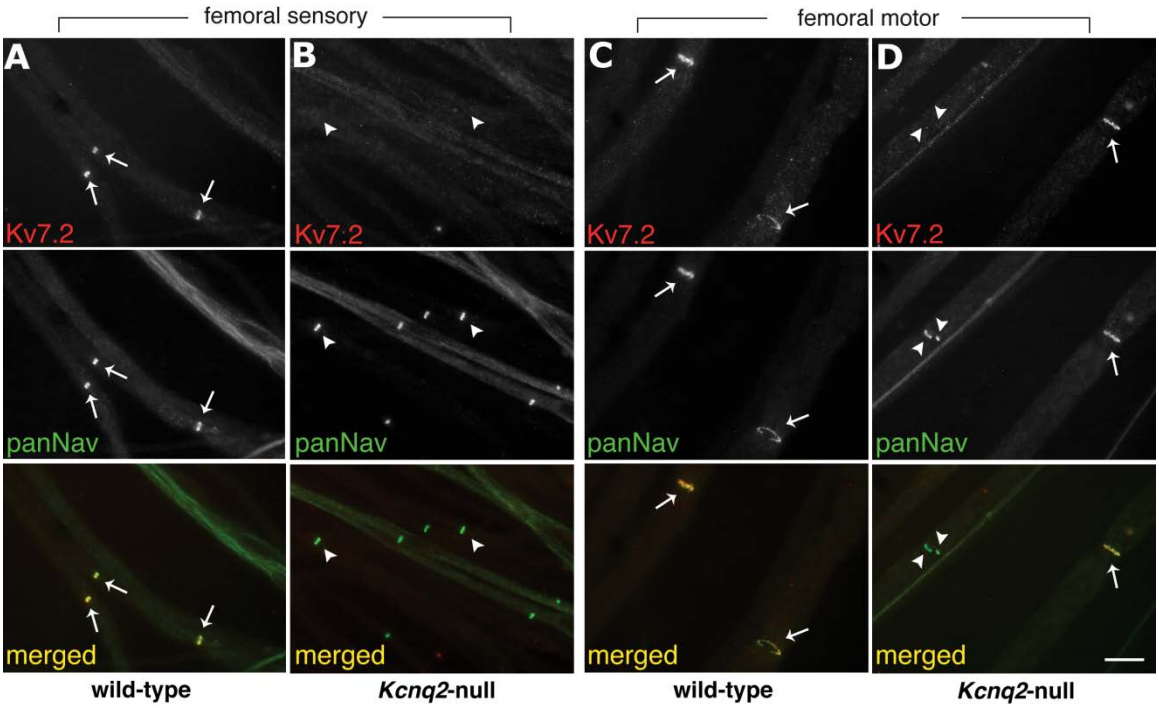

Figure 3-4: Selective loss of *Kcnq2* from the nodes of sensory axons.

These are digital images of unfixed teased fibers, double-labeled for Kv7.2 (red) and voltage-gated sodium channels (panNav; green). In the femoral sensory branch, Kv7.2 is found at all nodes of Ranvier (arrows) in wild-type animals, but is not detected at any nodes (arrowheads) in *Kcnq2*-null animals. In the femoral motor branch, Kv7.2 is found at all nodes of Ranvier (arrows) in wild-type animals, but is not detected at some nodes (arrowheads) in *Kcnq2*-null animals. Scale bar: 10 µm.

Figure 3-5

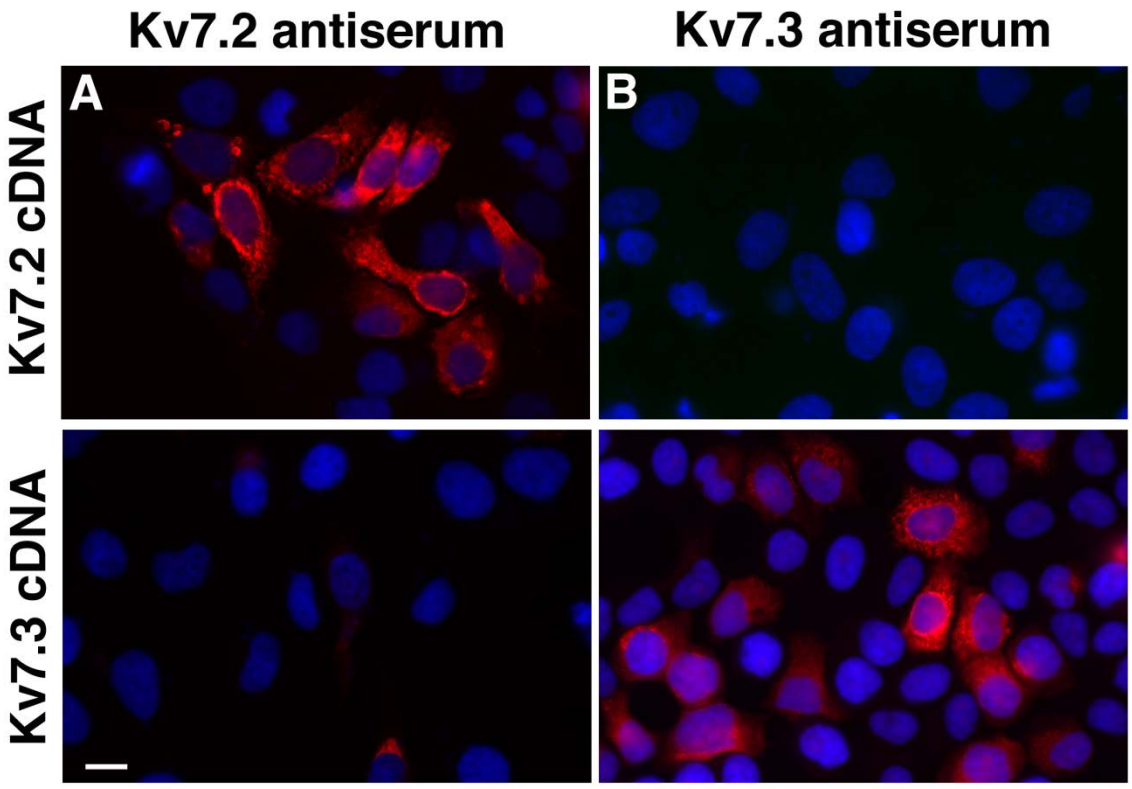

Figure 3-5: Kv7.2 antiserum recognized Kv7.2 but not Kv7.3.

These are images of HeLa cells transiently transfected to express human Kv7.2 or Kv7.3, labeled with the indicated antiserum and counterstained with DAPI. Note that the Kv7.2 antiserum (column A) labels cells expressing Kv7.2 and not Kv7.3, and that the Kv7.3 antiserum (column B) labels cells expressing Kv7.3 but not Kv7.2. Scale bar: 20 μm.

Figure 3-6

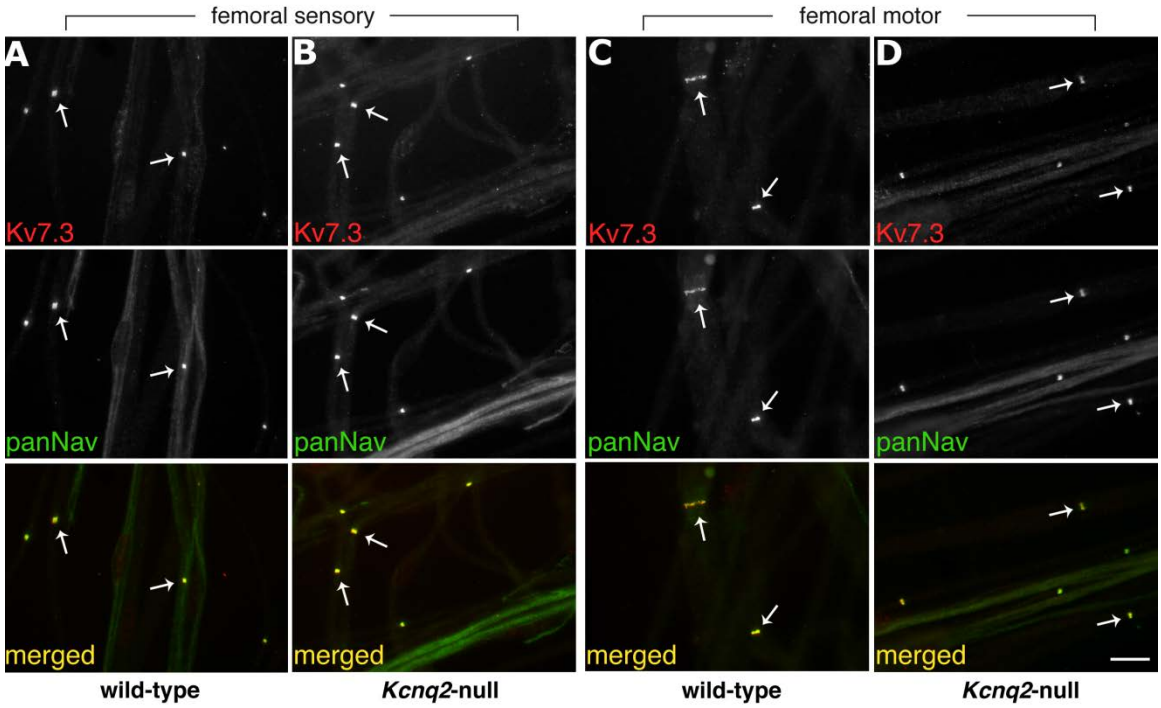

Figure 3-6: Kv7.3 is found at all nodes in *Kcnq2*-null mice.

These are digital images of unfixed mouse teased nerves, double-labeled for Kv7.3 (red) and panNav (green). In the femoral motor and sensory branches of both mutant and wild-type mice, all panNav positive nodes are also Kv7.3-positive (arrows). Scale bar: 10 µm.

Figure 3-7

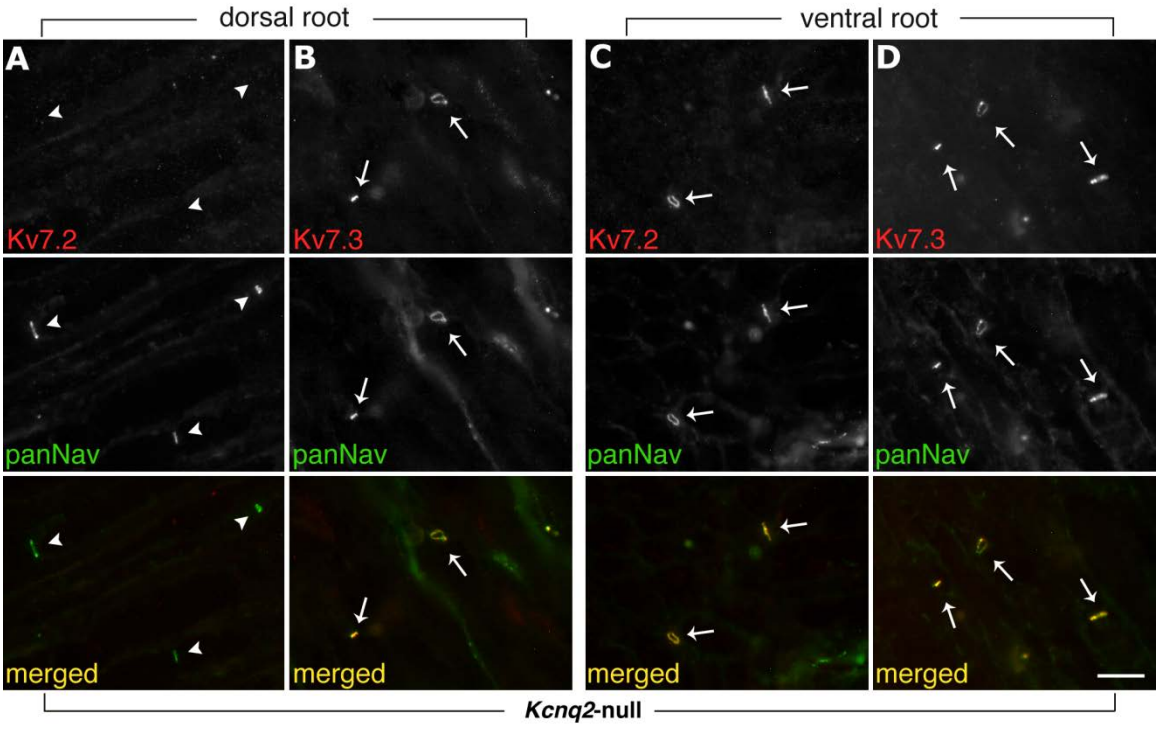

Figure 3-7: Selective loss of *Kcnq2* from the nodes of sensory axons.

These are digital images of unfixed mouse teased nerves, double-labeled for either Kv7.2 or Kv7.3 (red) and panNav (green). In the dorsal roots of mutant animals, Kv7.2 is not detected at any node (arrowheads), where Kv7.3 is found at every node (arrows). In the ventral roots of mutant mice, note that all nodes are Kv7.2- and Kv7.3-positive (arrows). Scale bar: 10 µm.

Figure 3-8

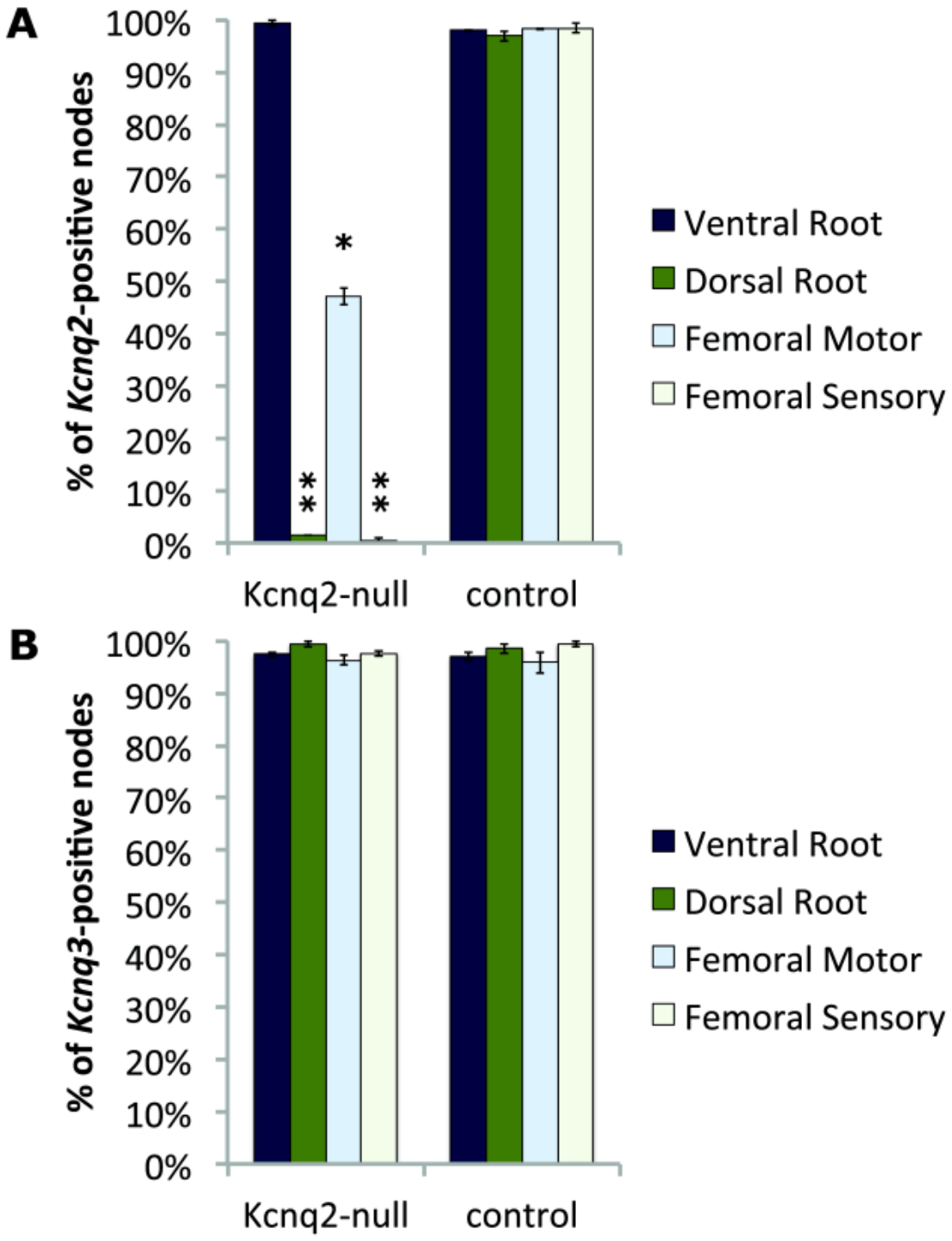
A
100%
90%
80%
70%
60%
50%
40%
30%
20%
10%
0%
% of Kcnq2-positive nodes
*
**
**
Kcnq2-null
control
Ventral Root
Dorsal Root
Femoral Motor
Femoral Sensory
B
100%
90%
80%
70%
60%
50%
40%
30%
20%
10%
0%
% of Kcnq3-positive nodes
Kcnq2-null
control
Ventral Root
Dorsal Root
Femoral Motor
Femoral Sensory

Figure 3-8: Selective loss of *Kcnq2*, but not *Kcnq3*, from the nodes of sensory axons.

The bar graphs represent average proportion of panNav-positive nodes that are Kv7.2- (panel A) or Kv7.3- (panel B) positive from the indicated source (n=3 for all samples). Note that ~0% of nodes in the dorsal root and femoral sensory branch, and 50% in the femoral motor branch, were Kv7.2-positive. Error bars represent SEM; * $P < 0.05$; ** $P < 0.01$ (two-way ANOVA).

Figure 3-9

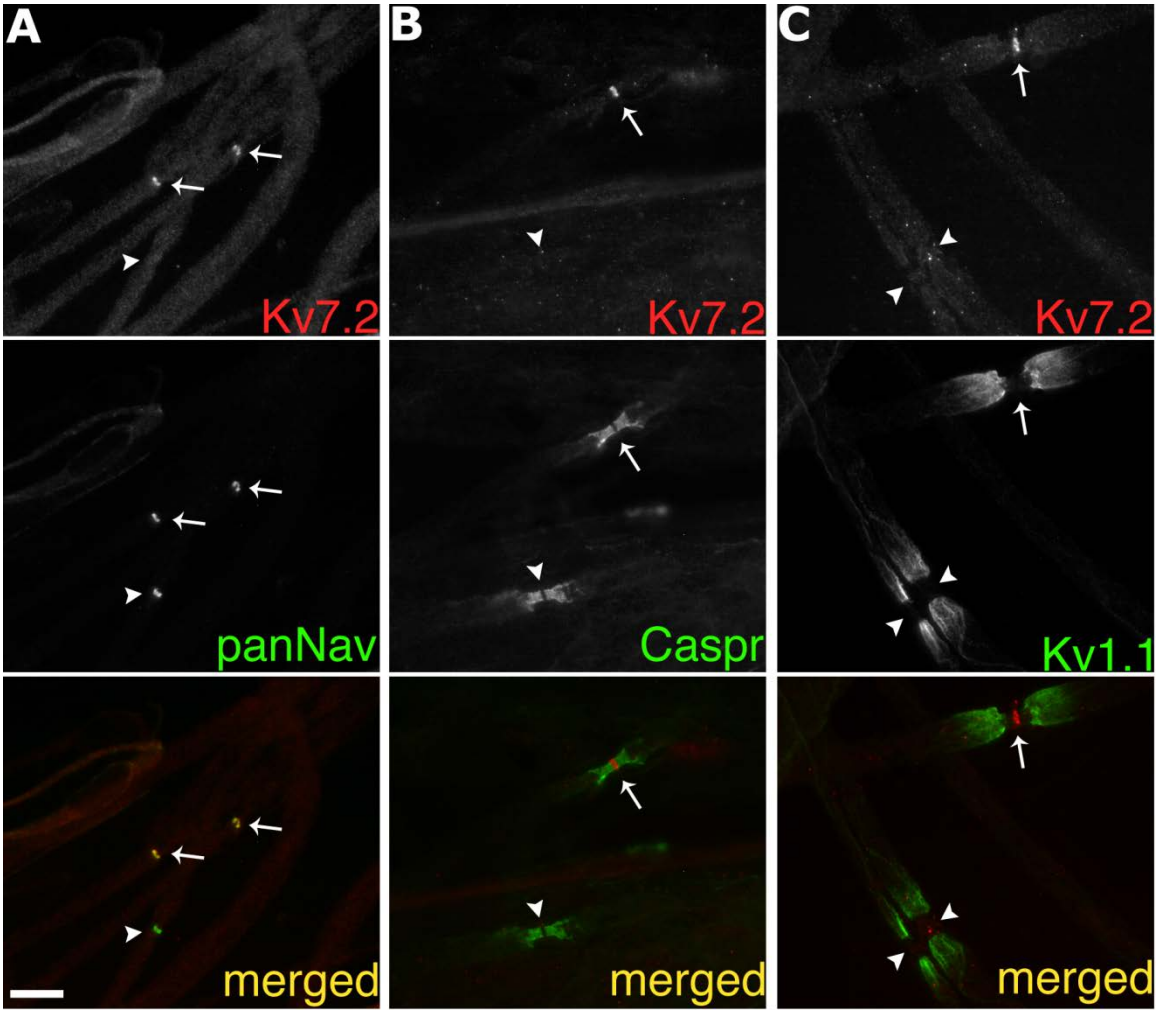

Figure 3-9: The molecular components of nodes, paranodes and juxtaparanodes are maintained in *Kcnq2*-null sensory axons.

These are digital images of teased fibers from unfixed mutant sciatic nerves, double-labeled for Kv7.2 (red) and either panNav (column A), Caspr (column B), or Kv1.1 (column C); all green. The selected nodal (panNav), paranodal (Caspr) and juxtaparanodal (Kv1.1) components are the same for myelinated axons with Kv7.2-positive (motor axons) or Kv7.2-negative (sensory axons) nodes. Scale bar: 10 µm.

Figure 3-10

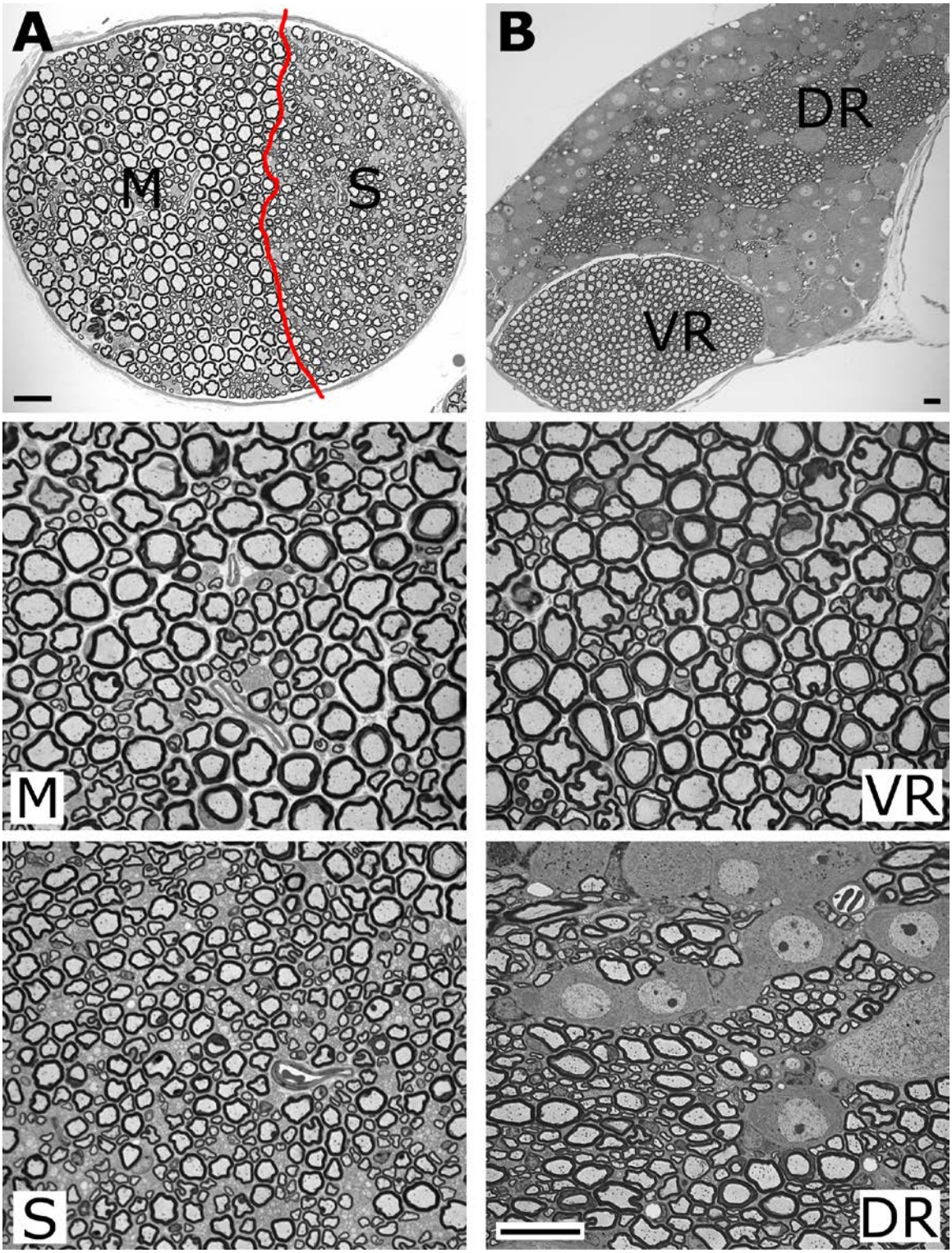

Figure 3-10: *Kcnq2*-null sensory axons in femoral sensory branch and dorsal root have normal cross-sectional appearance

These are digital images of 1 µm-thick *Kcnq2*-null femoral nerve and DRG cross-sections, stained with toluidine blue. First panel of column A shows a 20x magnification of the femoral nerve cross-section, with the division between motor (M) and sensory (S) branch approximately demarcated by the red line. The 100x magnification of both femoral motor and sensory branches show that myelinated axons look normal. First panel of column B shows a 10X magnification of the DRG cross-section, with accompanied ventral (VR) and dorsal (DR) roots. The 100x magnification of both ventral and dorsal roots show that myelinated axon look normal. Scale bars at all magnification: 20 µm.

Figure 3-11

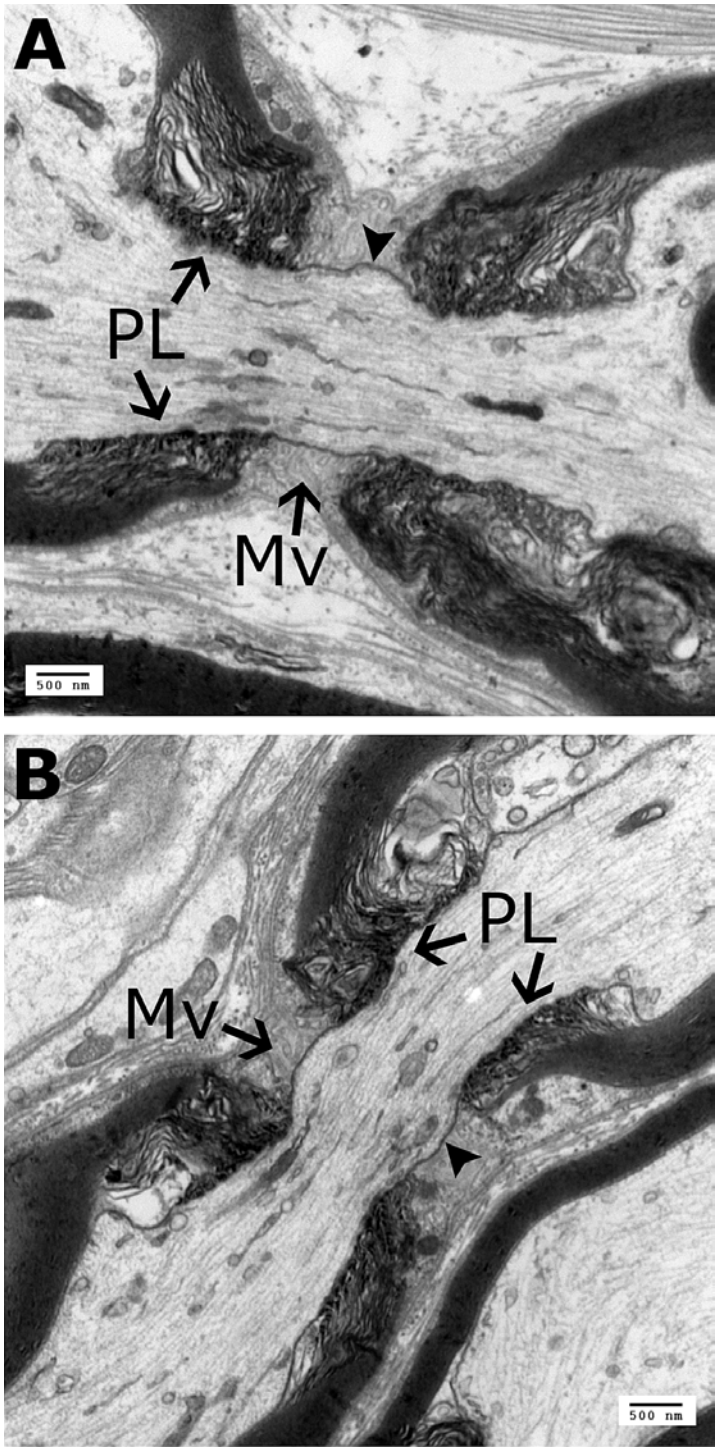

Figure 3-11: *Kcnq2*-null sensory axons have normal nodal and paranodal ultrastructure.

These are digital images of ultra-thin sections of femoral sensory nerves from wild-type (panel A) and mutant (panel B) mice. The appearance of the paranodal loops (PL), the nodal microvilli (Mv), and the nodal axolemma (arrowheads), were all similar. Scale bar: 500 nm.

Figure 3-12

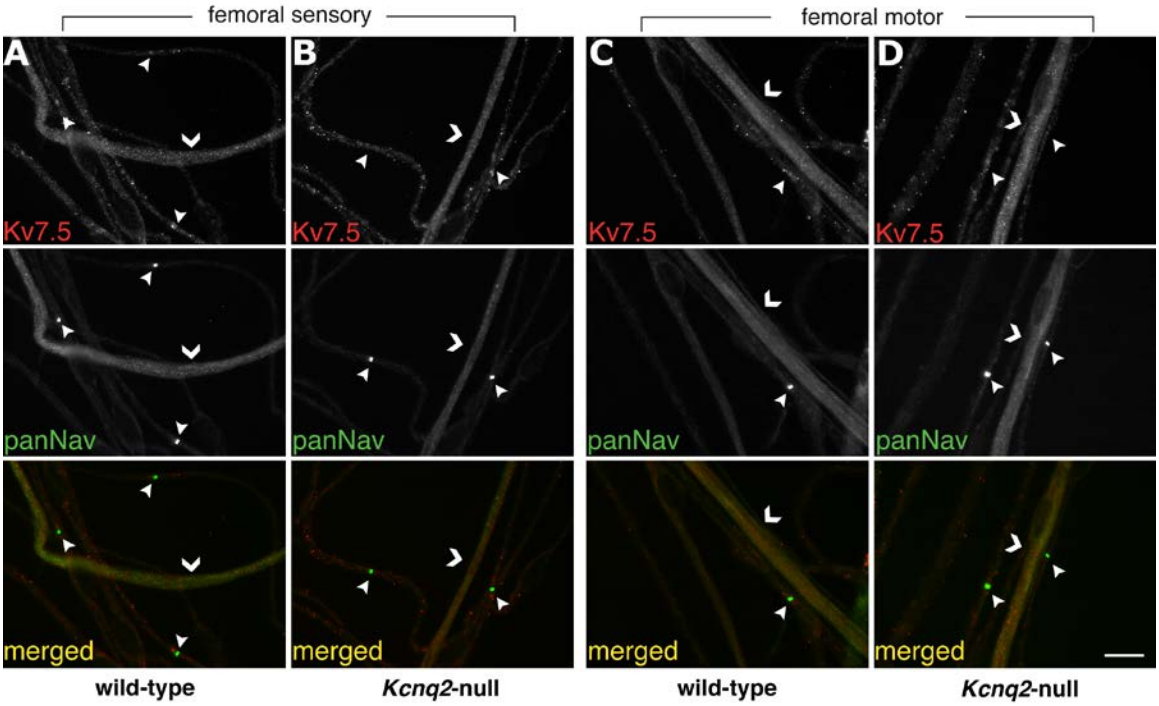

Figure 3-12: Remak fiber expression of Kv7.5 is maintained in *Kcnq2* mutant mice

These are digital images of unfixed mouse teased nerves, double-labeled for Kv7.5 (red) and panNav (green). In the femoral sensory and motor branches of both mutant and wild-type mice, all panNav-positive Remak fibers are Kv7.5-positive (chevrons), while all panNav-positive nodes are Kv7.5-negative (arrowheads). Scale bar: 10 µm.

Figure 3-13

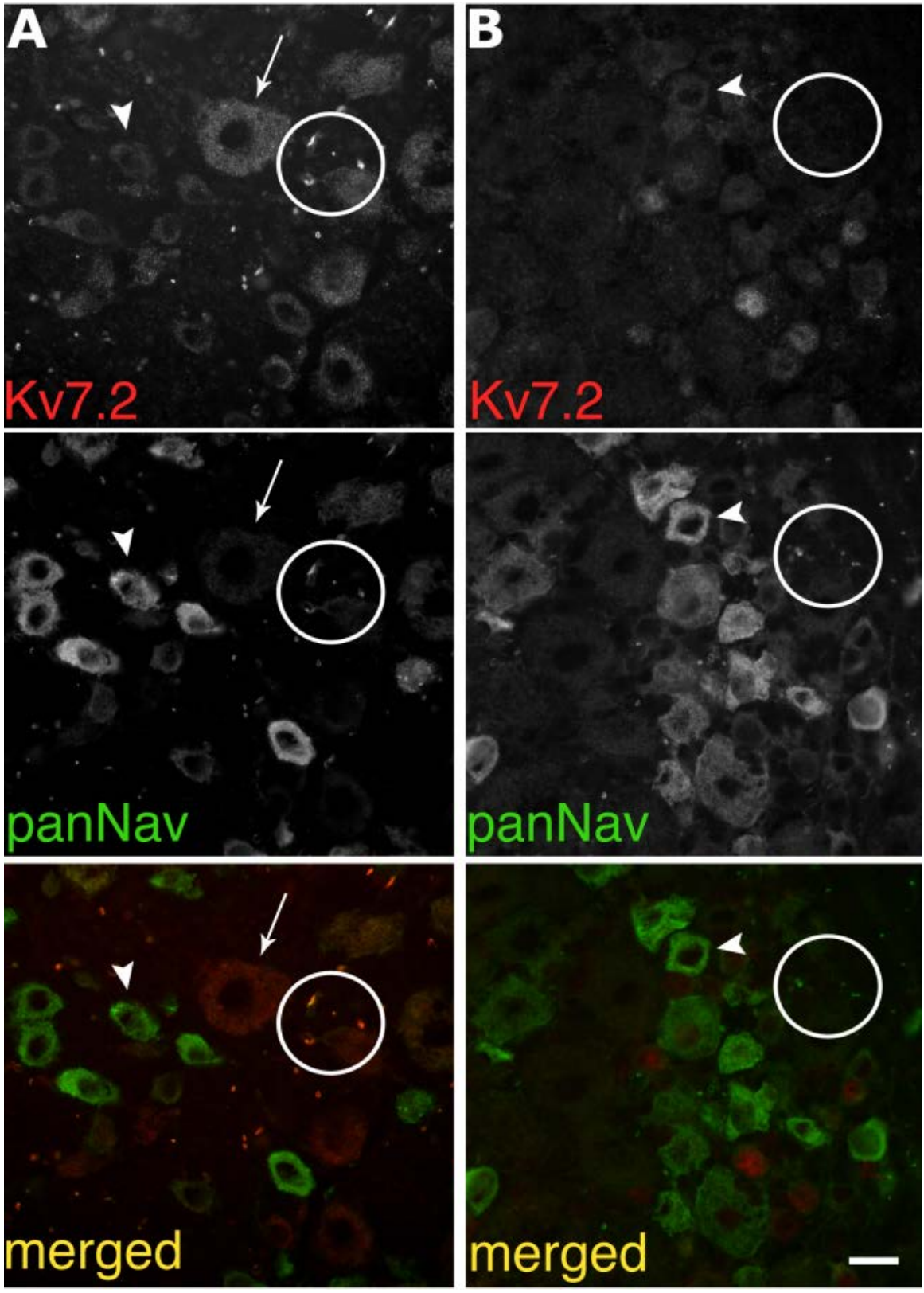

Figure 3-13: DRG neurons of *Kcnq2*-null mice do not express Kv7.2.

These are images of unfixed sections of lumbar dorsal root ganglia (DRG), double-labeled with a rabbit antiserum against Kv7.2 (red) and a panNav monoclonal antibody (green). In wild-type DRG (column A), the Kv7.2 antiserum labels large diameter neurons, one of which is indicated (arrow); these are relatively unlabeled by the panNav antibody. In contrast, in *Kcnq2*-null DRG (column B), the Kv7.2 antiserum does not label large neurons. In both wild-type and *Kcnq2*-null DRG, the panNav monoclonal labels small neurons, two of which are indicated (arrowhead). In addition, all nodes of wild-type neurons are double-labeled by both Kv7.2 and panNav (some enclosed within a circle), while none of the nodes of mutant neurons are Kv7.2-positive. Scale bar: 20 μm.

Figure 3-14

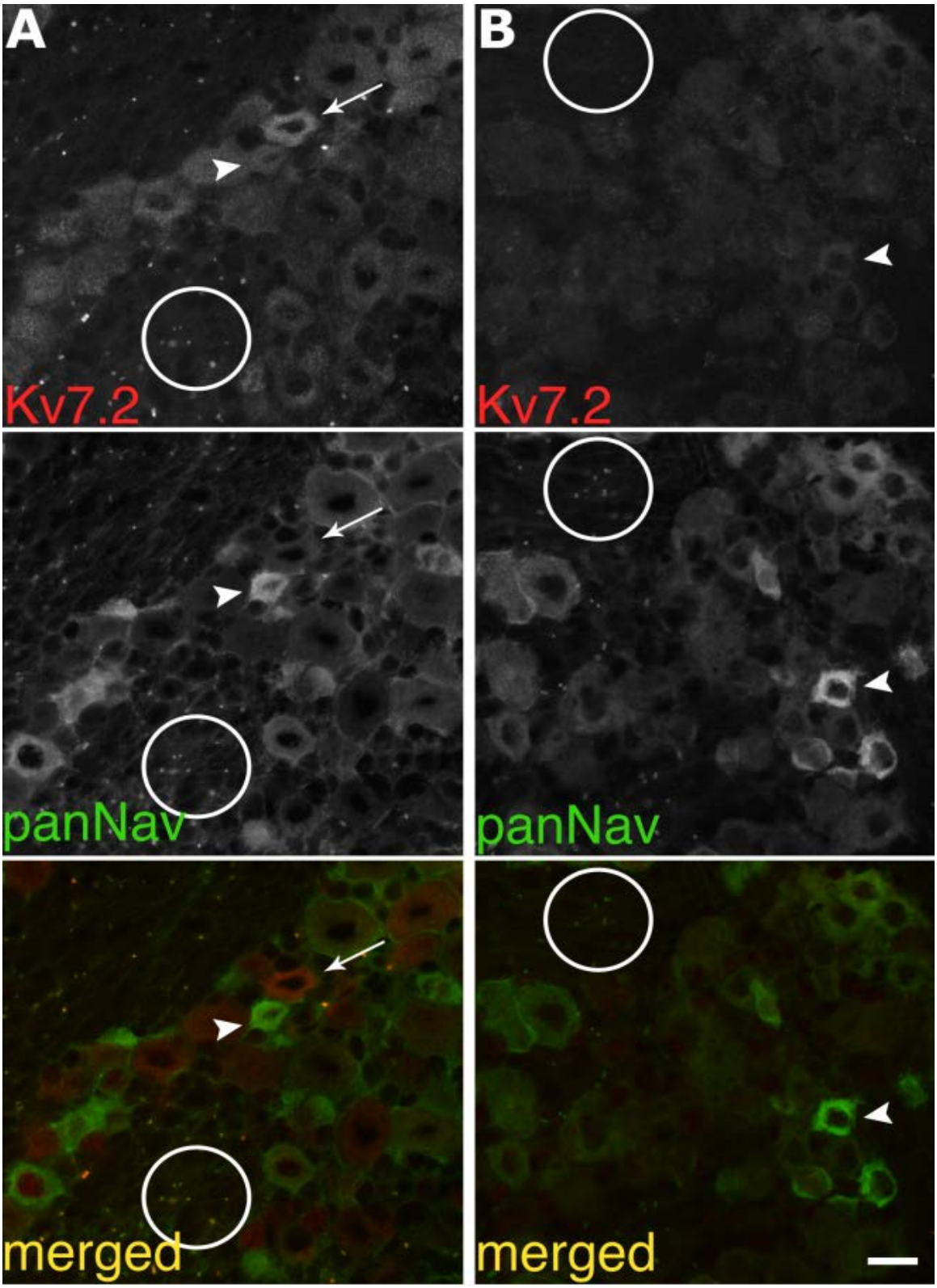

Figure 3-14: Trigeminal neurons of *Kcnq2*-null mice do not express Kv7.2.

These are images of unfixed sections of trigeminal ganglia, double-labeled with rabbit antiserum against Kv7.2 (red) and a panNav monoclonal antibody (green). In wild-type trigeminal ganglia (column A), the K7.2 antiserum labeled neurons that are relatively unlabeled by the panNav antibody, one of which is indicated (arrow). In contrast, in *Kcnq2*-null trigeminal ganglia (column B), the Kv7.2 antiserum does not label any neurons. In both wild-type and *Kcnq2*-null trigeminal ganglia, the panNav monoclonal labels small neurons, two of which are indicated (arrowhead). In addition, all nodes of wild-type neurons are double-labeled by both Kv7.2 and panNav (some enclosed within a circle), while none of the nodes of mutant neurons are Kv7.2-positive. Scale bar: 20 μm.

Figure 3-15

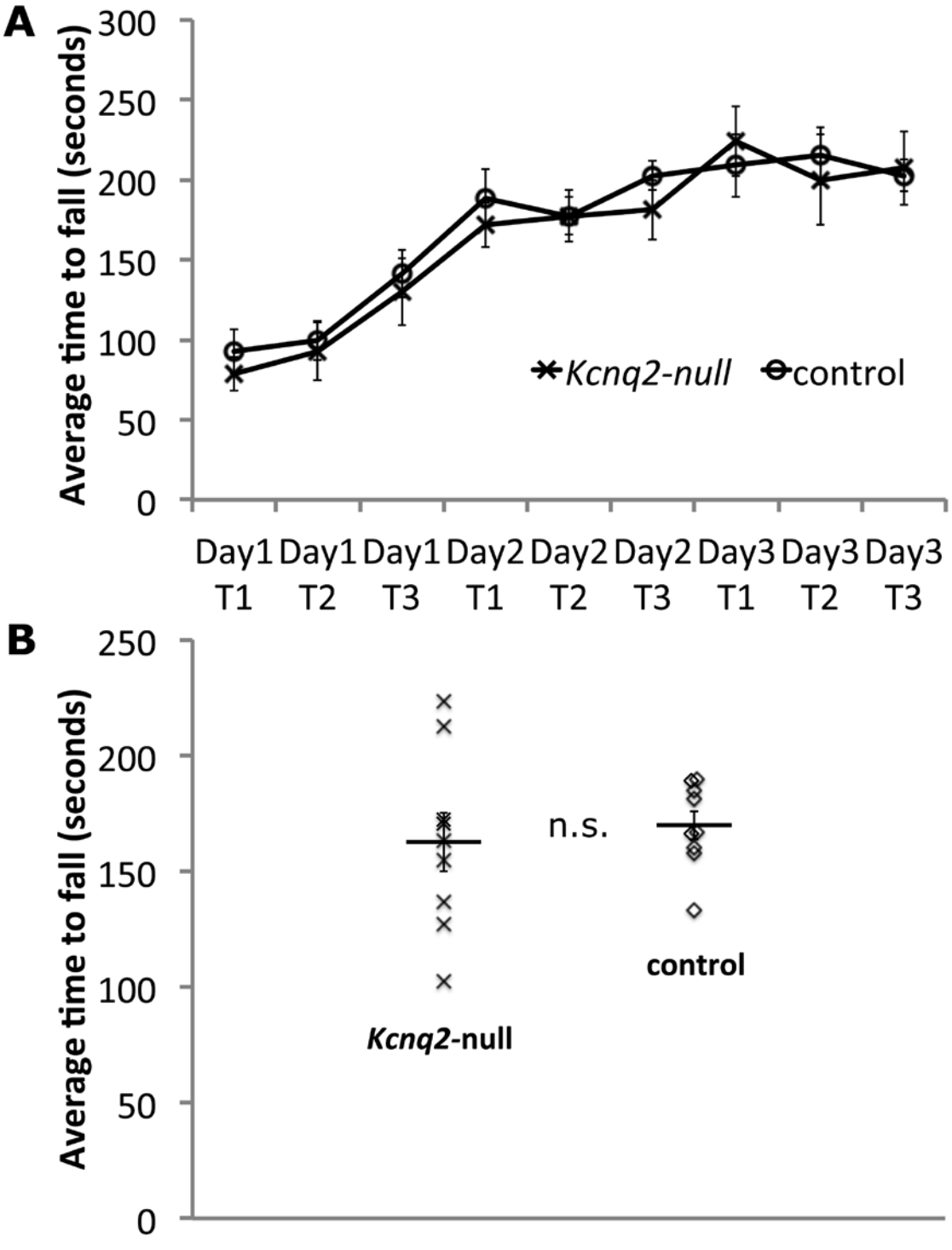
A
Average time to fall (seconds)
300
250
200
150
100
50
0
Kcnq2-null
control
Day1 T1
Day1 T2
Day1 T3
Day2 T1
Day2 T2
Day2 T3
Day3 T1
Day3 T2
Day3 T3
B
Average time to fall (seconds)
250
200
150
100
50
0
n.s.
Kcnq2-null
control

Figure 3-15: *Kcnq2*-null mice exhibited similar motor performance as control mice.

Mutant mice (n=9) and their wild-type littermates (n=9) were subjected to three consecutive days of testing on a rotarod (three tests per day), with motor performance measured by the time it took the mice to fall off the rotarod. Both the mutant and wild-type mice displayed a similar increase in motor performance over the course of nine testing sessions, with no statistical difference between the two groups (panel A; repeated measures ANOVA). In addition, that there was no statistical difference in the overall average time to fall between the mutant and control animals (panel B). Error bars represent SEM; N.S. = no significant difference (unpaired two-sample Student's t-test with equal variance).

Figure 3-16

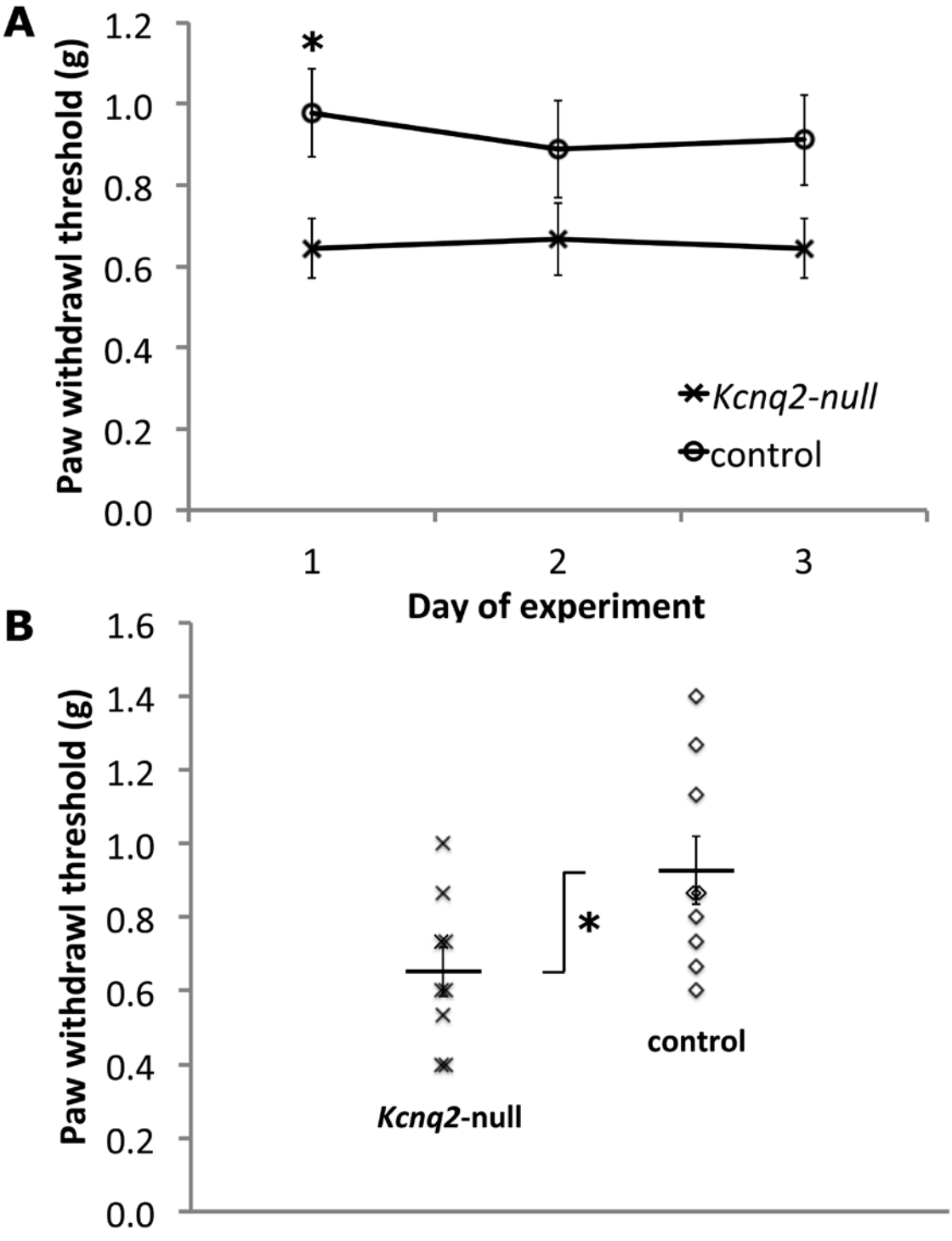
A
Paw withdrawl threshold (g)
1.2
1.0
0.8
0.6
0.4
0.2
0.0
*
Kcnq2-null
control
1
2
3
Day of experiment
B
Paw withdrawl threshold (g)
1.6
1.4
1.2
1.0
0.8
0.6
0.4
0.2
0.0
*
Kcnq2-null
control

Figure 3-16: *Kcnq2*-null mice displayed increased mechanical allodynia.

Both mutant mice (n=9) and wild-type littermates (n=9) were subjected to three consecutive days of testing with a series of von Frey hair filaments (0.4g, 0.6g, 1.0g, 1.4g, 2.0g; one up-and-down session per day). Mechanical allodynia determined by the lowest strength of hair filament capable of inducing a positive withdrawal response. The mutant animals showed consistently lower withdrawal threshold in each of the three testing days; this was significant only the first day (panel A). The overall average of all tests showed mutant animals have a statistically significant increase in mechanical allodynia (panel B). Error bars represent SEM; * $P < 0.05$ (unpaired two-sample Student's T-test with equal variance).

Figure 3-17

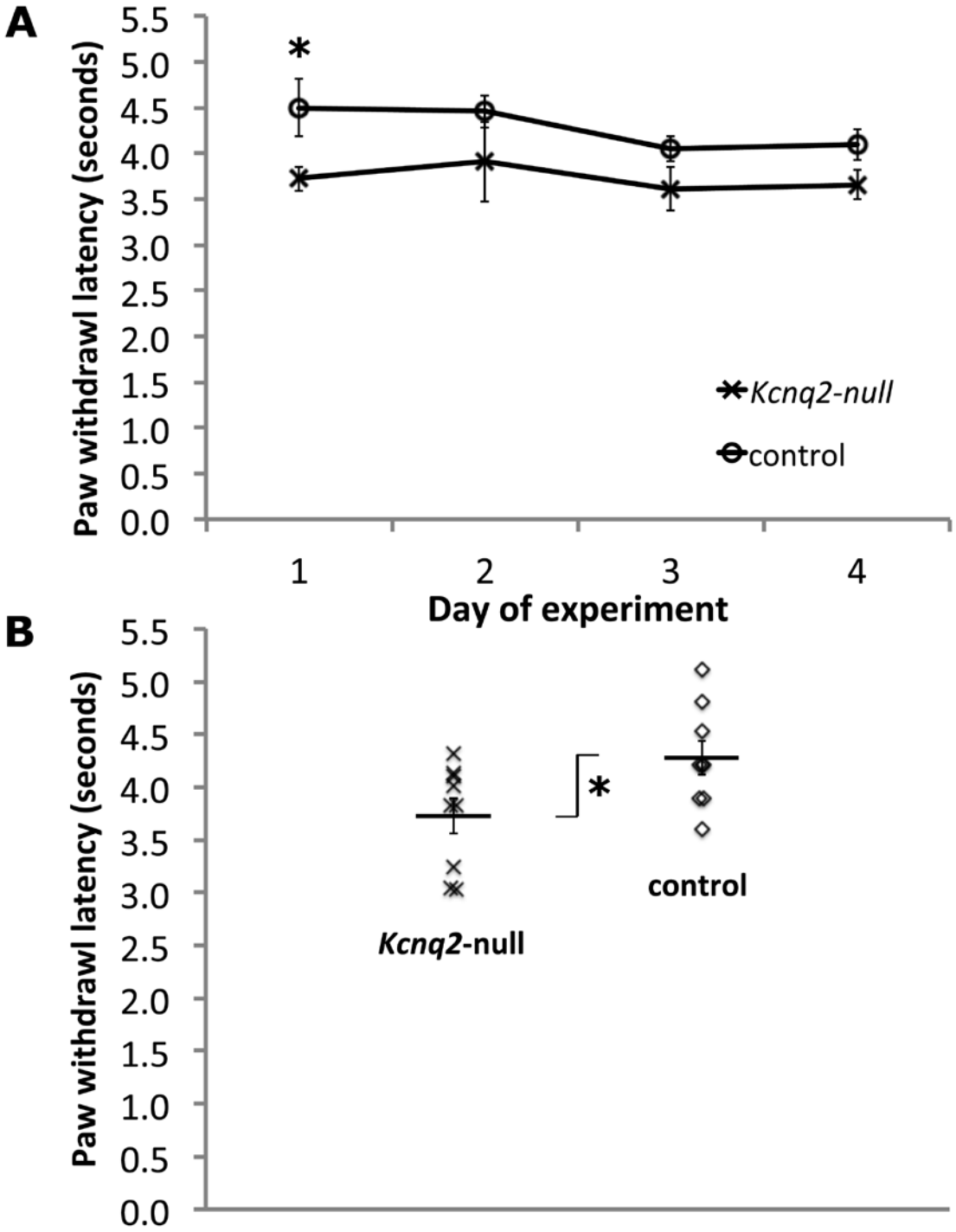
A
Paw withdrawl latency (seconds)
5.5
5.0
4.5
4.0
3.5
3.0
2.5
2.0
1.5
1.0
0.5
0.0
*
Kcnq2-null
control
1
2
3
4
Day of experiment
B
Paw withdrawl latency (seconds)
5.5
5.0
4.5
4.0
3.5
3.0
2.5
2.0
1.5
1.0
0.5
0.0
*
Kcnq2-null
control

Figure 3-17: *Kcnq2*-null mice have increased thermal hyperalgesia.

Both mutant mice (n=9) and their wild-type littermates (n=9) were subjected to four consecutive days (six trials per day) of thermal hyperalgesia measured by the withdrawal latency after thermal stimulation (on a Hargreaves chamber). The mutant animals showed consistently lower withdrawal latency during each of the four testing days; this was significant only the first day (panel A). The overall average of all tests showed mutant animals have a statistically significant increase in thermal hyperalgesia (panel B). Error bars represent SEM; * $P < 0.05$ (unpaired two-sample Student's t-test with equal variance).

Figure 3-18

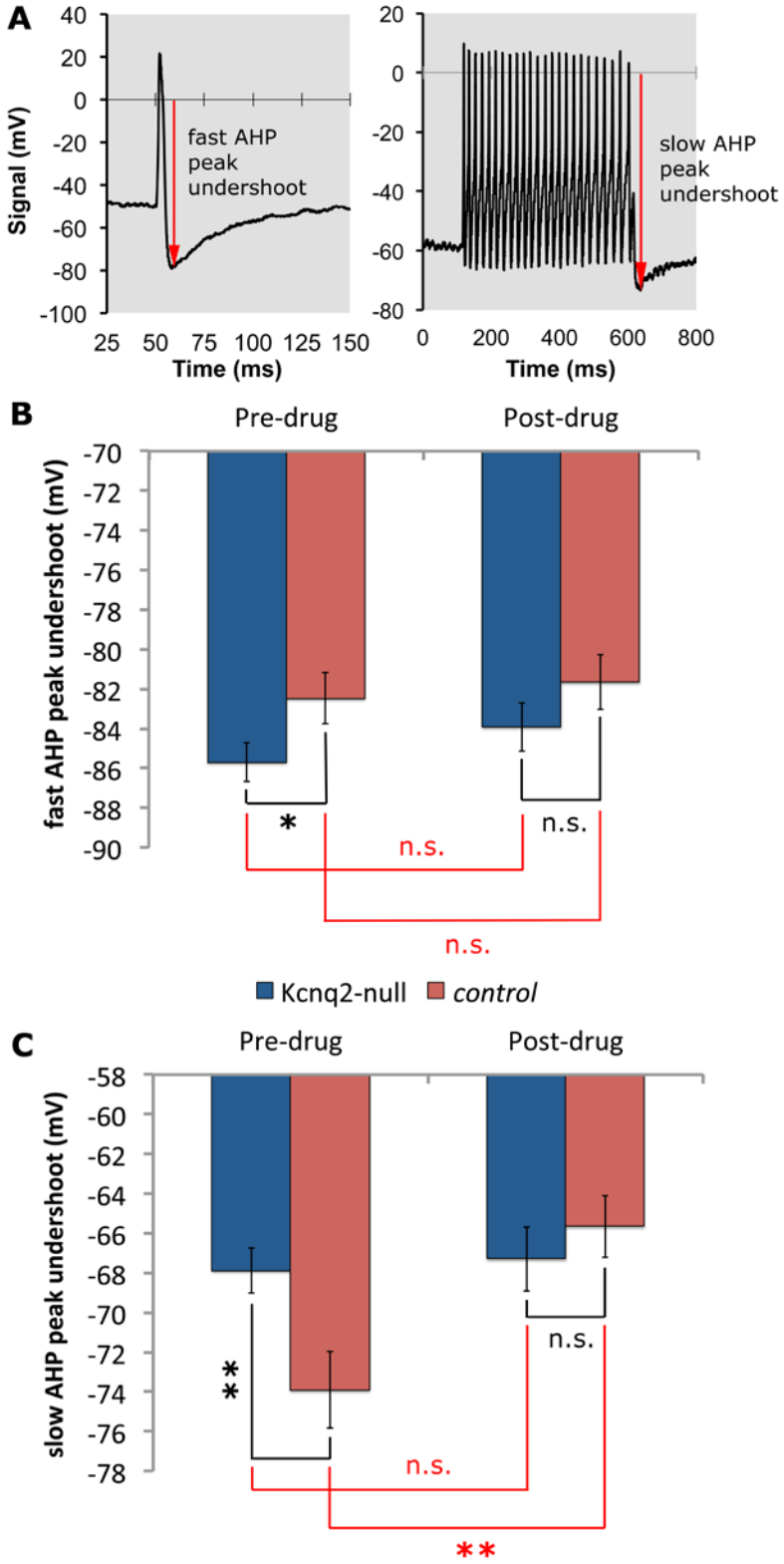
A
Signal (mV)
fast AHP peak undershoot
slow AHP peak undershoot
Time (ms)
Time (ms)
B
Pre-drug
Post-drug
fast AHP peak undershoot (mV)
*
n.s.
n.s.
n.s.
Kcnq2-null
control
C
Pre-drug
Post-drug
slow AHP peak undershoot (mV)
**
n.s.
n.s.
**

Figure 3-18: *Kcnq2*-null DRG neurons have a diminished slow afterhyperpolization (AHP) that is not affected by 3 mM TEA.

Panel A shows representative responses from a control DRG neuron given a brief (3 ms) depolarizing current step that generated a single action potential (AP), and a prolonged (500 ms) depolarizing current step that generated multiple APs, from which the magnitude of the fast and slow AHP peak undershoots, respectively, were measured.

Panel B shows that before 3 mM TEA, the average fast AHP peak undershoot of mutant neurons (n=25) was slightly more negative than that of control neurons (n=25). After applying 3 mM TEA, the fast AHP peak undershoot of both control and *Kcnq2*-null neurons did not change by a statistically significant amount.

Panel C shows that before 3 mM TEA, the average slow AHP peak undershoot of mutant neurons (n=25) was 8.8% more positive than that of control neurons (n=25) . After applying 3 mM TEA for 2 minutes, the slow AHP peak undershoot of control neurons became 11% more positive, while the slow AHP peak undershoot of *Kcnq2*-null neurons did not change by a statistically significant amount. * $p<0.05$; ** $p<0.01$ (2-way ANOVA).

Figure 3-19

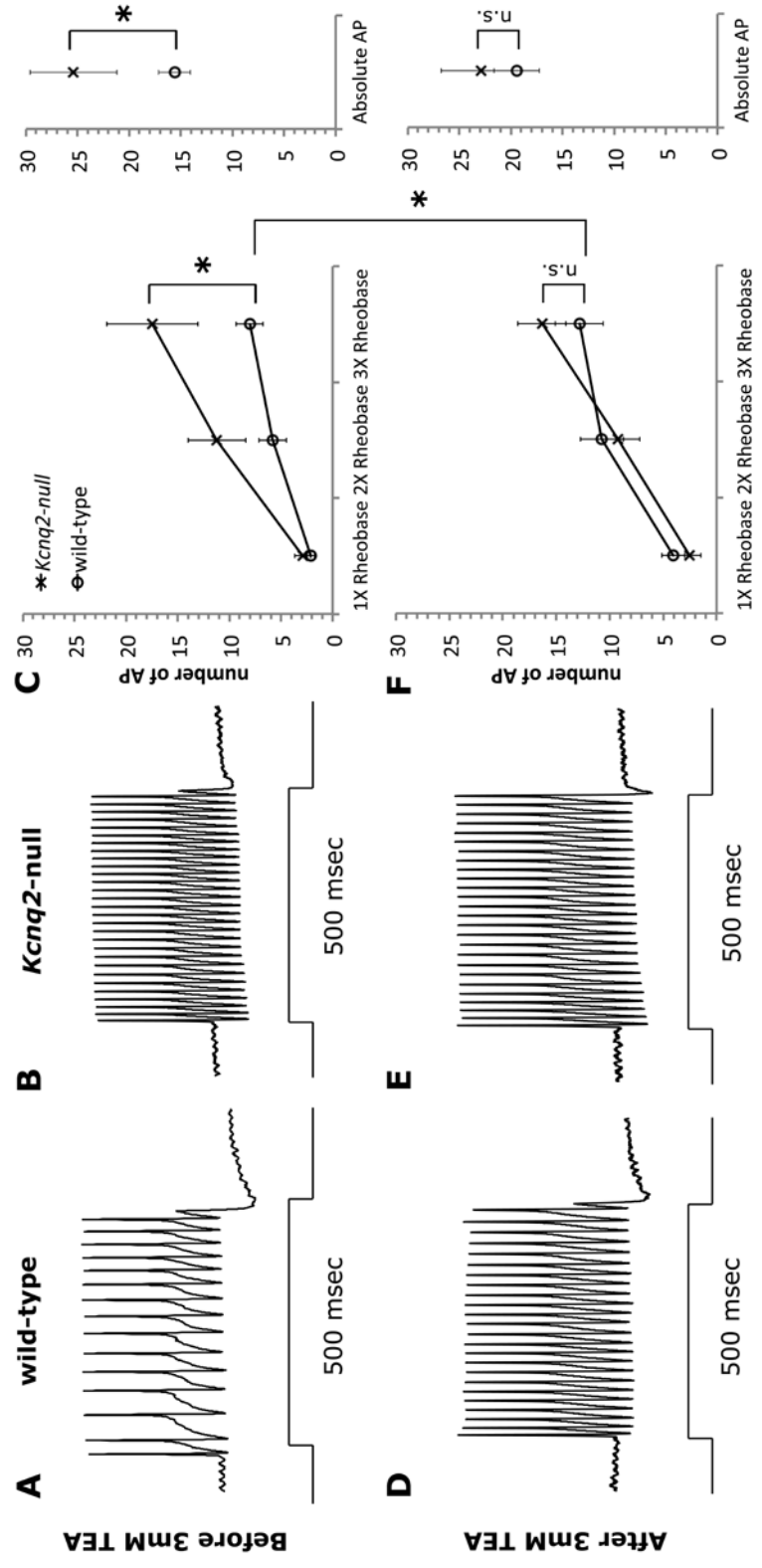
A
wild-type
B
Kcnq2-null
C
Kcnq2-null
wild-type
number of AP
1X Rheobase 2X Rheobase 3X Rheobase
Absolute AP
n.s.
D
E
F
Before 3mM TEA
After 3mM TEA
500 msec

Figure 3-19: *Kcnq2*-null DRG neurons have decreased spike-frequency adaption that is not affected by 3 mM TEA.

Single DRG neurons were injected with 500 ms depolarizing current steps of 1x, 2x, or 3x rheobase (A-F) into the cell from a holding level of between -50 to -60 mV before and after application of 3 mM TEA. Panels A-D show representative recordings of control (A&D) and mutant (B&E) neurons, before and after application of 3 mM TEA for 2 minutes. Panels C and F are summary diagrams showing the number of APs in mutant and control neurons, before and after applying TEA, respectively (* $p<0.05$; two-ways repeated measures ANOVA). Notably, after TEA application, control DRG neurons also showed a decrease in spike frequency adaption, and generated statistically similar numbers of APs at each rheobase as compared to mutant (n.s. = no significant difference; two-ways repeated measures ANOVA). In contrast, TEA application did not reduce spike-frequency adaptation of the mutant DRG neurons. In addition, we also injected 500 ms incremental current at set current step from 0.4nA to 3.6nA (in increments of 0.4nA) in order to determine the responsiveness of DRG neurons to absolute (as opposed to relative threshold as described above) depolarizing stimuli, and the spike frequency adaption was also significantly reduced in mutant DRG neurons in comparison to control neurons before TEA application; after TEA application the control neurons generated statistically similar number of APs in response to absolute stimuli as compared to mutant neurons.

Table 3-1

	control	*Kcnq2*-null
Passive properties		
C_m (pF)	39 ± 3.3	45 ± 4.1
Pre-drug firing properties		
Fast AHP peak (mV)	-83 ± 1.3	-86 ± 0.97*
AP rheobase (nA)	0.77 ± 0.23	0.81 ± 0.16
1 times rheobase (#APs)	2.1 ± 0.38	2.9 ± 0.75
2 times rheobase (#APs)	5.8 ± 1.3	11 ± 2.8
3 times rheobase (#APs)	8.0 ± 1.3	17. ± 4.4*
Absolute stimulus (#APs)	16 ± 1.6	25 ± 5.2*
Slow AHP peak (mV)	-74 ± 1.9	-68 ± 1.2**
Post-drug firing properties		
Fast AHP peak (mV)	-82 ± 0.97	-84 ± 1.21
AP rheobase (nA)	0.39 ± 0.07	0.88 ± 0.19*
1 times rheobase (#APs)	4.0 ± 1.1	2.5 ± 0.66
2 times rheobase (#APs)	11 ± 2.0	9.2 ± 2.2
3 times rheobase (#APs)	13 ± 2.2	16 ± 2.9
Absolute stimulus (#APs)	21 ± 2.2	23 ± 3.9
Slow AHP peak (mV)	-66 ± 1.2	-67 ± 1.6

Table 3-1: Passive and active membrane properties of control and *Kcnq2*-null DRG neurons.

Twenty-five DRG neurons from five animals were recorded in the control and *Kcnq2*-null groups. Values are means ± SEM. C_m = membrane capacitance; AHP = afterhyperpolarization potential; fast AHP peak = AHP undershoot peak magnitude after single 3-ms stimulus; AP rheobase = either the minimum amount of current required to evoke a single AP, or 0.1 nA (whichever one was smallest); 1, 2, and 3 times rheobase = the number of APs fired by a DRG neuron during a 500-ms depolarizing current step of a magnitude 1, 2, or 3 times its rheobase, respectively; absolute = the maximum number of APs fired in response to a single 500-ms depolarizing current step of 0.1-0.9 nA magnitude (in 0.1-nA increments); slow AHP peak = AHP undershoot magnitude after 500-ms stimulus at 0.4nA. Values of C_m of the control DRG neurons were compared to mutant neurons using unpaired 2-sample Student's t-test with equal variance; AHP and AP rheobase were compared with 2-way ANOVA with Tukey test; numbers of APs were compared with two-way repeated measures ANOVA. * $p<0.05$; ** $p<0.01$.

CHAPTER 4: CONCLUSIONS AND FUTURE DIRECTIONS

In this thesis I used immunohistochemical, behavioral, and electrophysiological tests to investigate the role of Kv7 in peripheral axons. While I was able to demonstrate the dichotomous expression of Kv7.2 and Kv7.5 in the myelinated and unmyelinated sensory axons, and also investigated the role of Kv7.2 in the regulation of myelinated axonal excitability, there are a number of possible future projects that should be undertaken to expand on the findings reported in this thesis.

The generation of other *Kcnq*-null mice

The *Kcnq2*-null mice allowed me study the specific expression and activity of Kv7.2 subunit while avoiding the disadvantages of using Kv7 blockers. However, because we have shown that the expression of *Pax3-Cre* is not limited to peripheral sensory neurons, I am unable to conclude that the lack of Kv7.2 activity in the peripheral sensory neurons is the cause of the increased thermal hyperalgesia and mechanical allodynia exhibited by the *Kcnq2*-null mice. Therefore, if and when a sensory neuron specific Cre line becomes available, it should be mated with mice carrying the floxed *Kcnq2* allele to generate sensory neuron-specific *Kcnq2*-null mice. Furthermore, although we had first hypothesized that proper Kv7.3 nodal localization depends on Kv7.2, our findings suggest that this is not the case. Thus we cannot exclude the possibility that Kv7.3 may at least be partially compensating the loss of Kv7.2 activity in our *Kcnq2*-null mice and masking the resulting behavioral and electrophysiological changes. To address this issue we should generate mice with double-knockout of *Kcnq2* and *Kcnq3*, which should

completely lack Kv7 activity in the myelinated sensory axons, and thus completely lack M-current. Furthermore, having such animals will also allow us to validate my Kv7.3 antiserum. In fact, Tzingounis and Nicoll (2008) have demonstrated that, unlike *Kcnq2*-null mice, *Kcnq3*-null animals are viable, so it is technically feasible to create double-null animals by crossing our conditional *Kcnq2*-null mice with their *Kcnq3*-null mice, and this approach should allow us to further understand the functional role of Kv7 channels in peripheral myelinated axons. Finally, although *Kcnq5*-null animal is currently unavailable, the generation of such animal will provide the ultimate method of confirming Kv7.5 expression in the Remak fibers, and electrophysiological studies of such animals should confirm if Kv7.5 does contribute to the regulation of C-fiber activity.

M-current-specific recording

As I have discussed in the introduction, Kv7 channels mediate spike-frequency adaptation and regulate neuronal excitability by generating M-current. Therefore, in chapter 3 I used decreased spike-frequency adaptation to indirectly demonstrate the lack of M-current in the *Kcnq2*-null DRG neurons. However, in their investigation of the functional role of Kv7 in nodose ganglia, Wladyka and Kunze (2006) used a novel pharmacological approach to separate M-current from other endogenous potassium currents, which normally only constitutes a small component of the total outward potassium current (Brown and Yu, 2000). They first applied the potassium channel blocker 4-AP, which because it blocks M-current poorly (Robbins, 2001), results in the elimination of the majority of non-Kv7 potassium currents. Next they used linopirdine or

XE991 to isolate the M-current from other 4-AP-insenstive current. (Wladyka and Kunze) found that along with M-current, this method blocks two other currents: a transient Kv4.3-like current that is present in most neurons by P3, which they minimized by recording from P1 cells, and a much faster activating current, which can also be minimized because its block by linopirdine or XE991 is rapidly reversible (while the M-current remain blocked throughout the course of their experiment). Thus, they were able to obtain total isolation of the M-current by subtracting the irreversibly blocked current from the total current recorded before linopirdine application. By using this method, the authors were able to measure M-current in both nodose ganglia and arterial baroreceptors (Wladyka and Kunze, 2006, Wladyka et al., 2008).

I believe their method should also allow us to directly measure M-current in the *Kcnq2*-null DRG neurons, and should allow us better determine if *Kcnq2*-null neurons have decreased M-current. We are currently in the process setting up collaboration with Dr. Diana Kunze's lab, and are shipping our *Kcnq2*-null mice and wild-type littermates to their lab.

Threshold tracking

Other than measuring spike frequency adaptation, another way to quantify axonal excitability is through threshold tracking, specifically by measuring the late subexcitability threshold. Schwarz et al. (2006) showed that, unlike superexcitability, which is influenced by transient sodium and fast potassium conductance, late subexcitability is primarily influenced by Kv7 channels. In addition, superexcitability is usually measured after a single conditioning stimulus, while late subexcitability is

measured after a conditioning train of multiple action potentials. We are currently setting up a collaboration with Dr. Martin Koltzenburg's lab at University College London, as he had used this technique before to record late subexcitability from isolated saphenous (femoral sensory) nerves (Achilli et al., 2009). Because we have demonstrated a complete loss of Kv7.2 nodal expression in the *Kcnq2*-null femoral sensory nerves, we expect these nerves to have decreased late subexcitability threshold, which if true, will help to support our hypothesis that the increased thermal hyperalgesia and mechanical allodynia exhibited by the *Kcnq2*-null mice is due to an increase excitability of the peripheral sensory axons.

REFERENCE

Allen Mouse Brain Atlas [Internet]. Seattle (WA): Allen Institute for Brain Science. ©2009. Available from: http://mouse.brain-map.org

Achilli F, Bros-Facer V, Williams HP, Banks GT, AlQatari M, Chia R, Tucci V, Groves M, Nickols CD, Seburn KL, Kendall R, Cader MZ, Talbot K, van Minnen J, Burgess RW, Brandner S, Martin JE, Koltzenburg M, Greensmith L, Nolan PM, Fisher EM (2009) An ENU-induced mutation in mouse glycyl-tRNA synthetase (GARS) causes peripheral sensory and motor phenotypes creating a model of Charcot-Marie-Tooth type 2D peripheral neuropathy. Dis Model Mech 2:359-373.

Aiken SP, Lampe BJ, Murphy PA, Brown BS (1995) Reduction of spike frequency adaption and blockade of M-crrent in rat CA1 pyramidal neurones by linopirdine (DuP 996), a neurotransmitter release enhancer. Br J Pharmacol 115:1163-1168.

Arroyo EJ, Bermingham JRJ, Rosenfeld MG, Scherer SS (1998) Promyelinating Schwann cells express Tst-1/SCIP/Oct-6. J Neurosci 18:7891-7902.

Averill S, McMahon SB, Clary DO, Reichardt LF, Priestley JV (1995) Immunocytochemical localization of trkA receptors in chemically identified subgroups of adult rat sensory neurons. The European journal of neuroscience 7:1484-1494.

Bal M, Zhang J, Zaika O, Hernandez CC, Shapiro MS (2008) Homomeric and heteromeric assembly of KCNQ (Kv7) K+ channels assayed by total internal reflection fluorescence/fluorescence resonance energy transfer and patch clamp analysis. J Biol Chem 283:30668-30676.

Blackburn-Munro G, Jensen BS (2003) The anticonvulsant retigabine attenuates nociceptive behaviours in rat models of persistent and neuropathic pain. European Journal of Pharmacology 460:109-116.

Brown BS, Yu SP (2000) Modulation and genetic identification of the M channel. Prog Biophys Mol Biol 73:135-166.

Brown DA, Adams PR (1980) Muscarinic suppression of a novel voltage sensitve K+ current in a vertebrate neuron. Nature 283:673-676.

Brown DA, Passmore GM (2009) Neural KCNQ (Kv7) channels. Br J Pharmacol 156:1185-1195.

Brueggemann LI, Moran CJ, Barakat JA, Yeh JZ, Cribbs LL, Byron KL (2007) Vasopressin stimulates action potential firing by protein kinase C-dependent inhibition of KCNQ5 in A7r5 rat aortic smooth muscle cells. Am J Physiol Heart Circ Physiol 292:H1352-1363.

Chaplan SR, Bach FW, Pogrel JW, Chung JM, Yaksh TL (1994) Quantitative assessment of tactile allodynia in the rat paw. J Neurosci Methods 53:55-63.

Cheng C, Zochodne DW (2002) In vivo proliferation, migration and phenotypic changes of Schwann cells in the presence of myelinated fibers. Neuroscience 115:321-329.

Chirgwin JM, Przbyla AE, MacDonald RJ, Rutter RJ (1979) Isolation of biologically active ribonucleic acid from sources enriched in ribonuclease. Biochem 18:5294-5299.

Cooper EC (2011) Made for "anchorin": Kv7.2/7.3 (KCNQ2/KCNQ3) channels and the modulation of neuronal excitability in vertebrate axons. Seminars in cell & developmental biology 22:185-192.

Cooper EC, Harrington E, Jan YN, Jan LY (2001) M channel KCNQ2 subunits are localized to key sites for control of neuronal network oscillations and synchronization in mouse brain. J Neurosci 21:9529–9540.

Crozier RA, Ajit SK, Kaftan EJ, Pausch MH (2007) MrgD activation inhibits KCNQ/M-currents and contributes to enhanced neuronal excitability. J Neurosci 27:4492-4496.

Cuellar JM, Manering NA, Klukinov M, Nemenov MI, Yeomans DC (2010) Thermal nociceptive properties of trigeminal afferent neurons in rats. Mol Pain 6:39.

Dedek K, Kunath B, Kananura C, Reuner U, Jentsch TJ, Steinlein OK (2001) Myokymia and neonatal epilepsy caused by a mutation in the voltage sensor of the KCNQ2 K+ channel. Proc Natl Acad Sci U S A 98:12272-12277.

Delmas P, Brown DA (2005) Pathways modulating neural KCNQ/M (Kv7) potassium channels. Nat Rev Neurosci 6:850-862.

Devaux JJ, Kleopa KA, Cooper EC, Scherer SS (2004) KCNQ2 is a nodal K+ channel. J Neurosci 24:1236-1244.

Dirig DM, Salami A, Rathbun ML, Ozaki GT, Yaksh TL (1997) Characterization of variables defining hindpaw withdrawl latency evoked by radiant thermal stimuli. J Neurosci Methods 76:183-191.

Dost R, Rostock A, Rundfeldt C (2004) The anti-hyperalgesic activity of retigabine is mediated by KCNQ potassium channel activation. Naunyn-Schmiedeberg's archives of pharmacology 369:382-390.

Dubner R, Bennett GJ (1983) Spinal and trigeminal mechanisms of nociception. Annu Rev Neurosci 6:381-418.

Farley FW, Soriano P, Steffen LS, Dymecki SM (2000) Widespread recombinase expression using FLPeR (Flipper) mice. Genesis 28:106-110.

Feltri ML, Scherer SS, Wrabetz L, Kamholz J, Shy ME (1992) Mitogen-expanded Schwann cells retain the capacity to myelinate regenerating axons after transplantation into rat sciatic nerve. Proc Natl Acad Sci U S A 89:8827-8831.

Fields HL (1987) Pain. New York: McGraw-Hill.

Gamper N, Li Y, Shapiro MS (2005) Structural requirements for differential sensitivity of KCNQ K+ channels to modulation by Ca2+/calmodulin. Mol Biol Cell 16:3538-3551.

Ghamari-Langroudi M, Bourque CW (2004) Muscarinic receptor modulation of slow afterhyperpolarization and phasic firing in rat supraoptic nucleus neurons. J Neurosci 24:7718-7726.

Giuliodori MJ, DiCarlo SE (2004) Myelinated vs. unmyelinated nerve conduction: a novel way of understanding the mechanisms. Adv Physiol Educ 28:80-81.

Goldman AM, Glasscock E, Yoo J, Chen TT, Klassen TL, Noebels JL (2009) Arrhythmia in heart and brain: KCNQ1 mutations link epilepsy and sudden unexplained death. Science translational medicine 1:2ra6.

Gollan L, Salomon D, Salzer JL, Peles E (2003) Caspr regulates the processing of contactin and inhibits its binding to neurofascin. J Cell Biol 163:1213-1218.

Gomez-Posada JC, Etxeberria A, Roura-Ferrer M, Areso P, Masin M, Murrell-Lagnado RD, Villarroel A (2010) A pore residue of the KCNQ3 potassium M-channel subunit controls surface expression. J Neurosci 30:9316-9323.

Griffin JW, Thompson WJ (2008) Biology and pathology of nonmyelinating Schwann cells. Glia 56:1518-1531.

Gu N, Vervaeke K, Hu H, Storm JF (2005) Kv7/KCNQ/M and HCN/h, but not KCa2/SK channels, contribute to the somatic medium after-hyperpolarization and excitability control in CA1 hippocampal pyramidal cells. J Physiol 566:689-715.

Hadley JK, Noda M, Selyanko AA, Wood IC, Abogadie FC, Brown DA (2000) Differential tetraethylammonium sensitivity of KCNQ1-4 potassium channels. Br J Pharmacol 129:413-415.

Hadley JK, Passmore GM, Tatulian L, Al-Qatari M, Ye F, Wickenden AD, Brown DA (2003) Stoichiometry of expressed KCNQ2/KCNQ3 potassium channels and subunit composition of native ganglionic M channels deduced from block by tetraethylammonium. J Neurosci 23:5012-5019.

Hamill OP, Marty A, Neher E, Sakmann B, Sigworth FJ (1981) Improved patch-clamp techniques for high-resolution current recording from cells and cell free membrane patches. Pflugers Arch 391:85-100.

Hargreaves K, Dubner R, Brown F, Flores C, Joris J (1988) A new and sensitive method for measuring thermal nociception in cutaneous hyperalgesia. Pain 32:77-88.

Hargreaves KM, Swift JQ, Roszkowski MT, Bowles W, Garry MG, Jackson DL (1998) Pharmacology of peripheral neuropeptide and inflammatory mediator release. Oral Surg Oral Med Oral Pathol 78:503-510.

Hasegawa H, Abbott S, Han BX, Qi Y, Wang F (2007) Analyzing somatosensory axon projections with the sensory neuron-specific Advillin gene. J Neurosci 27:14404-14414.

Heidenreich M, Lechner SG, Vardanyan V, Wetzel C, Cremers CW, De Leenheer EM, Aránguez G, Moreno-Pelayo MÁ, Jentsch TJ, Lewin GR (2011) KCNQ4 K+ channels tune mechanoreceptors for normal touch sensation in mouse and man. Nature Neuroscience 15:138-145.

Hill AS, Nishino A, Nakajo K, Zhang G, Fineman JR, Selzer ME, Okamura Y, Cooper EC (2008) Ion channel clustering at the axon initial segment and node of Ranvier evolved sequentially in early chordates. PLoS Genet 4:e1000317.

Hu B, Mooney DM (2005) Burst firing induces a slow after hyperpolarization in rat auditory thalamus. Neurosci Lett 375:162-164.

Hubbard RD, Winkelstein BA (2005) Transient cervical nerve root compression in the rat induces bilateral forepaw allodynia and spinal glial activation: mechanical factors in painful neck injuries. Spine (Phila Pa 1976) 30:1924–1932.

Ikeda SR, Schofield GG, Weight FF (1986) Na+ and Ca2+ currents of acutely isolated adult rat nodose ganglion cells. J Neurophysiol 55:527-539.

Ivanusic JJ (2009) Size, neurochemistry, and segmental distribution of sensory neurons innervating the rat tibia. J Comp Neurol 517:276-283.

Jentsch TJ (2000) Neuronal KCNQ potassium channels: physiology and role in disease. Nat Rev Neurosci 1:21-30.

Jessen KR, Morgan L, Brammer M, Mirsky R (1985) Galactocerebroside is expressed by non-myelin-forming Schwann cells in situ. J Cell Biol 10:1135-1143.

Jessen KR, Morgan L, Stewart HJ, Mirsky R (1990) Three markers of adult non-myelin-forming Schwann cells, 217c(Ran-1), A5E3 and GFAP: development and regulation by neuron-Schwann cell interactions. Development 109:91-103.

Ji G, Zhou S, Kochukov MY, Westlund KN, Carlton SM (2007) Plasticity in intact A delta- and C-fibers contributes to cold hypersensitivity in neuropathic rats. Neuroscience 150:182-193.

Karlsson M, Hildebrand C (1993) Routes of putative afferent axons in rat lumbosacral ventral roots and pia mater. Brain Res 600:298-304.

Kashiba H, Uchida Y, Senba E (2001) Difference in binding by isolectin B4 to trkA and c-ret mRNA-expressing neurons in rat sensory ganglia. Brain Res Mol Brain Res 95:18-26.

Kavanaugh MP, Varnum MS, Osborne PB, Christie MJ, Busch AE, Adelman JP, North RA (1991) Interaction between tetraethylammonium and amino acid residues in the pore of cloned voltage-dependent potassium channels. J Biol Chem 266:7583-7587.

Koltzenburg M, Lundberg LE, Torebjork HE (1993) Dynamic and static components of mechanical hyperalgesia in human hairy skin. Pain 51:207-219.

Kubisch C, Schroeder BC, Friedrich T, Lutjohann B, El-Amraoui A, Marlin S, Petit C, Jentsch TJ (1999) KCNQ4, a novel potassium channel expressed in sensory outer hair cells, is mutated in dominant deafness. Cell 96:437-446.

Lamas JA, Reboreda A, Codesido V (2002) Ionic basis of the resting membrane potential in cultured rat sympathetic neurons. Neuroreport 13:585-591.

Lancaster E, Oh EJ, Weinreich D (2001) Vagotomy decreases excitability in primary vagal afferent somata. J Neurophysiol 85:247-253.

Lang PM, Fleckenstein J, Passmore GM, Brown DA, Grafe P (2008) Retigabine reduces the excitability of unmyelinated peripheral human axons. Neuropharmacology 54:1271-1278.

Lee KE, Davis MB, Winkelstein BA (2008) Capsular ligament involvement in the development of mechanical hyperalgesia after facet joint loading: behavioral and inflammatory outcomes in a rodent model of pain. J Neurotrauma 25:1383-1393.

Lee V, Wu HL, Schlaepfer WW (1982) Monoclonal antibodies recognized individual neurofilament triplet proteins. Proc Natl Acad Sci U S A 79:6089-6092.

Lee VM, Page CD, Wu HL, Schlaepfer WW (1984) Monoclonal antibodies to gel-excised glial filament protein and their reactivities with other intermediate filament proteins. journal of neurochemistry 42:25-32.

Lerche C, Scherer CR, Seebohm G, Derst C, Wei AD, Busch AE, Steinmeyer K (2000) Molecular cloning and functional expression of KCNQ5, a potassium channel subunit that may contribute to neuronal M-current diversity. J Biol Chem 275:22395-22400.

Li J, Chen F, Epstein JA (2000) Neural crest expression of Cre recombinase directed by the proximal Pax3 promoter in transgenic mice. Genesis 26:162-164.

Linley JE, Rose K, Ooi L, Gamper N (2010) Understanding inflammatory pain: ion channels contributing to acute and chronic nociception. Pflugers Arch 459:657-669.

Linley JE, Rose K, Patil M, Robertson B, Akopian AN, Gamper N (2008) Inhibition of M current in sensory neurons by exogenous proteases: a signaling pathway mediating inflammatory nociception. J Neurosci 28:11240-11249.

Liu B, Linley JE, Du X, Zhang X, Ooi L, Zhang H, Gamper N (2010) The acute nociceptive signals induced by bradykinin in rat sensory neurons are mediated by inhibition of M-type K+ channels and activation of Ca2+-activated Cl– channels. J Clin Invest 120:1240-1252.

Lozeron P, Krarup C, Schmalbruch H (2004) Regeneration of unmyelinated and myelinated sensory nerve fibres studied by a retrograde tracer method. J Neurosci Methods 138:225-232.

Madison DV, Nicoll RA (1984) Control of the repetitive discharge of rat CA1 pyramidal neurons in vitro. J Physiol 354:319-331.

Malin SA, Davis BM, Molliver DC (2007) Production of dissociated sensory neuron cultures and considerations for their use in studying neuronal function and plasticity. Nat Protoc 2:152-160.

Maljevic S, Lerche C, Seebohm G, Alekov AK, Busch AE, Lerche H (2003) C-terminal interaction of KCNQ2 and KCNQ3 K+ channels. J Physiol 548:353-360.

Matthews EA, Linardakis JM, Disterhoft JF (2009) The fast and slow afterhyperpolarizations are differentially modulated in hippocampal neurons by aging and learning. J Neurosci 29:4750-4755.

Miceli F, Soldovieri MV, Martire M, Taglialatela M (2008) Molecular pharmacology and therapeutic potential of neuronal Kv7-modulating drugs. Current opinion in pharmacology 8:65-74.

Molliver DC, Wright DE, Leitner ML, Parsadanian AS, Doster K, Wen D, Yan Q, Snider WD (1997) IB4-binding DRG neurons switch from NGF to GDNF dependence in early postnatal life. Neuron 19:849-861.

Nagy A (2000) Cre recombinase: the universal reagent for genome tailoring. Genesis 26:99-109.

Nielsen AN, Mathiesen C, Blackburn-Munro G (2004) Pharmacological characterisation of acid-induced muscle allodynia in rats. Eur J Pharmacol 487:93-103.

Oliveira AM, Abel T, Brindle PK, Wood MA (2006) Differential role for CBP and p300 CREB-binding domain in motor skill learning. Behav Neurosci 120:724-729.

Otto JF, Kimball MM, Wilcox KS (2002) Effects of the anticonvulsant retigabine on cultured cortical neurons: changes in electroresponsive properties and synaptic transmission. Mol Pharmacol 61:921-927.

Otto JF, Yang Y, Frankel WN, White HS, Wilcox KS (2006) A spontaneous mutation involving Kcnq2 (Kv7.2) reduces M-current density and spike frequency adaptation in mouse CA1 neurons. J Neurosci 26:2053-2059.

Pan Z, Kao T, Horvath Z, Lemos J, Sul JY, Cranstoun SD, Bennett V, Scherer SS, Cooper EC (2006) A common ankyrin-G-based mechanism retains KCNQ and NaV channels at electrically active domains of the axon. J Neurosci 26:2599-2613.

Passmore GM, Selyanko AA, Mistry M, Al-Qatari M, Marsh SJ, Matthews EA, Dickenson AH, Brown TA, Burbidge SA, Main M, Brown DA (2003) KCNQ/M currents in sensory neurons: significance for pain therapy. J Neurosci 23:7227-7236.

Perry MJ, Lawson SN, Robertson J (1991) Neurofilament immunoreactivity in populations of rat primary afferent neurons: a quantitative study of phosphorylated and non-phosphorylated subunits. J Neurocytol 20:746-758.

Peters HC, Hu H, Pongs O, Storm JF, Isbrandt D (2005) Conditional transgenic suppression of M channels in mouse brain reveals functions in neuronal excitability, resonance and behavior. Nature Neuroscience 8:51-60.

Poliak S, Gollan L, Martinez R, Custer A, Einheber S, Salzer JL, Trimmer JS, Shrager P, Peles E (1999) Caspr2, a new member of the neurexin superfamily, is localized at the juxtaparanodes of myelinated axons and associated with K+ channels. Neuron 24:1037-1047.

Poliak S, Peles E (2003) The local differentiation of myelinated axons at nodes of Ranvier. Nat Rev Neurosci 4:968-980.

Poliak S, Salomon D, Elhanany H, Sabanay H, Kiernan B, Pevny L, Stewart CL, Xu X, Chiu SY, Shrager P, Furley AJ, Peles E (2003) Juxtaparanodal clustering of Shaker-like K+ channels in myelinated axons depends on Caspr2 and TAG-1. J Cell Biol 162:1149-1160.

Price DD, Dubner R (1977) Mechanisms of first and second pain in the peripheral and central nervous systems. J Invest Dermatol 69:167-171.

Priestley JV, Michael GJ, Averill S, Liu M, Willmott N (2002) Regulation of nociceptive neurons by nerve growth factor and glial cell line derived neurotrophic factor. Canadian Journal of Physiology and Pharmacology 80:495-505.

Quinn KP, Dong L, Golder FJ, Winkelstein BA (2010) Neuronal hyperexcitability in the dorsal horn after painful facet joint injury. Pain 151:414-421.

Rasband MN, Park EW, Vanderah TW, Lai J, Porreca F, Trimmer JS (2001) Distinct potassium channels on pain-sensing neurons. Proc Natl Acad Sci U S A 98:13373-13378.

Rasmussen HB, Frokjaer-Jensen C, Jensen CS, Jensen HS, Jorgensen NK, Misonou H, Trimmer JS, Olesen SP, Schmitt N (2007) Requirement of subunit co-assembly and ankyrin-G for M-channel localization at the axon initial segment. J Cell Sci 120:953-963.

Rau KK, McIlwrath SL, Wang H, Lawson JJ, Jankowski MP, Zylka MJ, Anderson DJ, Koerber HR (2009) Mrgprd enhances excitability in specific populations of cutaneous murine polymodal nociceptors. J Neurosci 29:8612-8619.

Remak R (1838) Observationes anatomicae et microscopicae de systematis nervosi structura. Berlin.

Rivera-Arconada I, Lopez-Garcia JA (2005) Effects of M-current modulators on the excitability of immature rat spinal sensory and motor neurones. The European journal of neuroscience 22:3091-3098.

Rivera-Arconada I, Lopez-Garcia JA (2006) Retigabine-induced population primary afferent hyperpolarisation in vitro. Neuropharmacology 51:756-763.

Rivera-Arconada I, Roza C, Lopez-Garcia JA (2009) Enhancing m currents: a way out for neuropathic pain? Frontiers in molecular neuroscience 2:10.

Robbins J (2001) KCNQ potassium channels: physiology, pathophysiology, and pharmacology. Pharmacol Ther 90:1-19.

Rose K, Ooi L, Dalle C, Robertson B, Wood IC, Gamper N (2011) Transcriptional repression of the M channel subunit Kv7.2 in chronic nerve injury. Pain 152:742-754.

Roza C, Lopez-Garcia JA (2008) Retigabine, the specific KCNQ channel opener, blocks ectopic discharges in axotomized sensory fibres. Pain 138:537-545.

Salzer JL, Brophy PJ, Peles E (2008) Molecular domains of myelinated axons in the peripheral nervous system. Glia 56:1532-1540.

Sauer B, Henderson N (1988) Site-specific DNA recombination in mammalian cells by the Cre recombinase of bacteriophage P1. Proc Natl Acad Sci U S A 85:5166-5170.

Schenzer A, Friedrich T, Pusch M, Saftig P, Jentsch TJ, Grotzinger J, Schwake M (2005) Molecular determinants of KCNQ (Kv7) K+ channel sensitivity to the anticonvulsant retigabine. J Neurosci 25:5051-5060.

Schmitt N, Schwarz M, Peretz A, Abitbol I, Attali B, Pongs O (2000) A recessive C-terminal Jervell and Lange-Nielsen mutation of the KCNQ1 channel impairs subunit assembly. EMBO J 19:332-340.

Schroeder BC, Hechenberger M, Weinreich F, Kubisch C, Jentsch TJ (2000) KCNQ5, a novel potassium channel broadly expressed in brain, mediates M-type currents. J Biol Chem 275:24089-24095.

Schwake M, Pusch M, Kharkovets T, Jentsch TJ (2000) Surface expression and single channel properties of KCNQ2/KCNQ3, M-type K+ channels involved in epilepsy. J Biol Chem 275:13343-13348.

Schwarz JR, Glassmeier G, Cooper EC, Kao TC, Nodera H, Tabuena D, Kaji R, Bostock H (2006) KCNQ channels mediate IKs, a slow K+ current regulating excitability in the rat node of Ranvier. J Physiol 573:17-34.

Selyanko A, Hadley JK, Brown DA (2001) Properties of single M-type KCNQ2/KCNQ3 potassium channels expressed in mammalian cells. J Physiol 534:15-24.

Shah MM, Migliore M, Valencia I, Cooper EC, Brown DA (2008) Functional significance of axonal Kv7 channels in hippocampal pyramidal neurons. Proc Natl Acad Sci U S A 105:7869-7874.

Shah MM, Mistry M, Marsh SJ, Brown DA, Delmas P (2002) Molecular correlates of the M-current in cultured rat hippocampal neurons. J Physiol 544:29-37.

Singh NA, Charlier C, Stauffer D, Dupont BR, Leach RJ, Melis R, Ronen GM, Bjerre I, Quattlebaum T, Murphy JV (1998) A novel potassium channel gene, KCNQ2, is mutated in an inherited epilepsy of newborns. Nature Genetics 18:25-29.

Soriano P (1999) Generalized lacZ expression with the ROSA26 Cre reporter strain. Nature Genetics 21:70-71.

Storm JF (1990) Potassium currents in hippocampal pyramidal cells. Prog Brain Res 83:161-187.

Suzuki R, Dickenson AH (2000) Neuropathic pain: nerves bursting with excitement. Neuroreport 11:R17-R21.

Suzuki R, Matthews EA, Dickenson AH (2002) Neurobiology of neuropathic pain: mode of action of anticonvulsants. Eur J Pain 6:51-60.

Tam SW, Zaczek R (1995) Linopirdine. A depolarization-activated releaser of transmitters for treatment of dementia. Adv Exp Med Biol 363:47-56.

Tatulian L, Brown DA (2003) Effect of the KCNQ potassium channel opener retigabine on single KCNQ2/3 channels expressed in CHO cells. J Physiol 549:57-63.

Toth SE (1966) A brief annotated synopsis of neural crest cell derivatives. Bios 37:164-167.

Tzingounis AV, Heidenreich M, Kharkovets T, Spitzmaul G, Jensen HS, Nicoll RA, Jentsch TJ (2010) The KCNQ5 potassium channel mediates a component of the afterhyperpolarization current in mouse hippocampus. Proc Natl Acad Sci U S A 107:10232-10237.

Tzingounis AV, Nicoll RA (2008) Contribution of KCNQ2 and KCNQ3 to the medium and slow afterhyperpolarization currents. Proc Natl Acad Sci U S A 105:19974-19979.

Van Camp G, Coucke PJ, Akita J, Fransen E, Abe S, De Leenheer EM, Huygen PL, Cremers CW, Usami S (2002) A mutational hot spot in the KCNQ4 gene responsible for autosomal dominant hearing impairment. Hum Mutat 20:15-19.

Vydyanathan A, Wu ZZ, Chen SR, Pan HL (2005) A-type voltage-gated K+ currents influence firing properties of isolectin B4-positive but not isolectin B4-negative primary sensory neurons. J Neurophysiol 93:3401-3409.

Wang HS, Brown BS, McKinnon D, Cohen IS (2000) Molecular basis for differential sensitivity of KCNQ and IKs channels to the cognitive enhancer XE991. Mol Pharmacol 57:1218-1223.

Wang HS, Pan Z, Shi W, Brown BS, Wymore RS, Cohen IS, Dixon JE, MckKinnon D (1998) KCNQ2 and KCNQ3 Potassium Channel Subunits: Molecular Correlates of the M-Channel. Science 282:1890-1893.

Wang Q, Curran ME, Splawski I, Burn TC, Millholland JM, VanRaay TJ, Shen J, Timothy KW, Vincent GM, de Jager T, Schwartz PJ, J.A. T, Moss AJ, Atkinson DL, Landes GM, Connors TD, Keating MT (1996) Positional cloning of a novel

potassium channel gene: KVLQT1 mutations cause cardiac arrhythmias. Nat Genet 12:17-23.

Watanabe H, Nagata E, Kosakai A, Nakamura M, Yokoyama M, Tanaka K, Sasai H (2000) Disruption of the epilepsy KCNQ2 gene results in neural hyperexcitability. J Neurochem 75:28-33.

Waxman S, Cummins T, Dib-Hajj S, Fjell J, Black J (1999) Sodium channels, excitability of primary sensory neurons, and the molecular basis of pain. Muscle Nerve 22:1177-1187.

Wen H, Levitan IB (2002) Calmodulin is an auxiliary subunit of KCNQ2/3 potassium channels. J Neurosci 22:7991-8001.

Wladyka CL, Feng B, Glazebrook PA, Schild JH, Kunze DL (2008) The KCNQ/M-current modulates arterial baroreceptor function at the sensory terminal in rats. J Physiol 586:795-802.

Wladyka CL, Kunze DL (2006) KCNQ/M-currents contribute to the resting membrane potential in rat visceral sensory neurons. J Physiol 575:175-189.

Wood MA, Kaplan MP, Park A, Blanchard EJ, Oliveira AM, Lombardi TL, Abel T (2005) Transgenic mice expressing a truncated form of CREB-binding protein (CBP) exhibit deficits in hippocampal synaptic plasticity and memory storage. Learn Mem 12:111-119.

Yang Y, Beyer BJ, Otto JF, O'Brien TP, Letts VA, White HS, Frankel WN (2003) Spontaneous deletion of epilepsy gene orthologs in a mutant mouse with a low electroconvulsive threshold. Human Molecular Genetics 12:975-984.

Yeomans DC, Proudfit HK (1996) Nociceptive responses to high and low rates of noxious cutaneous heating are mediated by different nociceptors in the rat: electrophysiological evidence. Pain 68:141-150.

Yue C, Yaari Y (2004) KCNQ/M channels control spike afterdepolarization and burst generation in hippocampal neurons. J Neurosci 24:4614-4624.

Ziegler EA, Mageri W, Meyer RA, Treede RD (1999) Secondary hyperalgesia to punctate mechanical stimuli: central sensitization to A-fibre nociceptor input. Brain 122:2245-2257.